INFORMATION TO USERS

This manuscript has been reproduced from the microfilm master. UMI films the text directly from the original or copy submitted. Thus, some thesis and dissertation copies are in typewriter face, while others may be from any type of computer printer.

The quality of this reproduction is dependent upon the quality of the copy submitted. Broken or indistinct print, colored or poor quality illustrations and photographs, print bleedthrough, substandard margins, and improper alignment can adversely affect reproduction.

In the unlikely event that the author did not send UMI a complete manuscript and there are missing pages, these will be noted. Also, if unauthorized copyright material had to be removed, a note will indicate the deletion.

Oversize materials (e.g., maps, drawings, charts) are reproduced by sectioning the original, beginning at the upper left-hand corner and continuing from left to right in equal sections with small overlaps.

Photographs included in the original manuscript have been reproduced xerographically in this copy. Higher quality 6" x 9" black and white photographic prints are available for any photographs or illustrations appearing in this copy for an additional charge. Contact UMI directly to order.

ProQuest Information and Learning
300 North Zeeb Road, Ann Arbor, MI 48106-1346 USA
800-521-0600

Validation of Three Multi-zone Airflow Models

Hongmin Li

A Thesis

in

The Department

of

Building, Civil and Environmental Engineering

Presented in Partial Fulfilment of the Requirements
for the Degree of Master of Applied Science at
Concordia University
Montreal, Quebec, Canada

January 2002

ABSTRACT

Validation of Three Multi-zone Airflow Models

Hongmin Li

Understanding airflow and contaminant transport patterns in building helps engineers to design systems that effectively ventilate all spaces. Computer simulation models are used to predict air and contaminant flow as inexpensive alternatives. Several airflow and contaminant dispersion models have been developed to study air distribution and indoor air quality in buildings.

A comprehensive research was conducted to validate the three multi-zone airflow models – COMIS, CONTAM and ESP-r. The validation process was carried out at different levels: fundamental comparisons of three models, validation with experimental data collected in a controlled environment test in a laboratory, and validation with field measurement data of two single-family houses in Ottawa. An approach was developed to distribute the measured air leakage characteristics of the whole house with the garage through cracks and gaps on exterior walls and roof, before the simulation with field measurement data. After that, COMIS and CONTAM were used to predict indoor air contaminant dispersion in the field measurement houses caused by car exhaust in the attached garages.

The validation comparisons indicate that there are good agreements between the predictions made by COMIS, CONTAM and ESP-r, there are, however, some differences between these models' predictions and the measured data. The contaminant concentrations predicted by COMIS and CONTAM illustrate that the air-tightness of garage/house interface wall has significant impact on the contaminant dispersion in the rooms of houses.

ACKNOWLEDGMENT

I would like to express my greatest gratitude to my supervisor, Dr. F. Haghighat, for his continued guidance, support, encouragement and patience.

Extended thanks go to Dr. Ian Beausoleil-Morrison and Dr. Kamel Haddad of Buildings Group of Natural Resources Canada (NRCan), for their offering of introductory ESP-r courses.

Special thanks go to Mr. Don Fugler of Research Division of Canada Mortgage and Housing Corporation (CMHC), for his kindly providing the field measurement data; to Dr. A. C. Megri, for his helpful suggestions and comments.

This work is also part of the Canadian contributions to the work of Annex 35 of the International Energy Agency (IEA).

My friends and colleagues from around the world I met at Concordia University and Montreal, thank you for your suggestions and help.

Finally, I want to express my deepest appreciation to my wife, Ping Zhang, my parents and my brother, for their love, understanding and support.

Table of Contents

List of Figures

List of Tables

Nomenclature

A	opening area (m^2)
C	crack flow coefficient ($m^3/s\ Pa^n\ m$)
C_d	discharge coefficient (-)
$C_{p,i,d}$	wind pressure coefficient for surface location "i" corresponding to wind from direction "d" (-)
D	dimension of the fan (m)
H_{NL}	height of neutral level (m)
H_s	specific humidity ($kg_{water}/kg_{dry\ air}$)
K	flow coefficient ($m^3/s\ Pa^n$)
L	crack length (m)
N	fan rotating speed (1/s)
P	absolute pressure (Pa)
P_a	reference pressure at zone A (Pa)
P_i	wind pressure on the building surface i (Pa)
P_r	reference pressure (Pa)
P_s	Pressure due to stack effect (Pa)
P_v	wind velocity pressure (Pa)
Q	volume air flow rate (m^3/s)
R	gas constant (287 for air) (J/kg K)
Re	Renolds number (-)

T	absolute temperature (^oK)
U	average velocity in duct (m/s)
U_{H}	approach wind speed at upwind wall height (m/s)
U_{ij}	air flow velocity at large opening between zone i and j (m/s)
W	opening width (m)
Z	vertical position (m)
Z_a	reference height for zone A (m)
a_i	coefficient for polynomial (-)
b	air density gradient (kg/m^4)
d	diameter of duct (m)
l	length of duct (m)
m	mass air flow rate (kg/s)
n	flow exponent (-)
ζ	local loss coefficient (-)
ε	surface roughness (m)
ρ	air density (kg/m^3)
λ	friction factor (-)
ω	relaxation coefficient (-)
ρ_a	ambient air density (kg/m^3)
ρ_b	air density at zone B (kg/m^3)
μ	viscosity (kg/s m)
ΔP	total pressure difference (Pa)
$\Delta P_{fitting}$	dynamic losses caused by fitting (Pa)

$\Delta P_{friction}$ friction losses in a section of duct (Pa)

[J] Jacobin matrix (-)

[X] pressure correction matrix (-)

CHAPTER 1

Introduction and Literature Review

1.1 Introduction to Multi-zone Airflow Models

Providing a comfortable and healthy indoor environment for building occupants is the primary concern of HVAC engineers. There are many factors that may influence indoor air quality (IAQ) and comfort, such as control of internal and external source of pollutant, supply of acceptable air, removal of unacceptable air, occupants' activities and preference, human's thermal regulation, and proper operation and maintenance of the building and its mechanical system. HVAC system designers, building occupants and owners must be aware of and address factors influencing indoor environment (ASHRAE, Fundamental Handbook, 1997). Air infiltration and ventilation has a strong impact on both indoor air quality and energy consumption, therefore it is important to be able to investigate and predict airflow behavior of buildings as effectively and reliably as possible.

The transport of airborne contaminants throughout a building is caused by air movements driven by pressure difference between individual zones. It is very important to know the airflow pattern within the building, in order to provide good indoor air quality, to understand inter-zonal airflow, to determine the impact of infiltration and natural or mechanical ventilation on indoor air quality. Accurate airflow information is also

necessary for aiding assessments of possible smoke distribution if fire strikes, correctly calculating cooling/heating load and sizing space-conditioning equipment (Feustel, 1999).

There are two techniques to predict the airflow rates in buildings: experimental investigation and mathematical modeling. The most straightforward experimental method is to measure infiltration directly, e.g., using the tracer gas technique. This method works only under prevailing leakage and weather conditions. Experimental investigation of full-scale buildings usually becomes extremely expensive because of high cost and the need for complex instrumentation. In the building environmental engineering field, numerical predictions (computer-based building simulation) by mathematical models are increasingly being used to address real world problems in the design of energy efficient buildings and health buildings.

The calculation results of simulation programs can be obtained with different external factors (e.g., outdoor air temperature variation), and any combination of these factors can be selected and given freely as input parameters to a simulation program. A very important issue is that the theoretical calculations can be performed independent of time (e.g., the annual energy consumption of a building can be calculated in a much shorter period of time than the measurements would require). The advantage of the theoretical calculations is, however, the complete information of the simulation process and less cost.

Numerical simulations naturally have their own disadvantages. Very complex processes are very difficult to simulate and consume resources. This can be relieved by simplifying the process to be simulated, but this simplification can become an essential source of errors. The major drawback is that sometimes not all physical phenomena have been modeled with reasonable confidence (e.g., turbulence effect of air flow).

According to the type of information requested, various airflow models and tools may be used. Mathematical models range from very simple empirical algorithms to calculate the global airflow rate to sophisticated computerized fluid-dynamic techniques solving the Navier-Stokes equations (Allard, 1998). In general, according to the complexity of modeling, airflow models can be grouped into two categories: detailed models for predicting airflow and contaminant distribution patterns in rooms – room air movement models, and simplified models for predicting such in buildings consisting of one or several "well-mixed" zone or zones – building airflow models.

Although the level of analysis is not nearly as detailed as a room air movement model, building airflow models is easy to use and it can provide an overall picture of airflow and contaminant concentration distribution pattern in the modeled building, and hence it is more frequently used.

Building airflow models can be divided into two main categories, single-zone models and multi-zone models. Single-zone models assume that the whole building can be described by a single and well-mixed zone. The major application of this model type is the single-

story, single-family house with no internal partitions (e.g., all internal doors are open). Multi-zone models allow the division of a building into separate zones, which may be at internal pressures and temperatures distinct from one another. Their solution can provide detailed results about the mass flow rates through all air flow paths. Figure 1.1 shows an example of a very simple multi-zone building (Liddament, 1986).

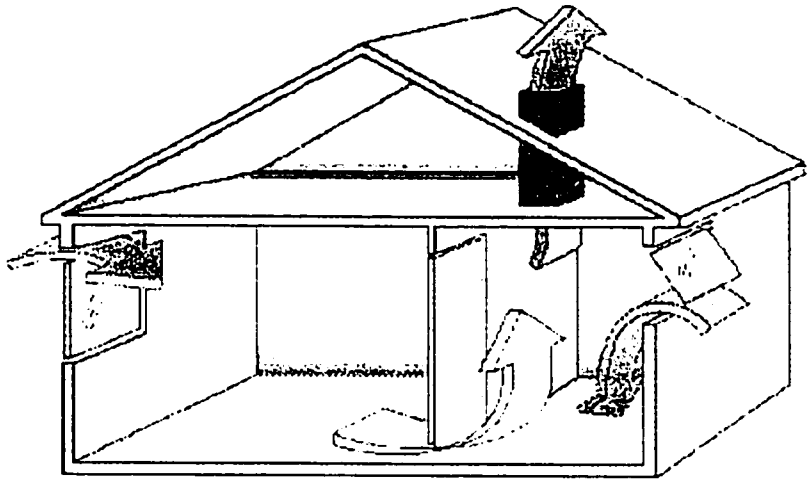

Figure 1.1. Example of a Simple Multi-Zone Structure (Liddament, 1986)

According to the concept of multi-zone airflow modelling, a building is represented by a grid that is formed by a number of nodes that stand for the simulated zones and exterior environment. Interaction between various zones is denoted by airflow paths linking their respective nodes. Thus, the rooms of a building are represented by nodes and the openings are represented by linking airflow paths. Interaction with the outdoor environment is represented by flow paths linking interior with exterior nodes. All nodes, interior and exterior, are attributed a pressure value.

The advantage of multi-zone models, besides being able to simulate infiltration in larger buildings, is that they can be used to calculate mass flow interactions between the different zones inside buildings. Understanding the airflow in buildings is important for several reasons: (Feustel and Dieris, 1992)

- Exchange of outside air with inside air is necessary for building ventilation;
- To calculate energy consumed for every room to heat or cool the infiltrated air to inside comfort temperature;
- Air needed for indoor combustion equipment;
- Airborne particles and germs transported by airflow in buildings space;
- Smoke distribution in case of fire.

The mechanical ventilation system can also be included in multi-zone network modeling, the duct system being treated like the other flow paths in the building. The advantage of calculating the airflow distribution effects of mechanical ventilation systems is that the duct pathways, as well as their connections with the building, are known. In the case of mechanical ventilation systems the fan can be described as one of the sources of pressure differences, changing the pressure difference between two nodes according to the characteristic curve of the fan (Feustel, et al, 1990).

1.2 Literature Review

A number of multi-zone airflow models have been developed during the last two decades. A literature survey by Feustel and Kendon (1985), revealed 26 papers describing 15 different multi-zone models. One of the first multi-zone models found was Jackman's model LEAK, which was published in 1970.

Liddament and Allen (1983) described the results of the Air Infiltration Center's program of model validation in their report. The task involved the selection, performance assessment and comparison of mathematical models. A total of ten models, including five multi-zone models, were selected for analysis. The principal objectives were to assess the reliability and applicability of mathematical models used in the air infiltration calculation, and to identify the key parameters for achieving reliable results. A survey of nine multi-zone models was carried out by Haghighat in 1989 (Haghighat, 1989)

In order to obtain more information on multi-zone airflow models, Feustel performed a second literature review and a questionnaire survey in 1989 (Feustel and Dieris, 1992), revealed the existence of 50 multi-zone airflow models. All these programs used similar flow equations for crack flow, but differed in the versatility to describe the full range of flow phenomena and the algorithm provided for solving the set of nonlinear equations. This survey found that newer models are able to describe and simulate the ventilation systems and interrelation of mechanical and natural ventilation.

The COMIS (Conjunction of Multizone Infiltration Specialist) workshop (October 1988 – September 1989) was a joint research effort to develop a multi-zone airflow model. The task was to develop a detailed multi-zone airflow program taking crack flow, HVAC-systems, single-sided ventilation and transport mechanism through large openings into account. The COMIS Fundamentals (Feustel and Raynor-Hoosen, 1990) contains an overview about airflow modeling as well as the physics and mathematics behind the COMIS model.

Herrlin (1992) developed a computer program (***Movecomp***) for simulating airflows and pollutant transports in multi-zone buildings and demonstrated its application to a typical Swedish multistory residential building, with emphasis on a comparison of exhaust and exhaust-supply ventilation systems. He also presented his understanding of how to approach airflow studies in multi-zone buildings.

Furbringer, Roulet and Brochiellin (1996), in the final report of IEA-ECBCS Annex 23 – Multi-zone Airflow Modeling, presented the inter-model comparison of COMIS simulation results with 14 different models including 9 multi-zone models – AIRNET, ASCOS, BREEZE, CBSAIR, CONTAM, ESP-r, MZAP, PASSPORT-AIR and VENCON. It was shown that COMIS is able to predict the air and contaminant flows as well as any of these other models and at the same time these other programs took benefit of the comparisons.

Yoshino, et al (1995) in their paper, described the measured and simulated results of air infiltration and decay profiles of tracer gas in a passive solar test house used to evaluate the simulation model COMIS. The relative error of the air change rates between measurement and simulation was mostly within ±25%.

Haghighat and Megri (1996) conducted a comprehensive validation of two multi-zone airflow models – COMIS and CONTAM. The validation process was carried out at three different levels: inter-program comparison; validation with the experimental data from a controlled environment test; and validation with the field measurements carried out in a residential building. This work provided also a platform for comparison of the other new airflow models with those discussed.

Zhao, et al (1998) in their paper, described the measured and simulated results of airflow rates and pollutant concentration profiles in an airtight test house in order to evaluate the model COMIS. The correlation coefficient between the measured and simulated air change rates was 0.72, and that for pollutant concentration was 0.94.

Orme (1999), in his report, discussed the applicable models for air infiltration and ventilation calculation and highlights areas of application. In these models there are seven multi-zone models that are currently available (AIOLOS, BREEZE, COMIS, CONTAM, NATVENT, PASSPORT).

Dols (2001) described that CONTAMW is the latest version in a family of multi-zone indoor air quality and ventilation analysis computer programs (CONTAM) developed by the Building and Fire Research Laboratory of the National Institute of Standard and Technology (NIST). This article introduced the program's capabilities, options and applications.

Upham, et al (2001) conducted a validation study of CONTAM as applied to a tall building. They compared the results from tracer gas tests in a university library with results from CONTAM simulations. They indicated that CONTAM can provide accurate airflow in tall buildings, but the modeling of contaminant concentrations cannot produce accurate results unless it's reasonable to assume average uniform concentrations in building zones.

1.3 Objectives of This Research

From the literatures of multi-zone airflow models, we can see that great efforts have been put in the development and validation of multi-zone airflow models. An essential part of the development of any computer model is its validation. This procedure should prove that the numerical results are actually the solution of the problem described in the input files. The validation can also be considered as the quality label of the program. It is a huge, complex and expensive task.

In the case of air infiltration models, errors or differences from the actual values can arise due to: the use of simplifying assumptions in the input data; differences in the actual building thermal characteristics and those used in the model; differences in the airflow mechanisms used by the model and the actual phenomena; differences between actual weather conditions and those used in the simulation; and programming or logic errors. (Walton, 1989)

The main objectives of this research are:

1. To carry out an inter-model comparison of three airflow models: COMIS, CONTAM, and ESP-r.
2. To validate the predictions made by these models with two sets of experimental data. The first set was collected in a controlled environment and the second one was field measurements from two houses in Ottawa.
3. To predict the indoor air contaminant dispersion in these houses caused by the car exhaust in attached garages.
4. To study the impact of garage/house common wall leakage on the indoor air contaminant dispersion in the houses.
5. To study the impact of considering the house as single zone or multi-zone on the indoor air contaminant concentration.

CHAPTER 2

Fundamentals of COMIS, CONTAM and ESP-r

2.1 Brief Descriptions of COMIS, CONTAM and ESP-r

The three models selected for this study, COMIS, CONTAM and ESP-r, are multi-zone air infiltration models. They use similar fundamentals including flow equations for airflow paths and algorithm for solving the equations. A brief description of the models follows.

2.1.1 COMIS

COMIS (Conjunction of Multizone Infiltration Specialists) is a multi-zone airflow and contaminant model which was developed in 1989 during a one year international workshop hosted by the Lawrence Berkeley National Laboratory (LBNL), by specialists coming from China, France, Italy, Japan, The Netherlands, Spain, Sweden, Switzerland and the United States. (Furbringer et al., 1996)

In 1990 the Executive Committee of the International Energy Agency's (IEA) Buildings and Community Systems Agreement instituted a working group (Annex 23) focusing on multi-zone airflow modeling. Annex 23 was supported between 1990 and 1996 by nine

participating nations: Belgium, Canada, France, Greece, Italy, Japan, Switzerland, the Netherlands, and USA. Its objectives were to study the physical phenomena causing air flow and pollutant transport in multi-zone buildings, develop numerical modules to be integrated in the COMIS multi-zone air flow modeling system, and evaluate the COMIS code. The programs developed within the frame of Annex 23 will be maintained by participating countries, and the official COMIS code was handed over to the Swiss agency EMPA (Swiss Federal Laboratories for Materials Testing and Research) in 1998.

COMIS is one of the most recently developed air flow models. It can be used as a stand-alone program with input and output features, or as an infiltration module that can be integrated into thermal building simulation programs. COMIS is a FORTRAN-based code. Because COMIS is not inherently a user-friendly program, several user interfaces were developed over time. The participants to the 1988-89 COMIS workshop developed COMIN (this user interface is no longer supported). Later, several interfaces were developed. They include COMERL (for the DOS operating system, Figure2.1), IISiBat (for the UNIX and Windows platforms, Figure2.2) and COMISexcel (spreadsheet user interface, Figure2.3).

The latest free version COMIS3.0 accompanying documents is a product of IEA Annex 23 and subject to IEA's copyright. A further improved commercial version of COMIS3.1 was presented at a workshop at EMPA in January 2001.

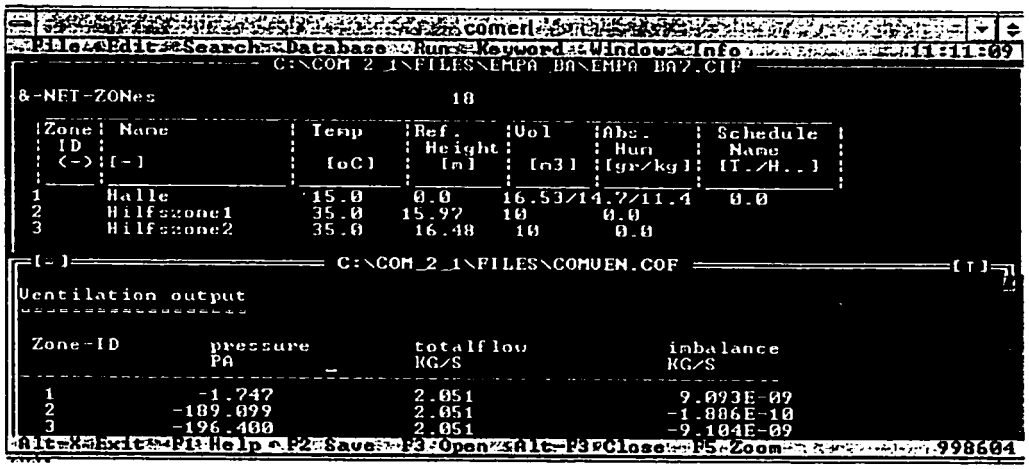

Figure 2.1 COMERL Interface for COMIS

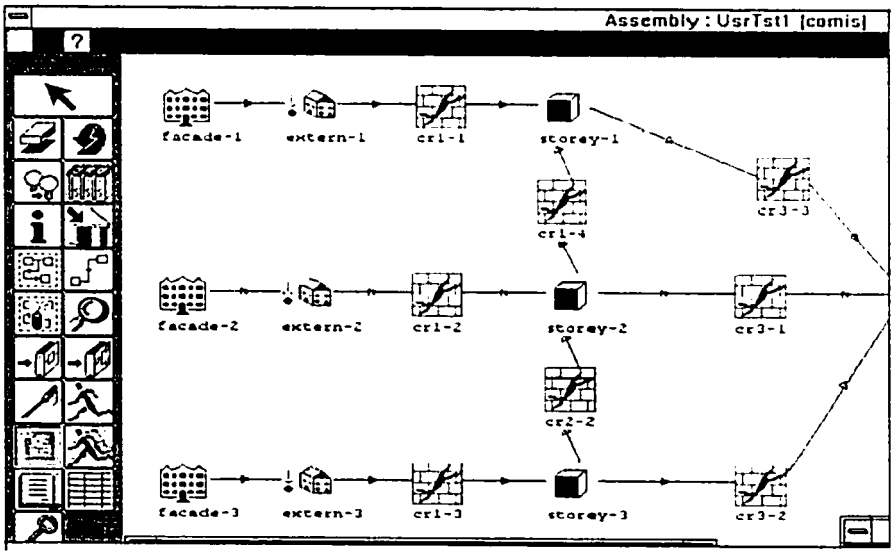

Figure 2.2 IISiBat Interface for COMIS

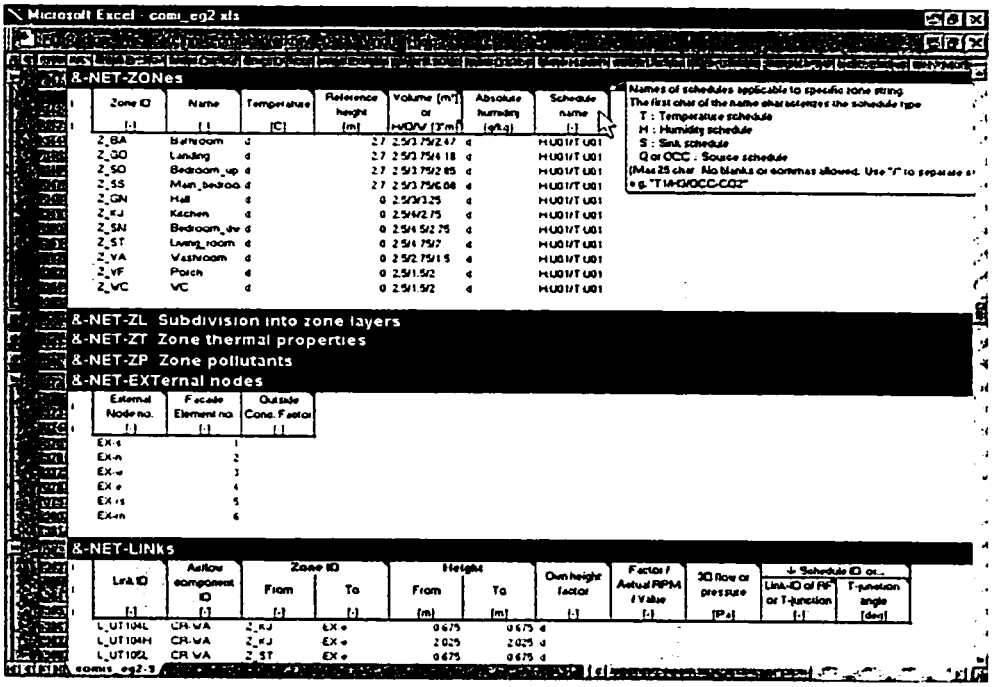

Figure 2.3 Spreadsheet Interface for COMIS

2.1.2 CONTAM

CONTAM is a multi-zone airflow and contaminant dispersal model designed to predict airflow, contaminant concentration and occupant exposure. It calculates pressures, airflow rates and contaminant concentrations in multi-zone buildings based on a graphic building description and contaminant source information. It performs steady-state, transient, and steady periodic (it is called "cyclic" in CONTAM and provides a method of simulating a typical pattern of operation by simulating only a representative time period, e.g. one day) analyses (Walton, 1997).

CONTAMW (Dols, et al. 2000) is a latest Windows version of CONTAM based on CONTAM96 (Walton, 1997) – the one of the CONTAM program series for DOS. The series includes CONTAM87 (Axley, 1988), CONTAM88 (Grot, 1991), CONTAM93 (Walton, 1994) and CONTAM96.

CONTAM employs a graphical user interface that simplifies the task of developing the zonal representation of a building (See Figure2.4). This user interface implements a "SketchPad" that lets the user draw schematic floor plans and establishes the geometric relationships of relevant building features such as zones, airflow paths, ventilation systems, contaminant sources, and building occupants. CONTAM translates the "SketchPad" diagram input by user into a system of equations that model the building system when performing simulations. (Dols, 2001)

User can view the simulation results on the screen and then to output them to a file for input to a spreadsheet program or a data analysis program developed by the user. Airflow and pressure differences at each flow element can be viewed directly on the "SketchPad". Contaminant concentrations for each zone can also be plotted as a function of time directly from the "SketchPad".

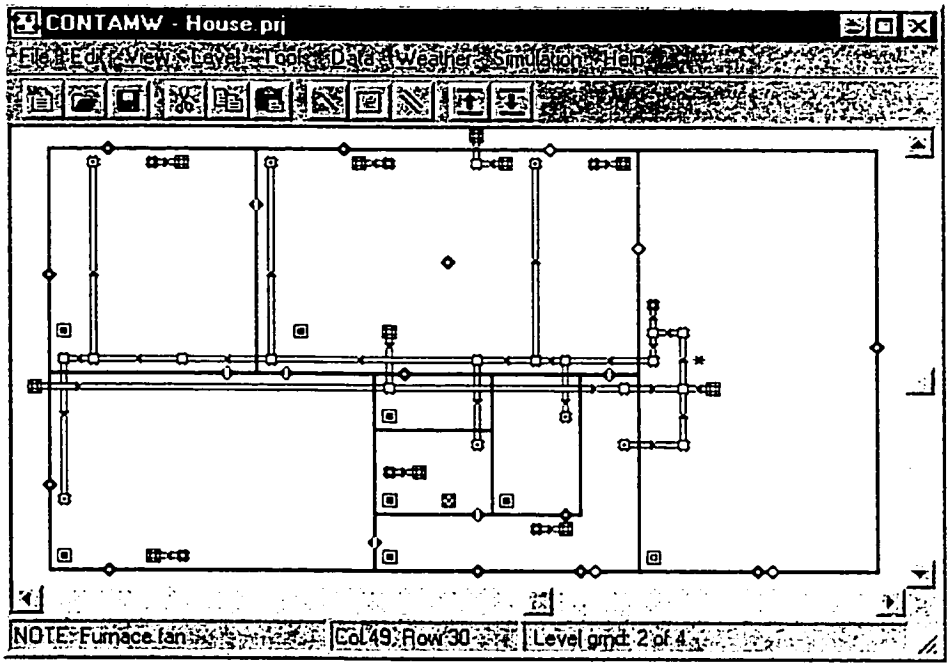

Figure 2.4 CONTAMW Graphic Interface

2.1.3 ESP-r

ESP-r (Environmental Systems Performance; r for "research") system has been evolved to its present form over more than two decades (ESRU, 1997). ESP-r is a transient energy simulation system, which is capable of modeling the energy and fluid flows within combined building and plant systems when constrained to conform to control action.

It is based on a finite volume, conservation approach in which a problem (specified in terms of geometry, construction, operation, leakage distribution, etc.) is transformed into

a set of conservation equations (for energy, mass, momentum, etc.) which are then integrated at successive time-steps in response to climate, occupant and control system influences.

The package comprises a number of interrelating program modules addressing project management, simulation, results recovery and display, database management and report writing. The simulation modules predict building and plant energy/fluid flows by a rigorous numerical method. The building/plant network is divided into a large number of finite volumes. Then at each time-step, as a simulation proceeds, an energy and mass balance is applied for all volumes, giving rise to a differential matrix for the entire system. This is then solved by custom matrix processing software in terms of any user-imposed control objectives.

The multi-zone network airflow model can be performed by the "Simulator Module" in tandem with the heat balance calculations. In this case, full account will be taken of buoyancy driven air movements between outside and inside and between internal zones. The stand-alone simulation module, *mfs*, allows independent airflow studies to predict infiltration and zone-coupled airflow. Buoyancy effects are still included but correspond to fixed zone temperatures assigned by the user. (ESRU, 1997)

Building geometry can be defined either using CAD tools or in-built facilities. ESP-r is compatible with the AutoCAD and Xzip CAD tools, which can be used to create a building representation of arbitrary complexity. (ESRU, 1997)

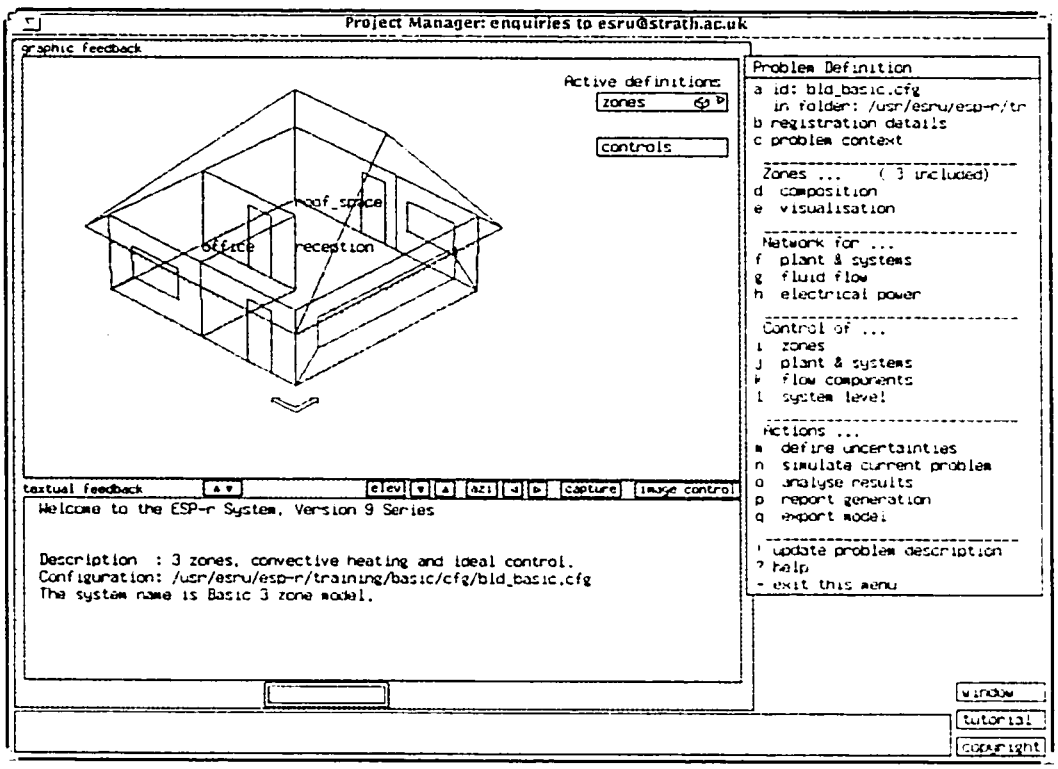

Figure 2.5 Example of Simple Building Model Definition in ESP-r

2.2 Fundamentals of Three Models

According to the concept of airflow network modeling, a building is represented by a grid that is formed by a number of nodes that stand for the simulated zones and the exterior environment. Flow paths linking their respective nodes denote interaction between various zones. Thus, the rooms of a building are represented by nodes and the openings are represented by linking flow paths. Interaction with the outdoor environment is

represented by flow paths linking interior with exterior nodes. All nodes, interior and exterior, are attributed a pressure value.

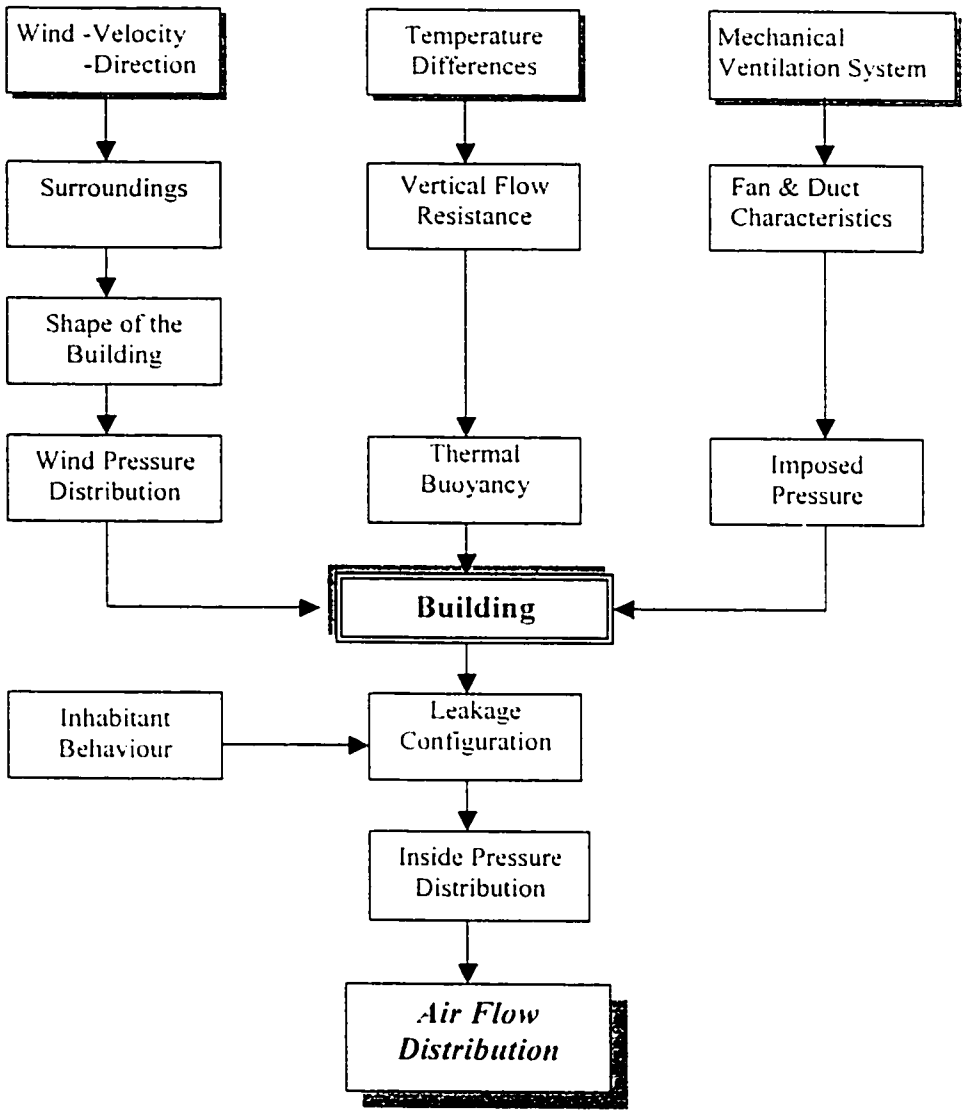

Figure 2.6 Influences on the Airflow Distribution in Buildings (Feustel et al. 1990).

The airflow distribution in a given building is caused by pressure differences evoked by wind, thermal buoyancy, mechanical ventilation system or a combination of them. Airflow is also influenced by the distribution of openings in the building shell and by the inner pathways. Actions by the occupants can also lead to significant differences in pressure distribution inside a building. Figure 2.6 shows various influences on airflow distribution (Feustel et al. 1990).

Every network approach airflow model is based on modeling the phenomena mentioned above. Mathematical formulation ought to be given to both driving forces and flow elements. After that, the whole set of equations (describing the process to be simulated) has to be solved, so that the conservation laws (for mass balance) will be fulfilled simultaneously. Because of the common non-linear dependency of the airflow rate on the pressure difference, the pressure distribution for a building can be calculated only by an iteration method.

2.2.1 Driving Forces

Airflow through the rooms of a building stems from pressure distribution around and within the building itself. Due to the turbulence of the wind flow in lower layers of the atmosphere the pressure field driven by wind on building surface is always unsteady. Pressure difference due to the stack effect depends on density field; and pressure difference due to mechanical ventilation depends on the characteristics of ducts and fans.

2.2.1.1 Wind Pressure

Wind flows produce a velocity and pressure field around buildings. Positive pressure is created on the sides of the building that face the wind (windward sides), whereas suction regions are formed on the opposite sides (leeward sides) and on the sidewalls. The pressures discussed here are time-averaged values.

The time-averaged surface pressures are proportional to the wind velocity pressure P_v (Pa) given by equation

$$P_v = \tfrac{1}{2} \rho_a U_H^{\,2} \tag{2.1}$$

Where U_H is the approach wind speed (m/s) at upwind wall height, and ρ_a (kg/m^3) is the ambient air density. The wind pressure distribution depends on the velocity and direction of the wind, the terrain surrounding of the building and its shape. This pressure distribution causes a horizontal air movement in the building. The wind pressure at each point on the building surface i is generally expressed as:

$$P_i = C_{p,i,d} P_v = C_{p,i,d} (\tfrac{1}{2} \rho_a U_H^{\,2}) \tag{2.2}$$

Where $C_{p,i,d}$ is the dimensionless pressure coefficient for a surface location i corresponding to wind from direction d, it is the ratio of the surface pressure to the dynamic pressure in the undisturbed flow pattern measured at a reference height.

The actual wind speed (U_H) is calculated as a function of available wind velocity measurements from typical meteorological data. As a result, the wind speed must be properly adjusted for a specific height and must take into account the building's orientation, the topography of the location and the roughness of the surrounding terrain in the direction of the wind. This can be calculated using three wind speed profiles: (Allard, 1998)

- The power law wind profile;
- The logarithmic wind profile;
- LBL model wind profile.

The pressure coefficient, C_p, is an empirically derived parameter that is a function of the pattern of flow around the building. It varies according to wind direction and position of the building surface. It is also significantly affected by neighboring obstruction with the result that similar buildings subjected to different surroundings may be expected to exhibit markedly different pressure coefficient patterns. Accurate evaluation of this parameter is one of the most difficult aspects of air infiltration modeling and, as yet, is not possible by theoretical means alone.

AIVC has a database of wind pressure coefficients (Orme et al., 1994) to present typical values of C_p for low rise buildings, high rise buildings and above roof level surrounded by different obstructions.

In COMIS, the C_p values are input using a table form for multiple wind directions. In addition to manual input for C_p, COMIS includes a sub-routine to automatically calculate the C_p values at any position on the building envelope for any wind angle. The calculation of C_p requires a description of environments, surrounding layout, building dimensions, building shapes and the relative location of a leakage path in the building envelope (Grosso, 1992). Because of a limited database, the application of this sub-routine is restricted to a certain a range (Feustel and Smith, 1997).

In CONTAM and ESP-r, there is a data file holding a collection of standard wind pressure coefficients sets that are based on published measurement results. A user can also input some specific C_p values by self.

For the wind speed profile, COMIS supports the two main approaches: the Power-Law profile and the Logarithmic profile. The user can chose the profile. The program uses the given wind speed at the meteo site to calculate the speed at 60m high (or higher if meteo or the building is in rough terrain). This speed at 60m (or higher) is assumed to be equal to the wind speed at the same height above the building. Along the profile near the building the velocity at the building reference height is calculated (Feustel and Smith 1997). The user can enter different wind profile exponents for different wind directions.

After the user inputs the value of local terrain constant and wind speed profile exponent, CONTAM uses the Power-Law wind speed profile approach to calculate the value of "wind pressure modifier", accounting for the difference of the wind speed at

meteorological station and building reference height. The value can typically be constant for all openings on a given building or to be set individually for each of these airflow paths.

In ESP-r, the ratio between the local wind speed at some reference height (building height) and the wind speed as read from the climate file, is called the "wind speed reduction factor". The user can input this value directly. Alternatively, ESP-r supports all the three wind speed profiles mentioned above to calculate the wind speed reduction factor for the whole building airflow paths when the user supplies additional data (regarding terrain roughness etc) (ESRU, 1996).

2.2.1.2 Thermal Buoyancy

Airflow by the stack effect occurs when temperature differences between a zone and the environment adjacent to it, be it another zone or the exterior, cause light warm air to rise and flow out of the warm zone, while cooler air flows in.

At normal temperature and pressure, the density of air is calculated by the ideal gas law:

$$\rho = \frac{P}{RT} \tag{2.3}$$

Where ρ (kg/m^3) is the air density, P (Pa) is the absolute pressure, R (J/kg K) is the gas constant (287 for air), and T (K) is the absolute temperature. This equation indicates that temperature variations cause air density variations that create the thermal buoyancy (stack effect).

In COMIS, the air density is mainly a function of temperature and moisture contents, and can be obtained by: (Feustel et al., 1990)

$$\rho = \frac{P(1 + H_s)}{461.518 \times T(H_s + 0.62198)} \tag{2.4}$$

Where H_s is the specific humidity (kg water/kg dry air), P (Pa) is the absolute pressure, and T (K) is the absolute temperature.

If P_r (Pa) is the stack pressure at the bottom of a zone, then the pressure due to the stack effect, at a height Z (m) of the zone is given by:

$$P_s = P_r - \rho g Z \tag{2.5}$$

This equation can be used to calculate the stack pressure difference ΔP_s at the height of Z across a vertical surface separating two zones. Z_a and Z_b are reference heights for room A and B:

$$\Delta P_s = P_a - P_b - \rho_a g(Z - Z_a) + \rho_b g(Z - Z_b) \quad (2.6)$$

COMIS, CONTAMW and ESP-r all employ this fundamental equation to calculate the thermal buoyancy between two points on the opposite side of an airflow path.

To be better equipped to handle some rare cases (an actual example is: a large mass flow network with relative few boundary nodes representing building zones and airflow paths) that may lead to unstable results, ESP-r offers an alternative stack pressure calculation model, which may be chosen by altering the user definable parameter. In this approach the stack pressure calculation is based on the average fluid density at the connected nodes (Hensen, 1991).

2.2.1.3 Mechanical Ventilation Systems

A mechanical ventilation system also introduces a pressure field within a building. The air movement can occur by mechanical systems such as a fan. Fan performance is usually expressed by the total pressure difference and the volume flow rate.

The effect of changing air density and fan rotating speed on volume flow rate and pressure is important for ventilation calculation. The fan laws relating to the effects of fan size, rotating speed and air density can be expressed by:

$$Q_1 = Q_2 \times \left[\frac{D_{F,1}}{D_{F,2}}\right]^3 \times \frac{N_{F,1}}{N_{F,2}} \tag{2.7}$$

$$P_{F,1} = P_{F,2} \times \left[\frac{D_{F,1}}{D_{F,2}}\right]^2 \times \left[\frac{N_{F,1}}{N_{F,2}}\right]^2 \times \frac{\rho_1}{\rho_2} \tag{2.8}$$

Where Q is the airflow rate, D is the dimension of the fan, N is the rotating speed, P is the pressure and ρ is the air density.

Subscript 1 denotes that the variable is for the fan under consideration; subscript 2 denotes that the variable is for the tested fan. If the same fan is considered ($D_{F1} = D_{F2}$), the equation (2.7) and (2.8) are simplified as:

$$Q_1 = Q_2 \times \frac{N_{F,1}}{N_{F,2}} \tag{2.9}$$

$$P_{F,1} = P_{F,2} \times \left[\frac{N_{F,1}}{N_{F,2}}\right]^2 \times \frac{\rho_1}{\rho_2} \tag{2.10}$$

On the basis of the data pair of the volume flow rate and the pressure difference, the fan performance curve is expressed by the approximate polynomial formula using the least square method. The pressure difference caused by a fan can be described for example by a cubic polynomial equation:

$$\Delta P = a_0 + a_1 Q + a_2 Q^2 + a_3 Q^3 \qquad (2.11)$$

Where ΔP (Pa) is the total pressure difference across the fan, Q (m^3/s) is the airflow rate through the fan, and a_i is the coefficient.

All three models use this cubic polynomial curve, expressed by 4 coefficients, to describe the relationship between the fan flow rate and the pressure. In ESP-r, the user has to input the four coefficients and the lower and upper validity limit of the polynomial. In COMIS, the user can either input the four coefficients directly or input 3 (minimum) to 12 (maximum) pairs of measured airflow-pressure data that will be used by the program to calculate the four coefficients. Between four and ten data points are required to fit a line for CONTAM to fit a cubic polynomial to create a performance curve for the fan.

2.2.2 Air Flow Elements

The relationship between air flow and pressure difference can be modeled by several empirical component models. The mathematical formulations of the models depend very much on the nature of the airflow which, in turn, depends on the type of flow path or opening. The openings can be placed into three categories:

- Purpose-provided openings (windows, doors, ducts, etc.).
- Component openings which are identifiable cracks around doors or windows.

- Background leakage areas which are the openings that remain after the first two types of openings are sealed, such as cracks between walls and floors.

The geometry of the first two openings can be measured but that of the third type of opening cannot be identified. The last two types of openings are collectively referred to as adventitious openings.

The airflow through a crack is always a mixture of laminar, turbulent and transition flow, the proportion of each regime depending on the shape of the crack and pressure difference. (Feustel et al. 1990)

2.2.2.1 Small Openings (Cracks)

The component openings and background leakage of buildings may be characterized fairly well by the crack flow equations. Generally, the flow of air through gaps and cracks in the building fabric is transitional between laminar and turbulent. The power law method assumes that infiltration is proportional to the product of the crack coefficient and the crack length.

$$Q = C \times L \times (\Delta P)^n = K(\Delta P)^n \qquad (2.12)$$

Where Q (m^3/s) is the volume flow rate, C ($m^3/s\ Pa^n\ m$) is the crack flow coefficient, L (m) is the crack length, ΔP (Pa) is the pressure drop, K ($m^3/s\ Pa^n$) is the flow coefficient, n is the flow exponent.

The value of the flow coefficient, K, is related to the size of the opening and the flow exponent, n, depends on the flow characteristics and varies in the range of 0.5 for fully turbulent flow, to 1.0 for fully laminar flow. Values of K and n are determined by the fan pressurization techniques with a blower door at a given temperature and pressure. AIVC has a database (Orme, 1994) for providing numerical guidance on typical leakage values for use in design and simulation when no other source of data is available.

Alternative representations of the airflow equation exist and, in most case, can be expressed by the Power-Law equation.

In COMIS, there is only one option to describe small crack airflow by the power-law equation. In ESP-r, more options are available. They include: three types of Power-Law; two types of Quadratic-Law and one Orifice flow component (Hensen, 1991).

- Power-Law flow component

$$\dot{m} = \rho a \Delta P^b \tag{2.13a}$$

$$\dot{m} = a \Delta P^b \tag{2.13b}$$

$$\dot{m} = a \sqrt{\rho} \Delta P^b \tag{2.13c}$$

Where m is the fluid mass flow rate through the component (kg/s), a is a flow coefficient, expressed in: $m^3/s.Pa^b$ (2.13a), $kg/s.Pa^b$ (2.13b), $(kg.m^3)^{1/2}/s.Pa^b$ (2.13c). ΔP is the total pressure loss across the component (Pa), and b is the flow exponent.

- Quadratic-Law flow component

$$\Delta P = a\frac{\dot{m}}{\rho} + b\left(\frac{\dot{m}}{\rho}\right)^2 \qquad (2.14a)$$

$$\Delta P = a\dot{m} + b\dot{m}^2 \qquad (2.14b)$$

Where a is a flow coefficient, expressed in: $Pa/(m^3/s)$ (2.14a), or $Pa/(kg/s)$ (2.14b). b is a flow coefficient, expressed in: $Pa/(m^3/s)^2$ (2.14a), or $Pa/(kg/s)^2$ (2.14b).

- Common orifice flow component

$$\dot{m} = C_d A\sqrt{2\rho\Delta P} \qquad (2.15)$$

Where C_d is the discharge factor and A is the opening area (m^2).

Compared with other two models, CONTAMW is more flexible for defining a small opening. It provides a few options to choose which is associated with the airflow element that the user is about to create.

1. $\underline{Q = K(\Delta P)^n}$ and $\underline{m = K(\Delta P)^n}$: This is the general form of the power-law model in volumetric flow and mass flow form that allows user to directly input the coefficient, K, and exponent, n.

2. Leakage Area Data: This model refers to effective leakage areas as described in Chapter 25 of the 1997 ASHRAE Handbook of Fundamentals.

3. Connection (ASCOS) Data: Refers to the airflow description used in the ASCOS program (Klote, 1981).

4. Orifice Area Data: Relates the opening description to the orifice area data.

5. Crack Description: A narrow opening described by its length and width using the power-law model.

6. Test Data (1-point): Uses a single flow rate and pressure drop along with an estimate for the pressure exponent, n.

7. Test Data (2-point): Uses two flow rates with their corresponding pressure drops to define the flow using the power-law model.

8. $\Delta P = aQ + bQ^2$ and $\Delta P = am + bm^2$: These models allow the user to directly input the "a" and "b" coefficients for the Quadratic models in mass flow and volume flow forms.

9. Crack Description: This model describes a narrow opening using Quadratic model in greater detail than the power-law version of the crack model.

10. Test Data (2-point): This model uses two flow rates and their corresponding pressure drops to define the flow using the quadratic model.

11. Backdraft Damper Model ($m = K(\Delta P)^n$ and $Q = K(\Delta P)^n$): Volume flow and mass flow forms of the Backdraft Damper model allow user to model a feature that has different resistances depending on the direction of the pressure drop, e.g., a smoke control damper. User input separate values of K and n depending on the sign of the pressure drop across the damper.

2.2.2.2 Large Openings

Airflow through large openings (e.g., open doorways or open windows) is a main contributor to the transfer of air, pollutants and thermal energy from one zone of a building to another zone or to the outside. In most circumstance, thermal differences and/or differences in thermal gradients on both sides of a large opening will cause two-way flows.

The prediction of airflow through large openings is difficult. Although good agreement exists in the literature regarding prediction of gravitational flows through large openings in steady-state conditions, large uncertainty remains regarding the definition of the discharge coefficient. Air flow through large openings involves a number of different physical phenomena, including steady-state gravitational flows, fluctuating flows resulting from wind turbulence, and re-circulation flows caused by boundary layer effects in a thermal driven opening. (Allard, 1992)

In network modeling the air flow through large openings is considered to be bi-directional. In the absence of wind, warm and light air flows through the upper part of an opening, while cool air flows through the lower part in the opposite direction. Thus, a level can be defined at which no air movement is observed, that is, no pressure difference occurs. This is called the 'neutral level' and is located at a height H_{NL} from the floor of the zone.

The way to solve this problem is to interpret the flow equations of large openings in terms of non-linear pressure laws. This method leads to the definition of new flow equations in pressure characterizing the behavior of large openings. In the case of a vertical opening between two isothermal zones i and j for steady-state flow, following the approximation of the Bernoulli equation, it is assumed that the velocity (U_{ij}) of the air flow at different heights (z) is given by the equation:

$$U_{ij}(z) = \left[2 \frac{P_i(z) - P_j(z)}{\rho} \right]^{1/2} \tag{2.16}$$

Where ρ represents the density of flowing air.

The hydrostatic equation is then used to relate the pressures in each room to the air densities at various heights, and the velocity equation becomes:

$$U_{ij}(z) = \left[2 \frac{(P_{i,0} - P_{j,0}) - gz(\rho_i - \rho_j)}{\rho} \right]^{1/2} \tag{2.17}$$

The height of the neutral level is given by $P_i(z) = P_j(z)$ or by setting the inter-zonal velocity to zero. H_{NL} may be found to lie in one of the following positions: (Figure 2.7) (Allard et al. 1998)

- Above the opening ($H_{NL} > H_T$, top of the opening)
- Below the opening ($H_{NL} < H_B$, bottom of the opening)
- Between the top and the bottom of the opening

If temperature stratification is to be taken into account, on each side of the opening, linear density stratification is assumed:

$$\rho_i(z) = \rho_{0,i} + b_i z \tag{2.18}$$

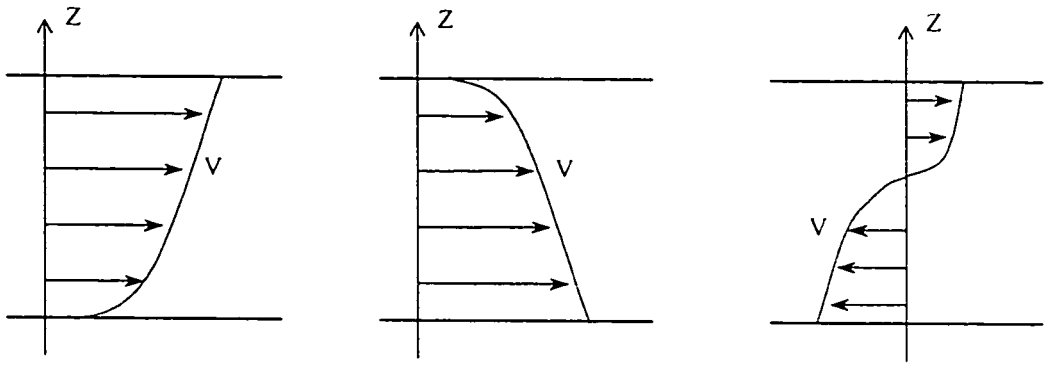

(a) $H_{NL} < H_B$ (b) $H_{NL} > H_T$ (C) $H_B < H_{NL} < H_T$

Figure 2.7 Airflow through Large Opening (No density gradient)

Where b is the air density gradient. The reference pressures on each side are given at the bottom of the opening. Assuming Bernoulli hypothesis on both sides of the opening the pressure difference can be defined at any level z as:

$$\Delta P_z = P_{1,0} - P_{2,0} - g\left[\left(\rho_{0,1} z + \frac{b_1 z^2}{2}\right) - \left(\rho_{0,2} z + \frac{b_2 z^2}{2}\right)\right] \qquad (2.19)$$

The location of the neutral plane can be obtained by equating the pressure difference to zero, which may have two, one or zero real solutions, since it is a second-order polynomial. (Figure 2.8) (Feustel and Raynor-Hoosen, 1990)

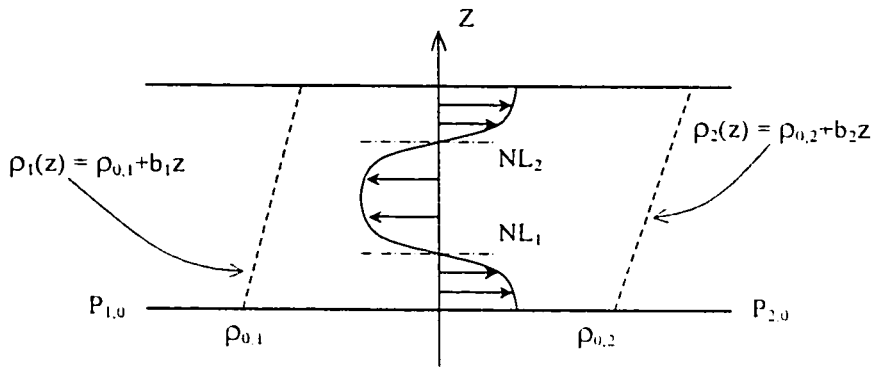

Figure 2.8 The General Problem of Gravitational Flow through a Vertical Opening

Once the height of the neutral level, H_{NL}, has been calculated, the rates for the various parts of the flow can be derived by integrating equation in the intervals defined by the physical limits of the opening and the position of the neutral planes:

$$\dot{m}_{HB,NL_1} = C_d \int_{Z=HB}^{Z=NL_1} \rho \cdot U(Z) \cdot W \cdot dz \qquad (2.20a)$$

$$\dot{m}_{NL_1,NL_2} = C_d \int_{Z=NL_1}^{Z=NL_2} \rho \cdot U(Z) \cdot W \cdot dz \qquad (2.20b)$$

$$\dot{m}_{NL_2,HT} = C_d \int_{Z=NL_2}^{Z=HT} \rho \cdot U(Z) \cdot W \cdot dz \qquad (2.20c)$$

These equations show that the flow through a large opening (W is the width of the opening) is proportional to an empirical discharge coefficient C_d. It is a phenomenological coefficient and depends on the fluid and the shape of the opening. Its value goes from 0.61 for sharp-edged orifices to 0.98 for trumpet shaped nozzles. (Feustel and Raynor-Hoosen, 1990)

COMIS uses this model to simulate the two-way airflow through windows and doors even slanted windows. Besides of this single opening model, CONTAM has an alternative model accounting for two-way flow over the height of large opening. It uses two power law flow models at different heights to approximate a single tall opening. This model divides an opening vertically and models the flow using two power-law models, one for each opening. Results are obtained in the form of the net flow rate in each direction.

ESP-r has a very different approach to simulate this type of airflow component: (Hensen, 1991)

$$\Delta P_v = \rho(2/3)\left[C_d W H (2/\rho)^{1/2} (C_a^{3/2} - C_b^{3/2}) / C_t\right] \qquad (2.21)$$

Where

$$C_a = (1 - r_p) C_t + (P_n - P_m)$$

$$C_b = (P_n - P_m) - r_p C_t$$

$$C_t = g P_o H / R (1/T_m - 1/T_n)$$

and C_d is the discharge factor, W is the opening width (m), H is the opening height (m), $r_p = H_r / H$, g is the acceleration due to gravity (= 9.81m/s^2), P_o is the atmospheric pressure

(=101325 P_a), R is the gas constant for dry air (= 28.1J/kgK), T is the node temperature (K), and H_r is the reference height above the base of the doorway (m).

On evaluation, this equation yields a sum of real and imaginary parts. The real part of the solution indicates the flow in the positive direction and the imaginary part indicates the flow in the other direction. The value which is used for the fluid density depends on the flow direction. In case of the opening height is very small (<0.01 m) or in case there is no or only a very small temperature difference (<0.01 K) a large opening component is treated as an ordinary airflow opening because in those cases the buoyancy effects may be disregarded (Hensen, 1991).

2.2.2.3 Ducts

Pressure losses through duct work are calculated based on friction losses and dynamic losses. The friction losses in a section of duct is described as:

$$\Delta P_{friction} = \lambda \frac{l}{d} \cdot \frac{\rho U^2}{2} \qquad (2.22)$$

Where λ is the dimensionless friction factor, l is the length of the duct (m), d is the diameter of the duct (m), U is the average velocity in the duct (m/s), and ρ is the air density in the duct (kg/m^3).

Dynamic losses result from flow disturbances caused by fittings that change the path of the airflow and/or its area. These fittings include entries, exits, transitions and junctions. The dimensionless coefficient zeta (ζ) is used for fluid resistance and has the same value in dynamically similar streams. It can be obtained from engineering handbooks.

$$\Delta P_{fittings} = \zeta \frac{\rho U^2}{2} \tag{2.23}$$

So the sum of all friction and dynamic losses is calculated by:

$$\Delta P_{loss} = \Delta P_{friction} + \Delta P_{fittings} = \lambda \frac{l}{d} \frac{\rho U^2}{2} + \sum \zeta \frac{\rho U^2}{2} \tag{2.24}$$

Based on this equation, COMIS, CONTAM and ESP-r model the airflow through a duct and the pressure drop. But they use different methods to calculate the value of λ.

In COMIS, within the region of laminar flow, (i.e., Reynolds number less than 2000) the friction is a function of the Reynolds number only, and can be written as:

$$\lambda = \frac{64}{\mathrm{Re}} \tag{2.25}$$

$$\mathrm{Re} = \rho U d / \mu$$

Where *Re* is the dimensionless Reynolds number, μ is the viscosity (kg/s m).

For turbulent flow (Reynolds numbers greater than 10^4), the friction factor depends on the Reynolds number, duct surface roughness, and internal protuberances (such as joints) can be calculated by Colebrook's equation:

$$\frac{1}{\sqrt{\lambda}} = -2 \log \left[\frac{\varepsilon}{3.75} d + \frac{2.51}{\mathrm{Re}} \sqrt{\lambda} \right] \qquad (2.26)$$

Where ε is the surface roughness (m). Since this equation cannot be solved explicitly for λ, an approximate explicit equation is used (Feustel and Raynor-Hoosen, 1990):

$$\lambda = 0.0055 \left[1 + \left(2000 \frac{\varepsilon}{d} + \frac{10^6}{\mathrm{Re}} \right)^{\frac{1}{3}} \right] \qquad (2.27)$$

For easier calculation in COMIS model, the relationship between the pressure loss and the volume flow rate of a duct is also modeled as the power law function. The flow coefficient K and the exponent n are calculated by means of iteration.

In ESP-r, the relationship between the pressure loss and the mass flow rate of a duct is derived from the equation (2.24) and expressed as follow: (Hensen, 1991)

$$\dot{m} = A \sqrt{\frac{2\rho\Delta P}{f L/D + \sum C_i}} \qquad (2.28)$$

Where f is the friction factor, L is the duct length (m), D is the hydraulic diameter (m), A is the cross- section area (m^2), C_i is the local loss factor due to fitting i.

For laminar flow (Re < 2300), the friction factor is calculated by equation (2.25).

In the transition region (2300<Re<3500), the friction factor is found by linear interpolation:

$$\lambda = \frac{\lambda_L (3500 - \mathrm{Re}) + \lambda_T (\mathrm{Re} - 2300)}{3500 - 2300} \tag{2.29}$$

Where λ_L is the friction factor for laminar flow at Re = 2300, and λ_T is the friction factor for turbulent flow at Re = 3500.

For Re>3500 the flow is assumed to be turbulent and the friction factor is calculated by:

$$\lambda = 1/\left[2 \cdot \log\left(5.74 / \mathrm{Re}^{0.901} + 0.27 \cdot \varepsilon / d\right)\right]^2 \tag{2.30}$$

Where ε is the surface roughness (m), d is the diameter of the duct (m).

CONTAMW uses the same equation (2.28) to describe the relationship of flow rate and pressure losses through a duct, but the friction factor is computed using the nonlinear Colebrook equation [ASHRAE 1997, p 2.9, equation. 29b]:

$$\frac{1}{\sqrt{f}} = 1.44 + 2 \cdot \log(D/\varepsilon) - 2 \cdot \log\left[1 + \frac{9.3}{\mathrm{Re} \cdot \varepsilon / D \cdot \sqrt{f}}\right] \qquad (2.31)$$

Where ε is the roughness dimension (m), D is the hydraulic diameter (m). This nonlinear equation may be solved by Newton's iteration method. (Walton, 1997)

2.2.3 Solution Methods for Airflow Network

Multi-zone airflow modeling is based on the concept that each zone of a building can be represented by a pressure node. Boundary nodes are also used to represent the environment outside the building. Nodes are interconnected by flow elements, such as cracks, windows, doors and shafts, to form a network. According to the network approach, a building with N zones is represented by a network of N pressure nodes. Some of them are connected with exterior nodes of known pressures, while others are only connected to interior nodes with unknown pressures. Calculation of unknown pressures is derived by application of mass balance equations at each node. Application of the mass balance equation to a zone i gives:

$$f(P_i) = \sum_{k=1}^{j} \rho_i Q_{ik} = 0 \qquad (2.32)$$

where Q_{ik} (m^3/s) is the volumetric flow from zone i to zone k and ρ_i (kg/m^3) is the air density in the direction of the flow.

Application of mass balance at each internal node of the network leads to a set of simultaneous non-linear equations, a non-linear system of N equations is formed. Solution of this system is based on the Newton or the improved Newton-Raphson iterative method. According to the method, a set of initial pressures is attributed to the unknown pressures. The node pressure is progressively adjusted until the convergence is reached. To minimize the residuals, at each iteration a new estimate of the pressure at each node is computed. For iteration k the new set of pressure is derived from:

$$P_n^{k+1} = P_n^k - X_n^k \tag{2.33}$$

where the matrix of the pressure corrections $[X]$ is defined for each iteration by the equation:

$$[J][X] = [F] \tag{2.34}$$

Where $[J]$ is the Jacobian matrix ($N \times N$) for the simulated building, and $[F]$ is a matrix ($N \times 1$) containing the residuals from application of equation (2.33) to each zone.

Numerical tests of the N-R method solution indicated occasional instances of very slow convergence. To accelerate convergence, various techniques have been introduced. In CONTAM, this is handled by using a relaxation coefficient ω to the equation (2.33).

$$P_n^{k+1} = P_n^k - \omega X_n^k \tag{2.35}$$

COMIS and ESP-r also use this solving method with a user defined fixed relaxation coefficient.

CHAPTER 3

Validation with Controlled Environment Test – OPTIBAT

An essential part of the development of any computer model is its validation. In the case of multi-zone airflow models, errors or differences from the actual values can arise due to: differences between actual weather conditions and those used in the simulation; the use of simplifying assumptions in the input data; differences in the actual building thermal characteristics and those used in the model; differences in the airflow mechanisms used by the model and the actual phenomena; and, finally, programming or logic errors (Haghighat and Megri, 1996).

One of the validation steps is the comparison with experiments – the results of the calculation based on measured input data on some selected cases can effectively be compared with the measured output data. In this validation study, experimental data was collected in a controlled environment.

3.1 Test Facility

OPTIBAT is a real scale experimental facility consisting of a 108m^2 four-room dwelling built in the laboratory hall at the INSA in Lyon (Furbringer et al. 1996). It is an exact replica of an existing apartment within a building located near Lyon. Climatic chambers are placed against the two facades of this dwelling to simulate the outdoor climate

(temperature and pressure). Other climatic chambers are added on each face of the experimental cell, in order to control the boundary conditions. The two main facades (Figure 3.1) can be submitted to temperatures between -10 and 30°C, to relative humidity between 30% and 80%. The pressure difference between the two facades could reach up to 200 Pa, which is equivalent to a wind velocity of 70 km/h. The other four faces (two walls, floor and ceiling) had thermal and pressure guards, simulating the adjacent apartments. (Furbringer et al, 1996)

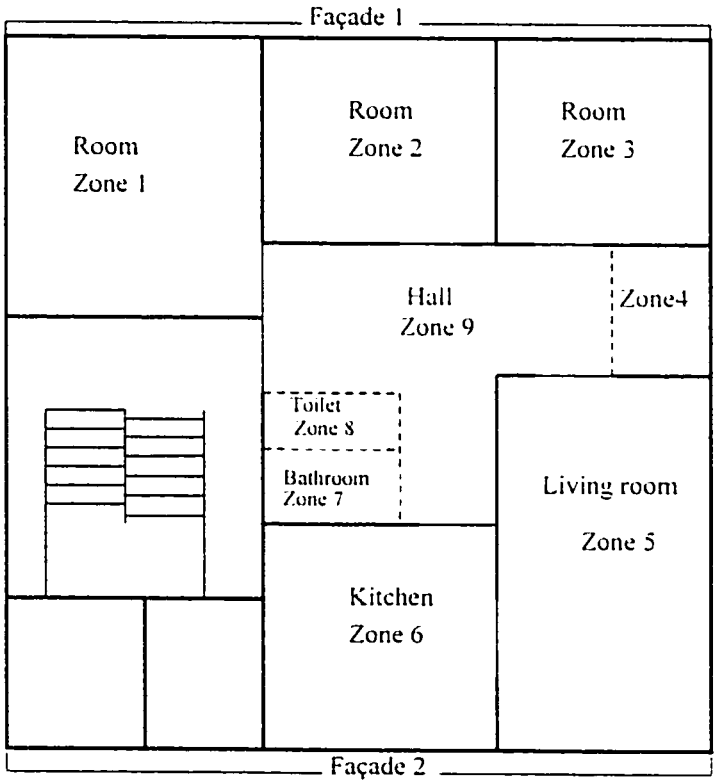

Figure 3.1 The OPTIBAT Facility for Infiltration Measurements

This facility allows measurements of air permeability and airflow in a very well controlled environment. Simulations can also be performed with very well controlled boundary conditions. The comparisons between simulations and experiments made with this facility are therefore much more accurate than those performed on real buildings. Since real pressures on facades were directly input for simulations, the possible discrepancies resulting from the use of pressure coefficients are avoided.

3.2 Measurements Performed

The fan pressurization test was used to measure the air leakage of the building envelope components such as windows, doors and walls. In order to minimize the error due to measurement techniques, both the active (guarded zone method) and passive methods were used. The guarded zone method employs two blower doors. The pressure difference across the outer walls of the primary zone is kept constant (i.e. at zero Pa), while the pressure in the secondary zone is varied between –200 and +200 Pa. The flow rates required to maintain the constant pressure difference across the external walls of the primary zone were recorded for different pressure levels in the secondary zone. See Figure 3.2.

In the passive method, one blower door is employed with the interior and exterior openings kept either closed or opened. The blower door is installed in the door of the room containing the element to be measured. The advantage of this method is that it is cheaper than the active method and easy to use. However it requires more time than the

active method and the estimation of the flow coefficients is more difficult because it requires the solution of a set of nonlinear equations coupled with statistical treatment.

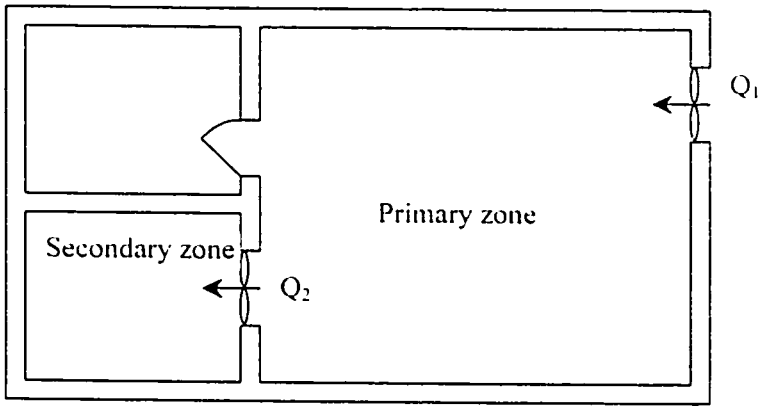

Figure 3.2 Fan Pressurisation Test of Active Method

A least square regression technique was used to estimate the flow coefficients, K and flow exponents, n. Table 3.1 (Furbringer et al, 1996) gives the values of these parameters for each component. In order to identify the components, they have been numbered clockwise starting from the door. Thus, '*Wil*' is wall number *l* of room number *i*.

The value of K and n obtained using active and passive techniques are not the same in all cases. The statistical error treatment however shows that, in most of the cases, the confidence intervals calculated using the two methods overlap with each other. This good agreement indicates that the possible error between the actual values (K and n) and those used as input in the models has been minimized (Furbringer et al, 1996).

The air leakage from the interior doors is not determined by the fan pressurization method, but estimated by $K = 0.83 \times S$, where S is the area of the crack (m^2), and $n = 0.5$ (Furbringer et al, 1996).

Component	Active method		Passive method	
	$K\ [m^3/(h.Pa^n)]$	n	$K\ [m^3/(h.Pa^n)]$	n
W11 = W22	0.01 ± 0.02	0.95 ± 0.05	0.14 ± 0.001	0.90 ± 0.001
W21	19.30 ± 0.38	0.71 ± 0.01	20.22 ± 1.03	0.78 ± 0.05
W22	0.01 ± 0.02	0.95 ± 0.05	0.14 ± 0.001	0.90 ± 0.001
W24	0.08 ± 0.02	0.99 ± 0.01	0.17 ± 0.01	0.87 ± 0.01
W31	14.17 ± 0.03	0.66 ± 0.001	14.94 ± 1.26	0.59 ± 0.004
W32 = W24	0.08 ± 0.02	0.99 ± 0.01	0.17 ± 0.01	0.87 ± 0.01
W41	2.54 ± 0.02	0.92 ± 0.03	2.49 ± 0.16	0.84 ± 0.02
W42	2.89 ± 0.21	0.66 ± 0.01	2.97 ± 0.08	0.65 ± 0.01
W44	5.48 ± 0.44	0.51 ± 0.002	5.64 ± 0.02	0.51 ± 0.01
W51	14.67 ± 1.54	0.71 ± 0.03	15.03 ± 0.64	0.76 ± 0.01
W54 = W62	6.47 ± 0.02	0.64 ± 0.01	6.29 ± 0.02	0.64 ± 0.001
W61 = W72	1.76 ± 0.26	0.74 ± 0.05	1.24 ± 0.21	0.81 ± 0.02
W64	1.64 ± 0.06	0.77 ± 0.02	1.99 ± 0.27	0.69 ± 0.06
W71	4.59 ± 0.99	0.89 ± 0.04	4.83 ± 0.31	0.80 ± 0.02
W72	1.76 ± 0.26	0.74 ± 0.05	1.24 ± 0.21	0.81 ± 0.02
W74	0.34 ± 0.01	0.97 ± 0.01	0.34 ± 0.01	0.97 ± 0.01
W82 = W74	0.34 ± 0.01	0.97 ± 0.01	0.34 ± 0.01	0.97 ± 0.01
W12				
W13				
W14	12.62 ± 1.04	0.59 ± 0.03	13.43 ± 0.91	0.58 ± 0.02
W23	13.93 ± 0.84	0.57 ± 0.02	11.82 ± 1.40	0.60 ± 0.04
W33	9.37 ± 1.15	0.61 ± 0.03	10.02 ± 1.08	0.55 ± 0.04
W34				
W43				
W52				
W53	13.52 ± 1.6	0.55 ± 0.03	13.34 ± 0.21	0.57 ± 0.01
W63	6.79 ± 1.15	0.52 ± 0.05	5.86 ± 0.02	0.56 ± 0.005
W73				
W83	3.34 ± 0.59	0.65 ± 0.05	3.94 ± 0.54	0.59 ± 0.04

Table 3.1 Value of K and n for the Internal and External Components

A smoke test was also performed to accurately find the location of these cracks. They were mainly located above the windows near the shutters, where the electric cables crossed (Amara, 1993).

Some climatic conditions, winter and summer, were simulated using the climate chambers (Table 3.2). The wind effect was simulated by pressure differentials at the facades. The temperature and pressure drop was measured in the middle of the room at height of 1.2m from the floor. The indoor air temperature was kept at 20°C throughout the apartment.

Scenario	T_{out} (°C)	T_{in} (°C)	ΔP_1 (Pa) (façade 1)	ΔP_2 (Pa) (façade 2)	ΔP_3 (Pa) (staircase)
Summer	20 ± 0.5	20 ± 0.5	16	-81	-2.8
Winter	-1.1 ± 0.5	20 ± 0.5	52	-121	-12.6

Table 3.2 Climatic Conditions Adopted for Measurements

The inter-zonal airflow rates from these boundary conditions were measured using multi-tracer gas technique and a Bayesian interpretation method. (Furbringer et al, 1996)

3.3 Simulation and Results

The OPTIBAT flat was modeled using the network illustrated in Figure 3.3. Node 4 includes bathroom (zone7), toilets (zone8), hall (zone9) and cupboard (zone 4). Interior

doors between these zones were opened for tracer gas measurements and simulations. (Door crack is *crp*, while *crw* is wall crack).

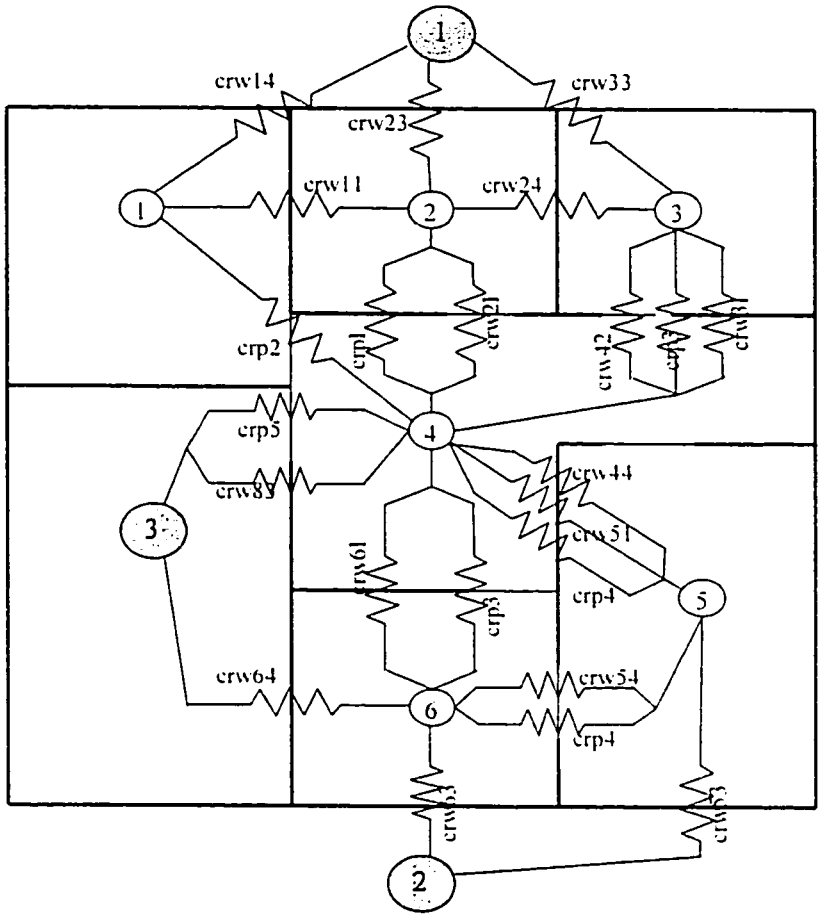

Figure 3.3 Network Modelling the OPTIBAT Flat

Simulations were performed with COMIS, CONTAM and ESP-r, using as input the measured boundary conditions (pressure differentials and temperature, see Table3.2) and the measured air permeability characteristics (Table 3.3). (Furbringer et al, 1996)

crack	Flow coefficient	exponent
	$K(m^3/(h\ Pa^n))$	n
CRW14	3.73E-03	0.58
CRW23	3.28E-03	0.6
CRW33	3.19E-03	0.58
CRW53	3.10E-03	0.54
CRW63	1.52E-03	0.56
CRW83	1.09E-03	0.59
CRW11	3.89E-05	0.9
CRW21	5.62E-03	0.78
CRW24	4.72E-05	0.87
CRW31	4.15E-03	0.59
CRW42	8.25E-04	0.65
CRW44	1.57E-03	0.51
CRW51	4.18E-03	0.76
CRW54	1.75E-03	0.64
CRW61	3.44E-04	0.81
CRW64	5.53E-04	0.69
CRP1	0.00825	0.5
CRP2	0.0166	0.5
CRP3	0.0249	0.5
CRP4	0.02075	0.5
CRP5	0.0249	0.5

Table 3.3 Input Air Leakage Parameters for Simulation

Simulation results of the inter-zonal airflow rates undertaken by three models are illustrated in Table 3.4 and Table 3.5 with summer and winter boundary conditions. The measurement data is from the thesis of Amara (1993).

ZONES	out	zone1	zone2	zone3	zone4	zone5	zone6	
out	183.0	44.7	37.6	83.7	0.5	18.3	0.0	measurement
	199.7	70.4	65.2	62.3	0.0	0.0	1.7	COMIS
	199.4	70.3	65.1	62.2	0.0	0.0	1.7	CONTAM
	196.6	69.3	64.2	61.3	0.0	0.0	1.7	ESP-r
zone1	1.9	45.2	0.2	0.0	43.1	0.0	0.0	measurement
	0.0	70.5	0.0	0.0	70.5	0.0	0.0	COMIS
	0.0	70.3	0.0	0.0	70.3	0.0	0.0	CONTAM
	0.0	69.3	0.0	0.0	69.3	0.0	0.0	ESP-r
zone2	4.5	0.3	38.3	1.4	32.1	0.0	0.0	measurement
	0.0	0.0	65.2	0.2	65.0	0.0	0.0	COMIS
	0.0	0.0	65.1	0.2	64.9	0.0	0.0	CONTAM
	0.0	0.0	64.2	0.2	64.0	0.0	0.0	ESP-r
zone3	13.5	0.0	0.2	85.0	68.5	0.0	0.0	measurement
	0.0	0.0	0.0	62.5	62.5	0.0	0.0	COMIS
	0.0	0.0	0.0	62.4	62.4	0.0	0.0	CONTAM
	0.0	0.0	0.0	61.5	61.5	0.0	0.0	ESP-r
zone4	57.7	0.2	0.3	0.6	145.3	30.0	56.5	measurement
	20.2	0.0	0.0	0.0	198.0	93.2	84.6	COMIS
	20.1	0.0	0.0	0.0	197.6	93.0	84.5	CONTAM
	19.0	0.0	0.0	0.0	194.8	92.2	83.6	ESP-r
zone5	67.2	0.0	0.0	0.0	0.5	67.8	0.1	measurement
	117.0	0.0	0.0	0.0	0.0	117.0	0.0	COMIS
	116.8	0.0	0.0	0.0	0.0	116.8	0.0	CONTAM
	116.0	0.0	0.0	0.0	0.0	116.0	0.0	ESP-r
zone6	36.6	0.0	0.0	0.0	0.5	19.5	56.5	measurement
	62.6	0.0	0.0	0.0	0.0	23.8	86.4	COMIS
	62.5	0.0	0.0	0.0	0.0	23.7	86.2	CONTAM
	61.6	0.0	0.0	0.0	0.0	23.7	85.3	ESP-r

Table 3.4 Inter-zonal Airflow Comparison between Measurements and Predictions (m^3/h) (Summer Condition)

ZONES	out	zone1	zone2	zone3	zone4	zone5	zone6	
out	350.0	91.2	77.1	142.5	7.0	30.2	1.5	measurement
	396.4	139.0	133.4	124.0	0.0	0.0	0.0	COMIS
	405.8	142.0	136.8	127.0	0.0	0.0	0.0	CONTAM
	408.8	143.1	137.5	128.2	0.0	0.0	0.0	ESP-r
zone1	8.2	99.6	0.4	0.0	91.0	0.0	0.0	measurement
	0.0	139.0	0.1	0.0	138.9	0.0	0.0	COMIS
	0.0	142.0	0.0	0.0	142.0	0.0	0.0	CONTAM
	0.0	143.1	0.1	0.0	143.0	0.0	0.0	ESP-r
zone2	9.9	0.6	85.4	0.6	74.3	0.0	0.0	measurement
	0.0	0.0	133.5	0.5	133.0	0.0	0.0	COMIS
	0.0	0.0	136.8	0.5	136.3	0.0	0.0	CONTAM
	0.0	0.0	137.6	0.5	137.1	0.0	0.0	ESP-r
zone3	19.0	0.0	1.4	155.1	134.7	0.0	0.0	measurement
	0.0	0.0	0.0	124.5	124.5	0.0	0.0	COMIS
	0.0	0.0	0.0	127.5	127.5	0.0	0.0	CONTAM
	0.0	0.0	0.0	128.7	128.7	0.0	0.0	ESP-r
zone4	211.0	0.6	0.6	1.1	307.7	29.9	64.5	measurement
	168.3	0.0	0.0	0.0	396.5	119.9	108.3	COMIS
	181.1	0.0	0.0	0.0	405.8	117.9	106.8	CONTAM
	184.7	0.0	0.0	0.0	407.9	117.1	106.0	ESP-r
zone5	76.2	0.0	0.0	0.0	0.0	80.0	3.8	measurement
	145.6	0.0	0.0	0.0	0.0	145.6	0.0	COMIS
	143.1	0.0	0.0	0.0	0.0	143.1	0.0	CONTAM
	142.9	0.0	0.0	0.0	0.0	142.9	0.0	ESP-r
zone6	52.6	0.0	0.0	0.0	0.0	17.5	70.1	measurement
	82.6	0.0	0.0	0.0	0.0	25.8	108.4	COMIS
	81.7	0.0	0.0	0.0	0.0	25.1	106.8	CONTAM
	81.2	0.0	0.0	0.0	0.0	25.0	106.2	ESP-r

Table 3.5 Inter-zonal Airflow Comparison between Measurements and Predictions (m^3/h) (Winter Condition)

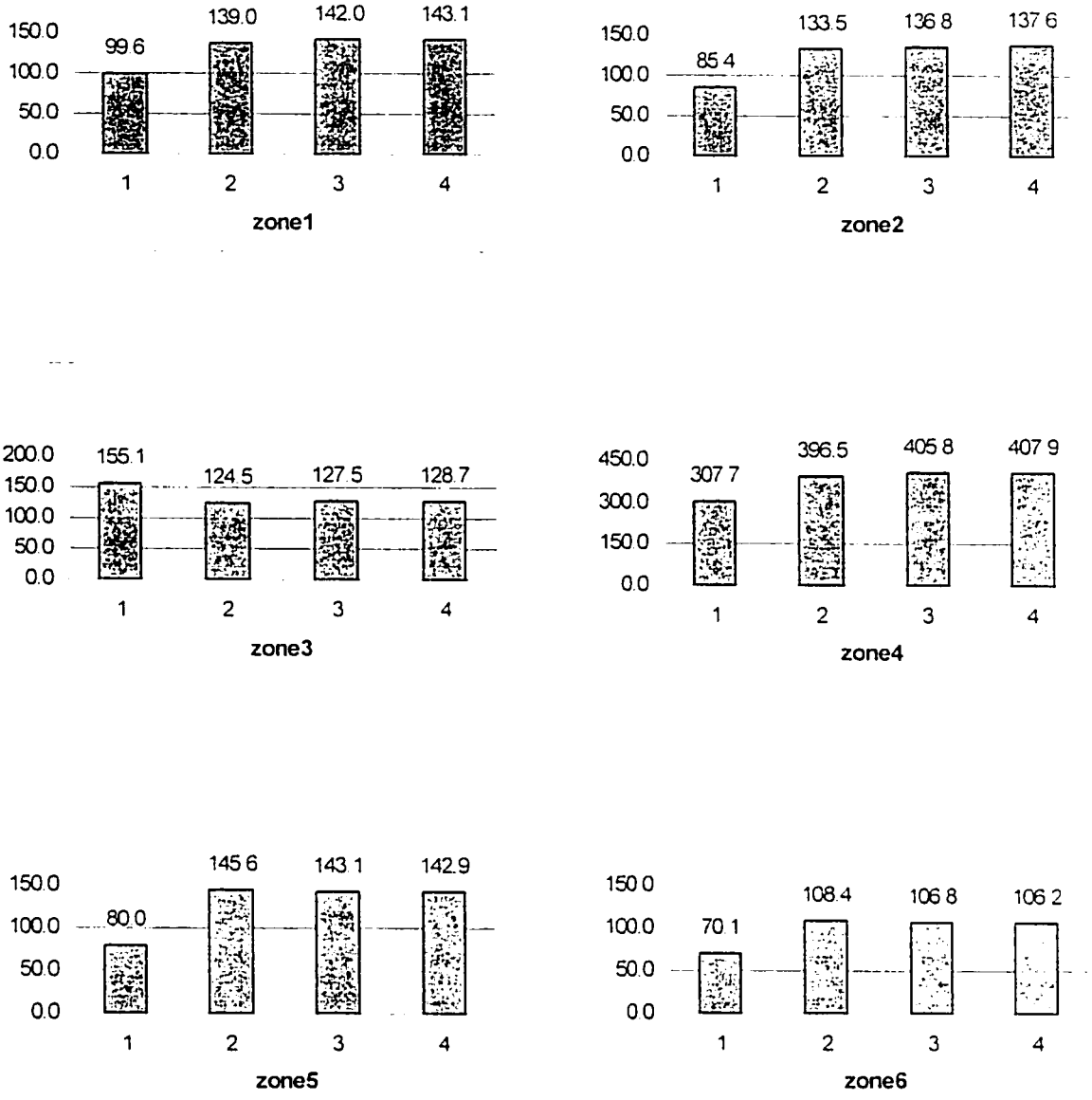

1-measurement, 2-COMIS, 3-CONTAMW, 4-ESP-r

Figure 3.4 Total Airflow Comparison between Measurements and Predictions for Every Zone(m^3/h) (Winter Condition)

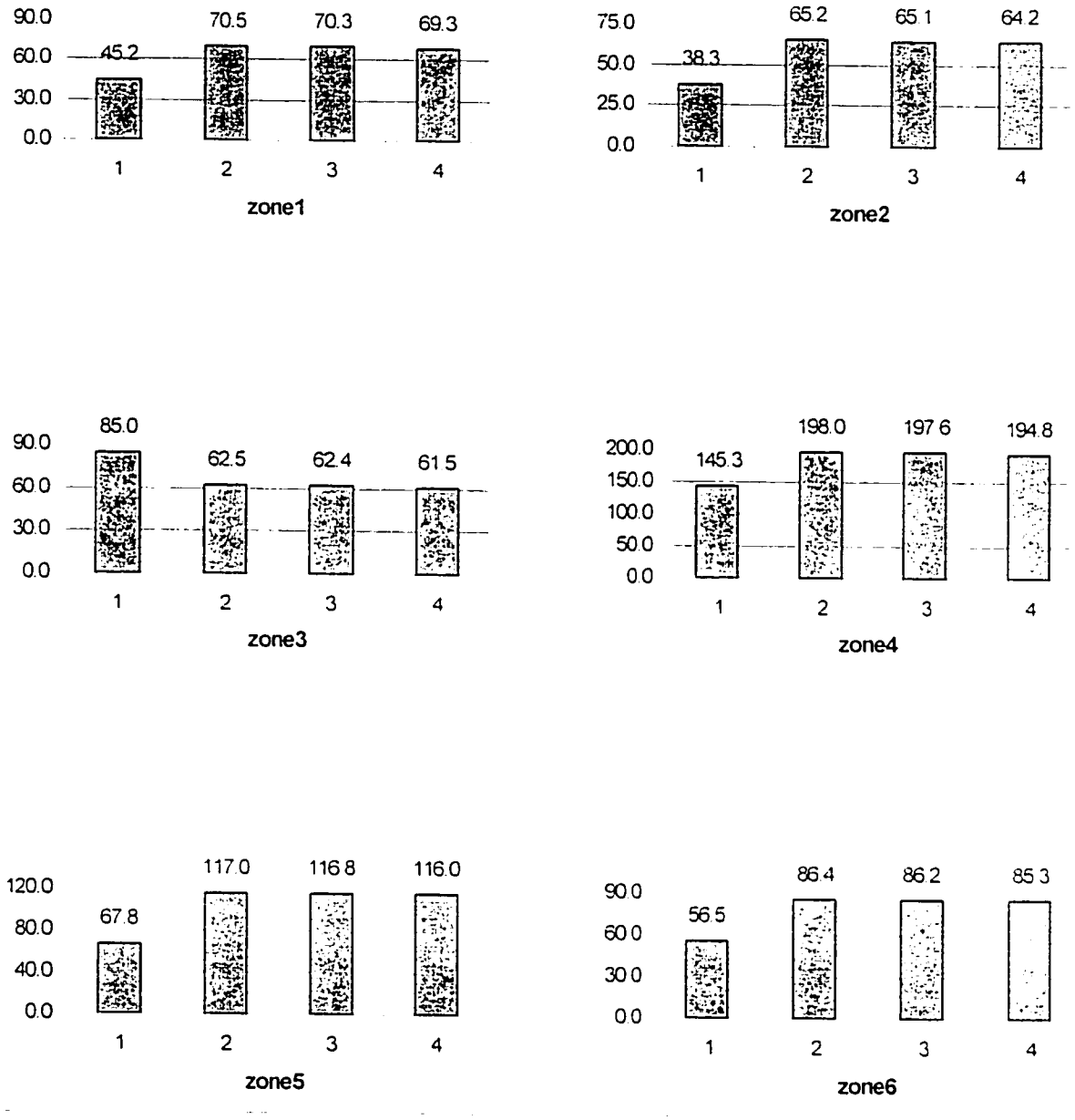

1-measurement, 2-COMIS, 3-CONTAMW, 4-ESP-r

Figure 3.5 Total Airflow Comparison between Measurements and Predictions for Every Zone(m^3/h) (Summer Condition)

3.4 Comparison and Analysis

In general, there is good agreement between the airflow rates predicted by COMIS, CONTAM and ESP-r. It was expected that the performances of three models are similar because they are based on almost the same fundamentals.

In two boundary conditions, the differences of predicted airflow rates between COMIS, CONTAM and ESP-r are under 5%, except one airflow path – from zone4 to the stairwell, in which the difference is about 10% under winter condition. Zone4 is the central node in this airflow network, and is connected to all the other zones. The differences of other airflow paths are accumulated into this link connected with a fixed boundary condition. This accumulation makes the significant difference.

In most cases, there are significant differences between simulated and measured airflow rates, even for total airflow rates in every zone (Figure 3.4 and Finger3.5). The relative differences are mostly between the range of 25% and 50%. These results agree with the experimental evaluation of COMIS presented in the final report of COMIS evaluation (Furbringer et al, 1996). Therefore the differences between measurement and prediction may be due to:

- The network used to simulate a building may not correspond to the real airflow pathway in a real building correctly. There are always hidden airflow paths between

walls. (There are several airflows that are not zero when measured, but there are zero when simulated. Maybe missing some links.)

CHAPTER 4

Validation with Field Measurements

A further validation of models was carried out with the field measurement tests performed in two single-family houses with attached garage. This type of house represents a typical Canadian house. The main difference between these houses is the heating type: house-1 is heated by electrical baseboard and house-2 is heated by a mechanical central air distribution system.

In order to simulate the airflow of two houses, the air leakage characteristics of the house, garage, and the house/garage interface are needed: they were determined by fan depressurization tests. For validation purposes, the pressure drop between the garage and the house was also measured during the test for each house (Haghighat and Megri, 1999).

The fan depressurization tests only can provide information about the global leakage characteristics of the house, garage, and the house/garage interface, but no information about the distribution of cracks and gaps on the exterior wall. This information is very essential for accurate prediction. An approach is developed in this study to evaluate the leakage distribution using the existing data.

The other required input parameters to simulate these houses are:

- Orientation of the building;

- Proximity of other buildings (shielding information);
- Physical dimensions of the house (including the sizes and locations of exterior doors, vent openings and windows, as well as interior doors);
- The location of all supply, return registers and vents as well as their respective airflow rate under normal conditions, if the house is mechanically ventilated;
- Temperature of the various rooms in the houses; and
- Local meteorological data (ambient temperature, wind speed and direction).

4.1 Measurements Methodology

The house preparation procedure followed for the air-tightness tests were according to the proposed revisions of the CGSB Standard (The Canadian General Standards Board Standard CAN/CGSB-149.10-M86, *Determination of the Air-Tightness of Building Envelopes by Fan Depressurization Method*) which allow the house to be tested as "occupied". This house preparation procedure basically does not require to seal intentional openings which would usually be left open during normal house operations. The houses were therefore prepared as they would be in winter, windows closed and latched. The "occupied' house condition provides a more realistic evaluation of the house leakage characteristics for air infiltration simulations.

To determine the air-tightness characteristics of the house, garage and their interface, two air-tightness tests were conducted as follows: (Haghighat and Megri, 1999)

- **Test 1.** House only air-tightness test. For this test the house is prepared for its winter operating conditions, and the garage door is opened. This air-tightness test is done to characterize the house envelope leakage characteristics independently from the garage. With the garage door opened, the house/garage interface leaks are included in the first test values.

- **Test 2.** House air-tightness test with the house/garage interface kept at zero pressure difference. The second house test (2h) is done with the garage door closed, and while the garage is simultaneously depressurized to eliminate the flows through common surfaces between the house and garage. The garage pressures and flows are also being recorded during this test (2g) to calculate the garage air-tightness.

Results from the two air-tightness tests provided the data required to characterize the house/garage interface. The value of flow coefficient, K, and the flow exponent, n, for the whole house envelope and the whole garage envelope were determined by regression analysis of the fan depressurization tests.

However, the value of K and n for the interface between the house and the garage are determined by mathematical manipulation of the two fan depressurization tests.

$$Q_{int} = K_{int}(\Delta P)^{n_{int}} = K_1(\Delta P)^{n_1} - K_2(\Delta P)^{n_2} \qquad (4.1)$$

Where, the subscript of "1" is for the test 1, "2" is for the test 2 (2h), "int" is for the interface. The air-tightness test results for two houses are showed in Table 4.1. (Haghighat and Megri, 1999)

Building	House		Garage		Interface	
	K [L/(s Pa^n)]	n	K [L/(s Pa^n)]	n	K [L/(s Pa^n)]	n
House-1	50.76	0.65	117.88	0.54	1.54	0.68
House-2	19.38	0.82	18.68	0.65	2.12	0.82

Table 4.1 Air Leakage Data Given by Air-Tightness Test and Calculation

A further assessment of the house/garage interface air leakage was done by pressurizing the garage and smoke pencilling. For this procedure, the garage is pressurized while the house remains under normal pressure. From inside the house, smoke pencils are used to locate the air leaks from the garage to the house. The leakage location observations from this procedure provide some indication of the airflow path distribution on this interface (Haghighat and Megri, 1999).

Some details about two houses and field test data are presented in Appendix A1.

At a specific day for each house, the meteorological data was collected. The pressure differences between the house and garage as well as the air temperature of garage and house were monitored.

4.2 Air Leakage Distribution

The fan depressurization tests provide only the information about the global air leakage characteristics of the whole unit (i.e. whole house, whole garage, etc.). This however, will not provide information about the distribution of cracks and gaps formed during the constructions of the building, such as the interface of window and door frame, ceiling/wall/floor interface, penetration of pipes, etc. This information is needed to run the simulation programs. It is, therefore, required that the global flow coefficient and exponent calculated by fan depressurization tests be distributed among cracks and gaps.

In this study, efforts and judgements have been made to evaluate the distribution of the air leakage paths around the building envelope by using some reliable data in the literature for every component.

Technical Note AIVC 44 (Orme et al 1994) developed a database to provide numerical guidance on typical leakage values for use in design and simulation when no other sources of data are available. These data are based on measurements published in over 80 technical publications and on measurements provided directly by many research organizations and groups.

One of the main criteria of data on leakage values selection from literature is that it must match the construction material and condition of the tested building such as the construction materials (concrete, timber or steel), the type of windows and doors

(weather-striped, unweather-striped), penetrations (location of the installations, etc.), wall junctions, etc. In general, the median value of flow coefficients was used except when a major airflow path was observed during the smoke test. In this case, the upper quartile value given in the literature was considered.

If no value for a component (i.e. type of window) was found in the literature, a K value was calculated by considering the airflow path as an orifice and estimating the leakage area. It is assumed the discharge coefficient C_d is equal to 0.61 (Orme et al 1994).

$$Q = C_d A \sqrt{\frac{2}{\rho} \Delta P} = C_d A \sqrt{\frac{2}{\rho}} \Delta P^{0.5} \tag{4.2}$$

$$K = C_d A \sqrt{\frac{2}{\rho}} \tag{4.3}$$

Where Q (m^3/s) is the volume flow rate, A is the opening area (m^2), ρ (kg/m^3) is the air density, ΔP (Pa) is pressure difference.

It is assumed that the air flow paths of the investigated buildings have similar characteristics as those given in the AIVC 44, but not necessarily the same value (only the flow exponent for every component is equal to that given in literature). The total envelope leakage airflow under a specific pressure differential (e.g. 50 Pa) can be calculated by adding leakage airflow for all components (literature value) at the same pressure differential. Equation 4.4 expresses the relationship between this total value and the leakage airflow determined by air-tightness test for the whole envelope.

$$\frac{\sum K_{i,lit}(\Delta P)^{n_{i,lit}}}{K_{test}(\Delta P)^{n_{test}}} = \frac{K_{i,lit}}{K_i} \tag{4.4}$$

Convert this equation, the flow coefficient for each air flow path, i, is calculated by:

$$K_i = K_{i,lit} \times \left[K_{test}(\Delta P)^{n_{test}}\right] / \sum K_{i,lit}(\Delta P)^{n_{i,lit}} \tag{4.5}$$

Where, $K_{i,lit}$ and $n_{i,lit}$ is the value of the flow coefficient and exponent for component i from the literature AIVC 44; and the K_{test} and n_{test} is the global flow coefficient and exponent of the whole unit (house, garage or their interface) measured by air-tightness test (Table 4.1)

It was also assumed that the house envelope is insulated with an air barrier and the flow coefficients of wall and ceiling were distributed proportionally to the wall area and ceiling area of each room.

In order to properly model the leakage airflow due to stack-effect (which is important in winter), every façade of the buildings is divided into two horizontal strips – the flow direction may be different between the lower and upper strip. For similar reason, every window is divided into two leakage flow paths – top and bottom.

The calculation spreadsheets for air leakage distribution along the exterior air flow components are presented in Appendix A2.

Since the airflow characterization of interior components is not available in the literature, the airflow path distribution in the interface of house and garage is based on the observation made during the test (Haghighat and Megri, 1999).

4.3 Assumptions and Parameters for Simulation

The important emphasis of this study was to ensure that identical input data is used in all of the three models – COMIS, CONTAM and ESP-r, and then to check how they respond.

The attic is treated as an unheated and well-ventilated area and the ceiling is totally insulated. It is assumed that the temperature of attic zone is the same as the ambient, and that the wind pressure in the attic is zero.

The garage air temperature is treated as constant during the simulation period, using the garage mean temperature during test period. The temperature inside the house is assumed to be uniform.

The fireplaces and exhaust fans in kitchens and bathrooms were not in use during the measurements and the dampers were closed.

The house-2 has a mechanical ventilation system and the supply and return airflow rates to each zone are measured, and then used as input for the simulation. But due to inaccessibility or other reasons, it was not possible to measure the supply or return airflow in certain zones. In this case, the values are obtained by performing a simple mass balance for the zone, floor or whole house with an assumption that there is no leakage on the air distribution ducts and trunks.

Wind velocity at the building height and the value of pressure coefficient are two parameters that have impact on the determination of wind induced surface pressure. In this study, the urban area wind velocity profile is used to calculate the wind velocity at building height. The pressure coefficient used here is from the literature, Technical Note AIVC44, for a low-rise building, surrounded on all sides by obstructions equal to the height of the building (Orme et al. 1994).

4.4 Models Configuration and Simulation

There are many factors that may influence the results predicted by multi-zone models. The limitations of the models themselves, due to physical approximations, are what should be found and compared in this study. On the other hand, lack of clarity or misunderstanding of the constructions of buildings and the misusing of simulation program can also give rise to incorrect results. This type of problem is easier to rectify, once it has been identified. Because of this, model configuration – building up an airflow network according to the real building, before simulation is very important.

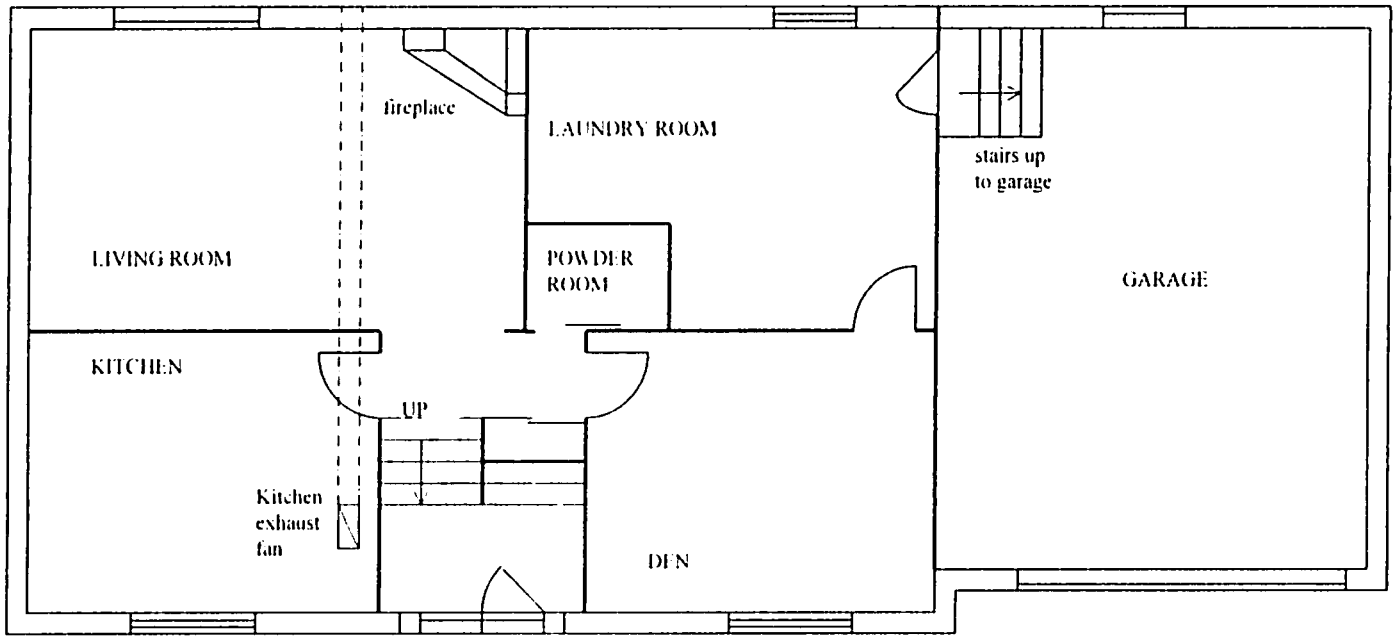

Figure 4.1 House-1 Basement Plan

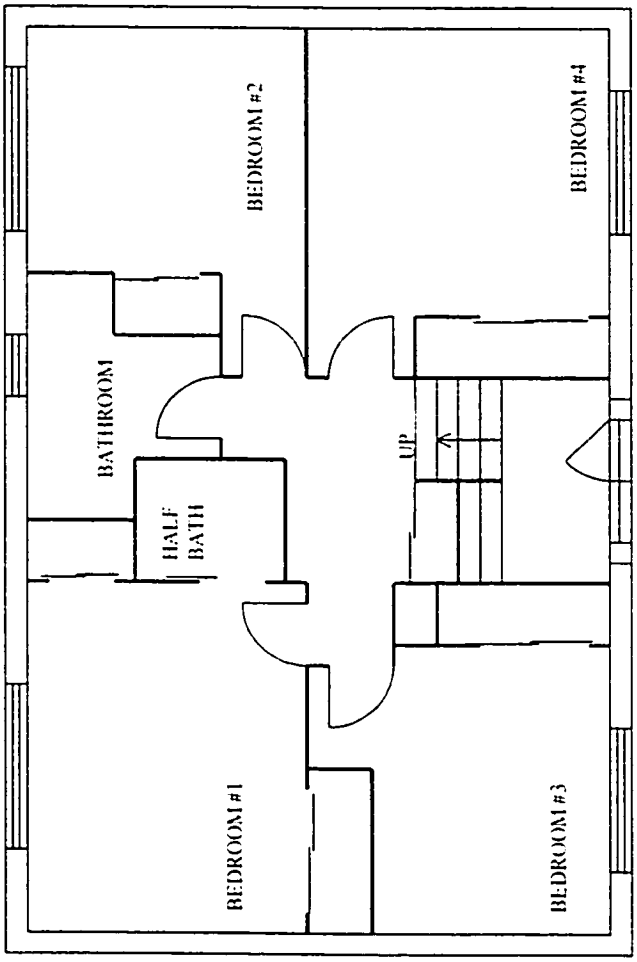

Figure 4.2 House-1 Main Floor Plan

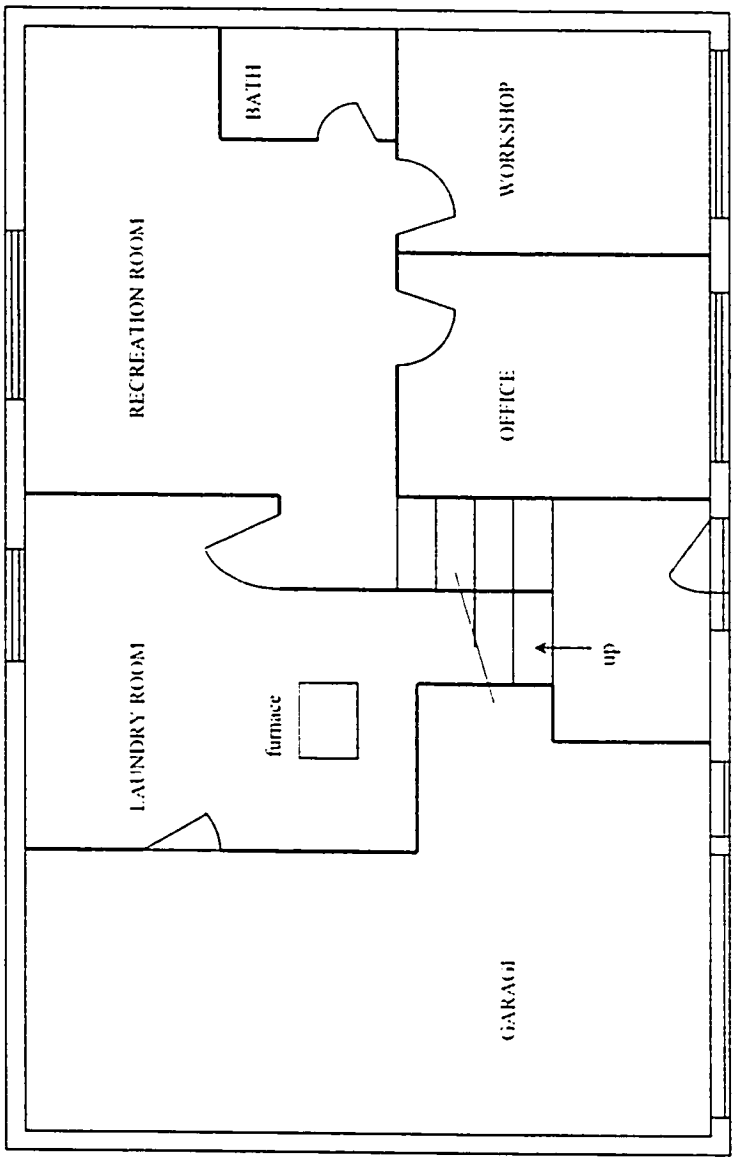

Figure 4.3 House-2 Basement Plan

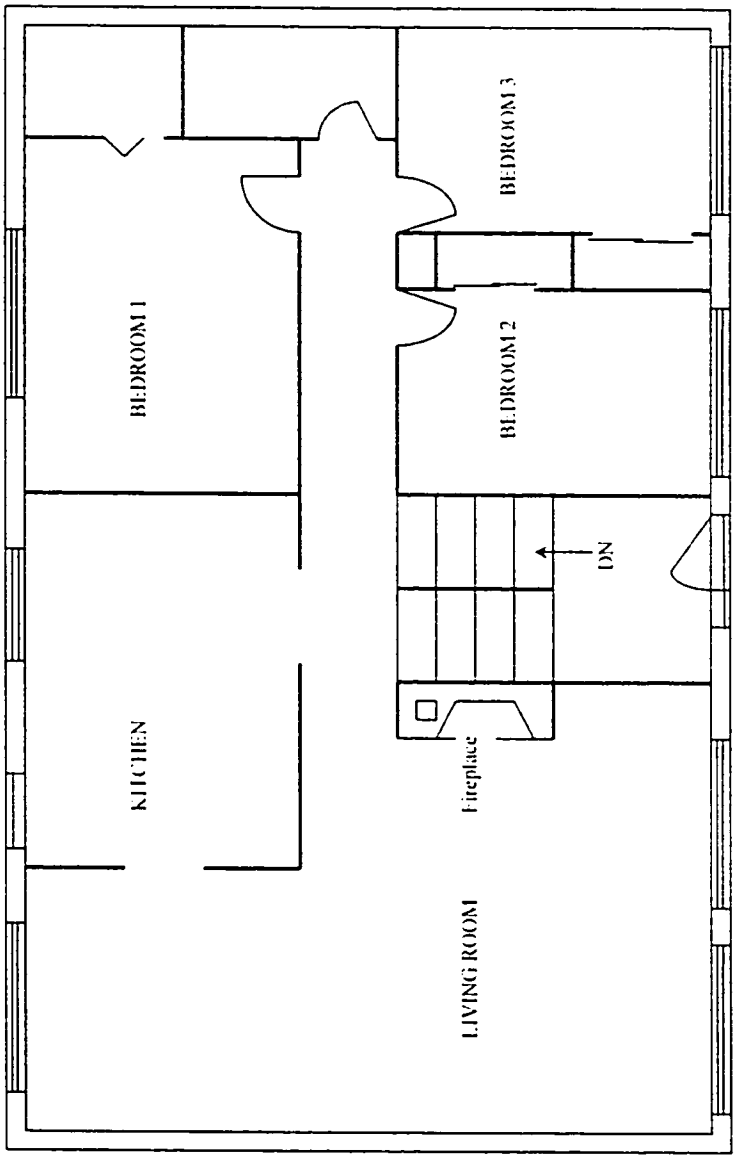

Figure 4.4 House-2 Main Floor Plan

Configuration errors may be avoided with graphical user interfaces, which allow floor plans to be drawn and leakage openings positioned correctly. By the comparison and analysis of Chapter 2, it can be seen that CONTAM has this facility (the layouts exported from CONTAM Sketchpad are shown in Appendix A3). The rough-scaled sketches of two houses are shown in Figure 4.1 to Figure 4.4.

COMIS and ESP-r are all based on text input to set up network models for building airflow. In ESP-r, the number of airflow components is limited to be less than 50, and the number of connections (airflow paths) is limited to be less than 99. In COMIS and CONTAM, there is no limitation like this.

For these two real buildings, there are a large number of airflow paths because they are calculated by air leakage distribution approach from the measured global air-tightness of house and garage. In order to handle the limitation in ESP-r, some approximations have to be made to reduce the number of airflow components (for example, to approximate two very close flow coefficient values to be one value) and remove some connections (airflow paths) with relatively very small values. So, the set of input data of ESP-r is not completely identical with that of COMIS and CONTAM, but the difference is very small.

The fireplaces in the two buildings are not in use during the measurements and the damper in each fireplace is closed. In this condition, the airflow velocity and the friction pressure losses in the chimney are very small, so the significant pressure drop in the chimney is on the damper. In order to simplify the model configuration, the fireplace is

described as a flow component from the living room to the roof of building without consideration of the friction loss in chimney. In CONTAM this can be implemented by describing some segments of ducts (represent the chimney) with zero friction loss coefficient and assuming the temperature in duct to be uniform and 20°C.

In COMIS and ESP-r, the fireplace damper can be described by a crack flow component linking the interior node of living room and the exterior node of the top of building. The height of this link influences the calculation of stack effect across the fireplace damper. Above the link, the temperature in the chimney is at outdoor temperature; below the link, it is at indoor temperature. In order to keep the same condition with CONTAM, the height of the fireplace damper has to be defined at the top of the chimney in the airflow network of COMIS and ESP-r.

For the mechanical air distribution heating system in House2, CONTAM uses a simple air handling system (AHS) to provide a means of approximating the operation of most air handling systems without going into the details of describing the duct network. AHS consists of 2 implicit airflow nodes (return and supply), 3 implicit flow paths (recirculation, outdoor, and exhaust air flow path), and multiple supply and return points in the building zones. The implicit nodes and flow paths do not appear on the SketchPad, but are represented in the AHS model of CONTAM (Walton, 1997). They are depicted in Figure 4.5.

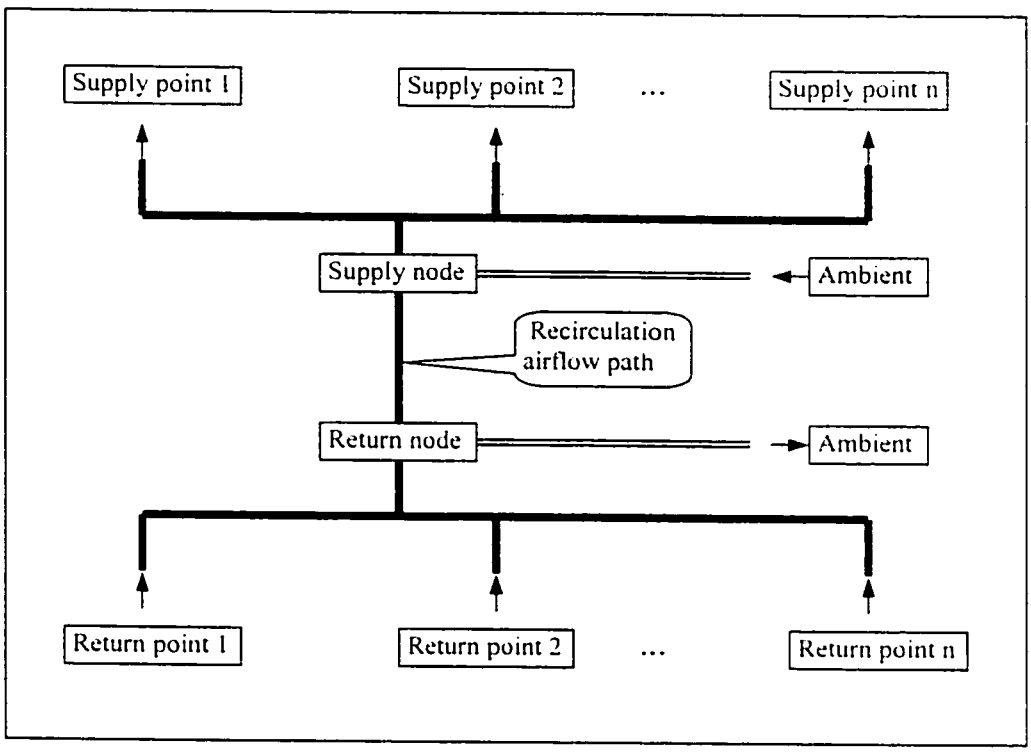

Figure 4.5 Implicit Nodes and Flow Paths for AHS in CONTAM (Walton, 1997)

In this study of house-2, there is no airflow through the outdoor air path and the exhaust air paths. The supply and return nodes are connected to every building zone by the supply and return points (measured constant airflow rates for every register). The supply node is connected with the return node by the re-circulation airflow path (measured constant airflow rate of the air handling system).

In COMIS and ESP-r the AHS airflow network is also built up based on this diagram. Because COMIS has no airflow component to describe the supply and return register

with a constant flow rate, the "Fan" component can be used by defining the fan curve slope to be zero and only one polynomial coefficient – C_0.

The purpose of the above working is to make sure that the identical networks for simulation with three models can be built up correctly. Only under this condition, the results from different models can be compared.

4.5 Comparison and Analysis

The comparisons between the predictions of COMIS, CONTAM and ESP-r and the measured pressure differences across house/garage interface for two houses are showed in Figure 4.6 and Figure 4.7. In general, there are good agreements between the predicted and measured values and the simulation results predicted by the three models are very close.

From the comparison between predictions and measurements, it can be seen that the three simulation models often over-estimated the pressure differences for two buildings. But even the biggest difference between the prediction and measurement is not out of the range of ±25%. This is acceptable and reasonable because the drive of natural ventilation is unsteady and is treated by average data, e.g. the wind pressure coefficients. The other reasons may be due to errors in measured data and parameters used for the building description.

Figure 4.6 shows that there are some differences between predictions and measurements at 8:00 AM and 9:00 AM. This is mainly due to the way that the experiment was carried out. The garage door was opened and the car was driven out and then the door was closed. This will affect the garage air temperature. In simulation, it was assumed a constant air temperature.

From the comparison between the predictions of the three simulation models, the results indicate that the sequence (from maximum to minimum) of prediction values during the measurement period for the two buildings is the same – COMIS, ESP-r, CONTAM. The differences of predicted values between ESP-r and CONTAM are smaller than that between COMIS and two others. This is due to the different approach used to convert wind velocity from meteorological station to building height. In CONTAM and ESP-r, a wind speed reduction factor (or wind speed modifier, which accounts for the difference between reported velocity and wind speed at building height) was input directly to keep the sets of input data identical. But in COMIS there is no such option. The program uses the given wind speed at the meteorological site and calculates the speed at 60m high (or higher if meteo or the building is in rough terrain and wind speed profile exponent, α, is greater than 0.34. In this condition, COMIS program calculates the height of the boundary layer). This speed at 60m (or higher) is assumed to be equal to the wind speed at the same height above the building. Along the profile near the building, the velocity at the building reference height is calculated (Feustel and Smith, 1997). Therefore, it is impossible in COMIS to get the same wind velocity at building height as that in

CONTAM and ESP-r. This resulted in different wind pressures and caused the different performance of the three models.

Another comparison conducted is about the airflow rates of every zone predicted by COMIS, CONTAM and ESP-r during the same period as the pressure difference comparison. The airflow rates are presented in Table 4.2 and Table 4.3 for House-1 and House-2 respectively. From the comparison, the good agreement can be seen and the relative differences are bigger in House-1 than that in House-2. That is because there is a constant airflow rate (air supply and return of mechanical heating system) in every zone of House-2. Therefore the airflow rates are much higher than the natural ventilated House-1.

These results also show that the approximation made in the ESP-r simulation did not significantly impact the predictions. This means that the small difference of airflow network description will not induce big discrepancy in results. From this, one can conclude that locating and sizing the airflow components with relative bigger values (for example the observed house air leakage paths) should be considered more carefully than the general background leakage (see section 2.2.2), because these elements influent the simulation results very much.

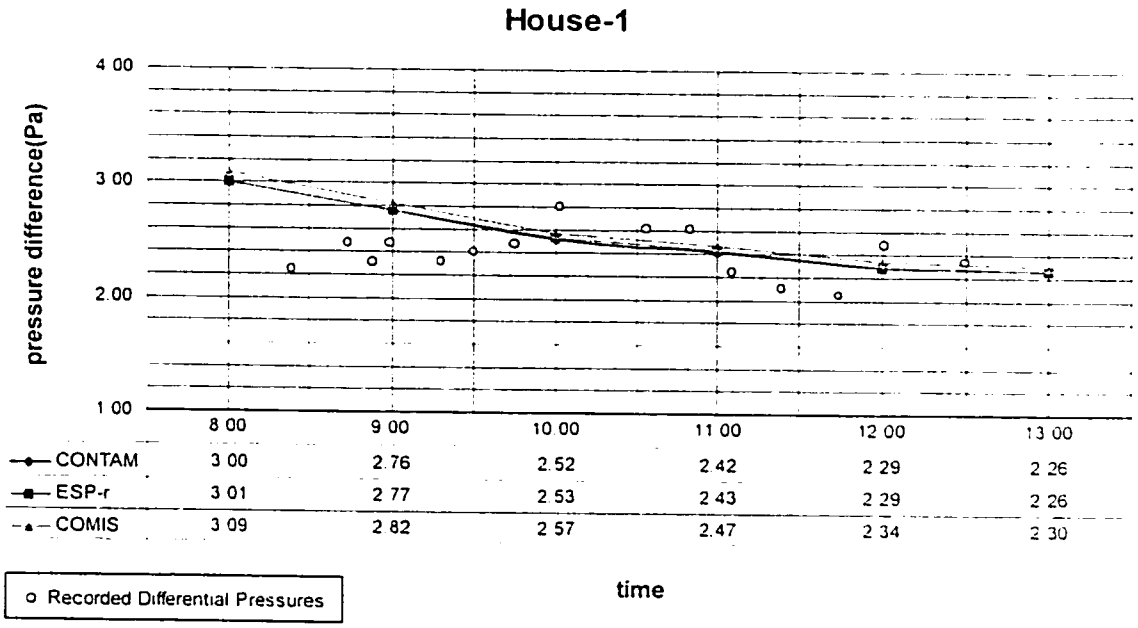

Figure 4.6 Measured and Predicted Differential Pressure across Garage-House Interface of House-1

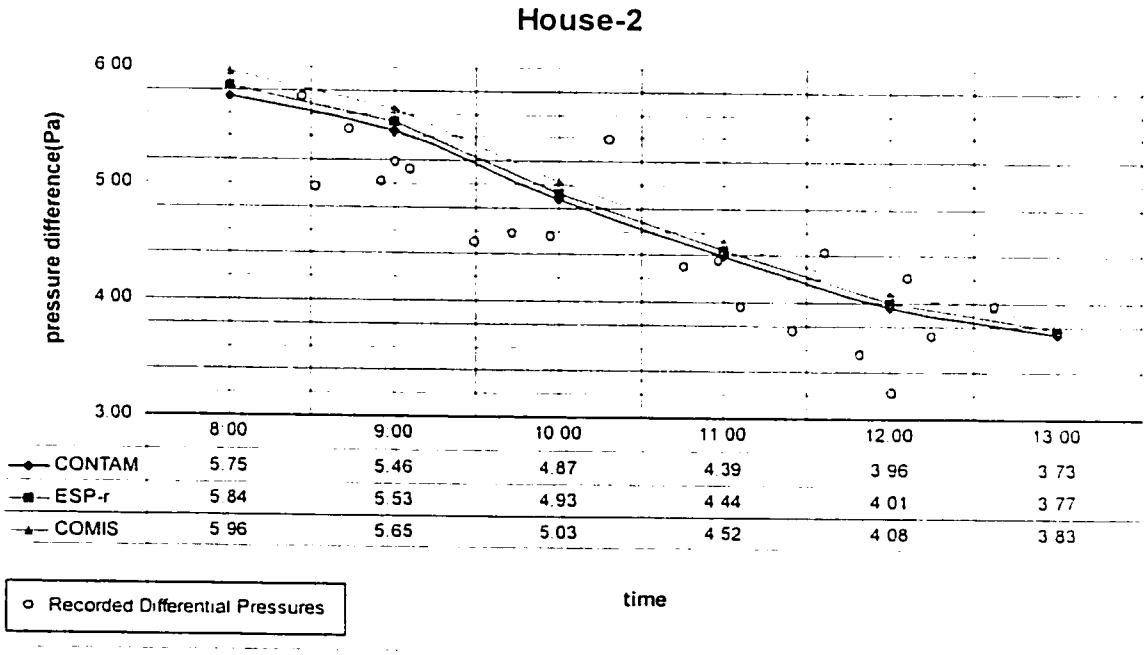

Figure 4.7 Measured and Predicted Differential Pressure across Garage-House Interface of House-2

	8:00	9:00	10:00	11:00	12:00	13:00	
Living Room	145.2	140.8	132.3	127.1	119.3	119.8	COMIS
	138.7	133.3	125.4	121.1	114.8	114.7	CONTAM
	143.0	138.1	129.7	125.0	117.9	118.0	ESP-r
Laundry Room	49.7	48.2	45.3	44.1	42.6	42.1	COMIS
	51.2	49.4	46.4	45.1	43.4	43.0	CONTAM
	51.9	50.0	46.7	45.4	43.6	43.1	ESP-r
Kitchen	41.5	40.0	37.5	36.4	34.9	34.6	COMIS
	42.2	40.3	37.7	36.6	35.1	34.8	CONTAM
	43.2	41.3	38.5	37.2	35.5	35.2	ESP-r
DEN	63.7	61.1	57.3	55.8	53.7	53.1	COMIS
	65.4	62.6	58.6	56.9	54.6	54.1	CONTAM
	66.4	63.4	59.0	57.3	54.9	54.4	ESP-r
Entrance	132.6	127.2	119.8	115.9	110.3	109.9	COMIS
	129.1	123.5	116.0	112.4	107.5	106.9	CONTAM
	132.3	126.9	118.4	115.2	109.5	109.1	ESP-r
Garage	60.9	48.9	21.4	24.7	41.9	44.3	COMIS
	62.5	48.8	21.1	24.6	42.3	44.7	CONTAM
	63.0	48.8	20.5	25.6	43.0	45.3	ESP-r
Bedroom 1	6.9	7.1	6.5	6.2	5.7	5.8	COMIS
	6.5	6.2	5.8	5.6	5.3	5.3	CONTAM
	6.6	6.7	6.3	5.9	5.5	5.5	ESP-r
Bedroom 2	5.7	5.6	5.2	5.1	5.0	4.9	COMIS
	5.6	5.5	5.1	5.0	4.9	4.7	CONTAM
	5.7	5.6	5.2	5.1	4.9	4.8	ESP-r
Bedroom 3	6.2	5.6	5.2	5.0	4.6	4.6	COMIS
	5.7	5.0	4.6	4.5	4.2	4.2	CONTAM
	5.8	5.3	5.0	4.7	4.4	4.4	ESP-r
Bedroom 4	3.9	3.4	3.2	3.2	3.2	3.1	COMIS
	3.7	3.5	3.1	3.0	3.0	2.9	CONTAM
	3.8	3.4	3.1	3.0	3.2	2.9	ESP-r
Bath Room	10.0	8.6	8.1	8.6	9.4	8.6	COMIS
	12.6	11.6	10.6	10.6	10.8	10.3	CONTAM
	12.6	11.4	9.9	10.4	10.3	10.1	ESP-r

Table 4.2 Predicted Airflow Rates for Each Zone in House-1

	8:00	9:00	10:00	11:00	12:00	13:00	
Office	93.6	93.5	93.2	92.9	92.6	92.5	COMIS
	95.3	95.1	94.7	94.3	94.0	93.8	CONTAM
	94.3	94.0	93.6	93.2	92.8	92.7	ESP-r
Workshop	101.1	100.8	100.2	99.6	99.2	99.0	COMIS
	103.1	102.7	101.9	101.3	100.8	100.5	CONTAM
	99.4	99.0	98.4	97.9	97.5	97.3	ESP-r
Half Bath	23.5	23.4	23.2	23.1	23.0	22.9	COMIS
	23.9	23.8	23.5	23.4	23.2	23.2	CONTAM
	23.7	23.6	23.4	23.2	23.1	23.0	ESP-r
Recreation	335.2	334.5	332.5	330.8	329.3	328.6	COMIS
	341.4	340.3	337.8	335.9	334.2	333.3	CONTAM
	332.9	331.7	329.6	327.9	326.4	325.6	ESP-r
Laundry	29.5	28.2	25.4	23.1	21.0	19.8	COMIS
	31.0	29.7	26.8	24.3	22.1	20.9	CONTAM
	31.3	29.7	26.9	24.4	22.2	20.9	ESP-r
Garage	30.3	28.7	25.3	22.6	20.3	19.0	COMIS
	32.1	30.3	26.7	23.8	21.4	20.1	CONTAM
	31.8	29.3	26.4	23.8	21.4	20.0	ESP-r
Entrance	562.2	560.6	556.6	553.1	550.5	549.5	COMIS
	569.9	567.8	563.3	559.8	556.9	555.5	CONTAM
	560.9	559.5	554.4	550.9	548.0	546.7	ESP-r
Bedroom 2	20.2	20.2	20.0	19.9	19.7	19.7	COMIS
	20.5	20.4	20.3	20.1	20.0	19.9	CONTAM
	19.5	19.8	19.1	19.0	18.9	18.9	ESP-r
Bedroom 3	44.4	44.3	43.9	43.6	43.3	43.3	COMIS
	45.1	44.9	44.5	44.1	43.9	43.8	CONTAM
	43.9	43.8	43.3	43.0	42.8	42.7	ESP-r
Bedroom 1	123.4	123.2	122.9	122.5	122.1	121.9	COMIS
	125.0	124.8	124.4	124.1	123.8	123.5	CONTAM
	123.7	123.7	123.1	122.7	122.3	122.0	ESP-r
Bath Room	108.2	108.2	108.2	108.1	108.0	108.1	COMIS
	110.0	109.9	109.7	109.6	109.5	109.5	CONTAM
	106.6	106.6	106.6	106.6	106.6	106.6	ESP-r
Walk-in Closet	48.5	48.4	48.3	48.1	48.0	48.0	COMIS
	49.2	49.1	48.9	48.7	48.6	48.5	CONTAM
	48.8	48.6	48.5	48.3	48.1	48.1	ESP-r
Kitchen	210.3	209.4	207.2	205.3	203.7	202.9	COMIS
	212.8	211.7	209.4	207.6	205.8	204.9	CONTAM
	209.5	208.5	205.9	204.0	202.3	201.4	ESP-r
Living Room	772.5	771.1	767.1	763.4	760.4	759.0	COMIS
	781.5	779.4	775.0	771.3	768.0	766.3	CONTAM
	772.5	770.6	765.6	761.8	758.5	756.8	ESP-r

Table 4.3 Predicted Airflow Rates for Each Zone in House-2

CHAPTER 5

Predicting the Indoor Air Contaminants Dispersion

A further study was carried out to predict the indoor air contaminant dispersion in the same houses. Carbon monoxide and acetylene are the results of morning vehicle coldstart exhaust emission in the garage. The predictions of contaminant concentration are based on the results of airflow simulation.

5.1 Indoor Pollutants Transport Models

In parallel with the development of the multi-zone airflow models, multi-zone pollutants transport models defining the mass balance of each pollutant in each zone of a multi-zone building were developed. The main assumption is that the pollutant is transported by the airflow from one zone to another zone and instantaneous perfect mixing occurs within each zone. COMIS and CONTAM use similar equations to describe this mass balance. ESP-r does not have contaminant transport module yet, so the simulations were carried out only by COMIS and CONTAM.

Contaminant dispersal analysis requires additional information, including the initial concentration specified in each zone, contaminant source strength, contaminant removal rate from indoor sink, filter efficiency, and outdoor contaminant concentration. In COMIS, there is only a constant coefficient model (constant generation or sink rate). In

CONTAM, there are several models for describing contaminant source and sink element. These models include "Constant Coefficient", "Pressure Driven", "Cutoff Concentration", "Decaying Source", "Boundary Layer Diffusion Controlled", and "Burst Source". Additionally, a kinetic reaction effect (modeled as first-order exponential functions between contaminants) is also included for each zone in CONTAM to account for the chemical reaction influence. (Walton, 1997)

In COMIS, one zone can be divided vertically into several sub-zones (zone layers) by horizontal partition. Sub-zones can be used to account for different sources, sinks and temperature in different heights of a zone (e.g. shafts, staircases and atria). In CONTAM, a "Phantom" zone is used to indicate that there is no floor below the enclosed region on a given level. That is, the region on this level is actually part of the zone below and has the same temperature and contaminant concentration. Therefore, if it is necessary to have different temperature or contaminant concentrations at the different levels in a big zone, these levels must be modeled as individual zones connected by horizontal large openings.

The steps that COMIS and CONTAM follow to calculate the contaminant concentration are as follows: they first calculate the pressure difference across each flow path by iteration method. After the solution converged, they use the pressure difference to calculate the airflow in and out of each zone. Then these airflow rates are used to estimate the contaminant concentration.

Time step is the period between events during a transient simulation. Simulations are performed for a time period defined by a start and stop time provided by the user. Airflow is a quasi-steady-state phenomenon and can be assumed to be steady state but pollutant transport and the related contaminant concentration variation are dynamic physical phenomena. Therefore, it is critical to use a time step short enough to represent the dynamic effect.

COMIS works with two different time steps, one for the airflow calculation and another for calculation of pollutant transport. The time step for airflow is determined by the change of boundary conditions with time, i.e. weather data, fan schedule, etc. In order to use a time step short enough to represent the dynamics, COMIS calculates the time step for contaminant transport as a function of the shortest time constant of all zones considered (Feustel, 1999). The user can not set it.

In CONTAM, the same simulation time step is used for both transient airflow and contaminant simulation and it is set by the user. If the period of time steps of weather file is longer than that of the simulation time step, the weather data for every simulation time step will be computed by linear interpolation between two steps in the weather file.

5.2 Data and Parameters for Simulations

The focus of this study is to predict the spatial distribution of contaminant concentration in the garage and room adjacent to it. The basic constant coefficient source model is used

in this study. The contaminants of interest in this study are acetylene and carbon monoxide from the car exhaust. Table 5.1 gives the emission rates of these contaminants, used as input data for simulation (Haghighat and Megri, 1999).

House	Acetylene (mg/s)	CO(g/s)
House-1	0.027625	0.0054236
House-2	0.030097	0.0057864

Table 5.1 Pollutant Emission Rate of Car Cold-Start

Some assumptions are made for simulation: contaminant removal rates from indoor sinks are zero; initial concentrations in each zone are zero; all filter efficiencies are zero; and outdoor contaminant concentrations are zero. The volume of the garage is assumed to be represented by the gross volume of the garage, into which the contaminant is released, ignoring the volume of the car.

The cold-start contaminant distributions were simulated for the same specific days as the airflow simulations of the two houses. Therefore, the input files for airflow simulations were used, some data for the contaminant sources and source schedules were added, and the time steps for transient contaminant simulations were changed. The cold-start emission was performed according to the following assumed procedure, the car exhaust emission in house-1 started at 8:00am, stopped at 8:01am, in house-2 started at 8:21am, stopped at 8:22am.

5.3 Simulation Results and Analysis

There has been good agreement between the predicted pressure drop and the measured data (see Chapter4). COMIS and CONTAM use the airflow to estimate the contaminant concentration, therefore, one expects that, in general, there should be good prediction of contaminant concentration.

The concentrations of acetylene and carbon monoxide in the garage and laundry room of house-1 and house-2 predicted by COMIS and CONTAM are presented on Figure 5.1 to Figure 5.4.

Comparisons and analysis of these predictions were carried out on the following subjects:

- Comparison between the garage and laundry room

The figures indicate that the peak concentrations in the laundry rooms are much less than the peak concentrations in the garage and the time delays between the peak values in the garages and the laundry rooms are about one and half hour.

- Comparison between COMIS and CONTAM

Comparing between Figure 5.1 and Figure 5.2, it can be found that the concentration values in the garage and the laundry room of house-1 predicted by COMIS are about 5%-10% different from that predicted by CONTAM. This is because the airflow rates of the garage and laundry room calculated by COMIS are different from that by CONTAM (see

Table 4.2 and 4.3, the airflow rates in laundry). Similar results can be found from the comparison between Figure5.3 and Figure5.4.

From the careful comparison between Figure5.1 and Figure5.2, another phenomenon can be found that the concentration in the garage predicted by COMIS is not always higher than that predicted by CONTAM during the simulation period. The reason is that COMIS uses two time steps, but CONTAM uses one, for both transient airflow and contaminant simulations (see section 5.1). In this case, the time step for airflow simulation in COMIS is **one hour**, which is scheduled by the time step of weather data. In CONTAM, the time step for airflow and contaminant simulation is set to be **ten seconds** in order to satisfy the contaminant simulation (the time step must be less than the time period of contaminant emission). At the time between two time steps of weather data, CONTAM uses the weather data calculated with the linear interpolation to do airflow simulation.

For example, at the time 9:30am of the specific day, the airflow rate for concentration calculation in COMIS is the same as that at 9:00am, because it uses the time step of one hour that is scheduled in the weather file. Therefore, the airflow rate is constant from 9:00am until the next time step, 10:00am. CONTAM calculates the airflow rate at 9:30am by using the weather data computed with the linear interpolation of the weather data at 9:00am and 10:00am. If the value (e.g. temperature or wind speed) of weather data increases from 9:00am to 10:00am, the calculated value of weather data at 9:30am will be higher than at 9:00am. If the value of weather data decreases from 9:00am to 10:00am, the calculated value of weather data at 9:30am will be lower than at 9:00am.

This calculated weather data makes the difference of airflow calculations, which induce the different concentrations predicted by COMIS and CONTAM at the time between two time steps of weather file.

Therefore, the variation of value from one time step to another in weather data will impact on the difference between contaminant concentrations predicted by COMIS and CONTAM.

- Comparison between house-1 and house-2

From the figures, it can been seen that in house-1, the peak concentration in the laundry room is approximately **ten times** less than the peak concentration in the garage. In house-2, the peak concentration in the laundry room is approximately **two and half times** less than the peak concentration in the garage. This is a big difference. The reason is the different air-tightness of the common wall between the garage and house in house-1 and house2 (See Table 4.1) (House-1, k = 1.54 (L/s Pa), n = 0.68; house-2, k = 2.12 (L/s Pa), n = 0.82). This indicates that the garage/house interface wall in house-2 is leakier than that in house-1. The tight wall could minimize the indoor air pollutant concentration in the laundry room much more than the leaky wall. Therefore, these simulation results predict that the leakage of garage/house interface wall has big impact on the indoor air contaminant dispersion in the houses.

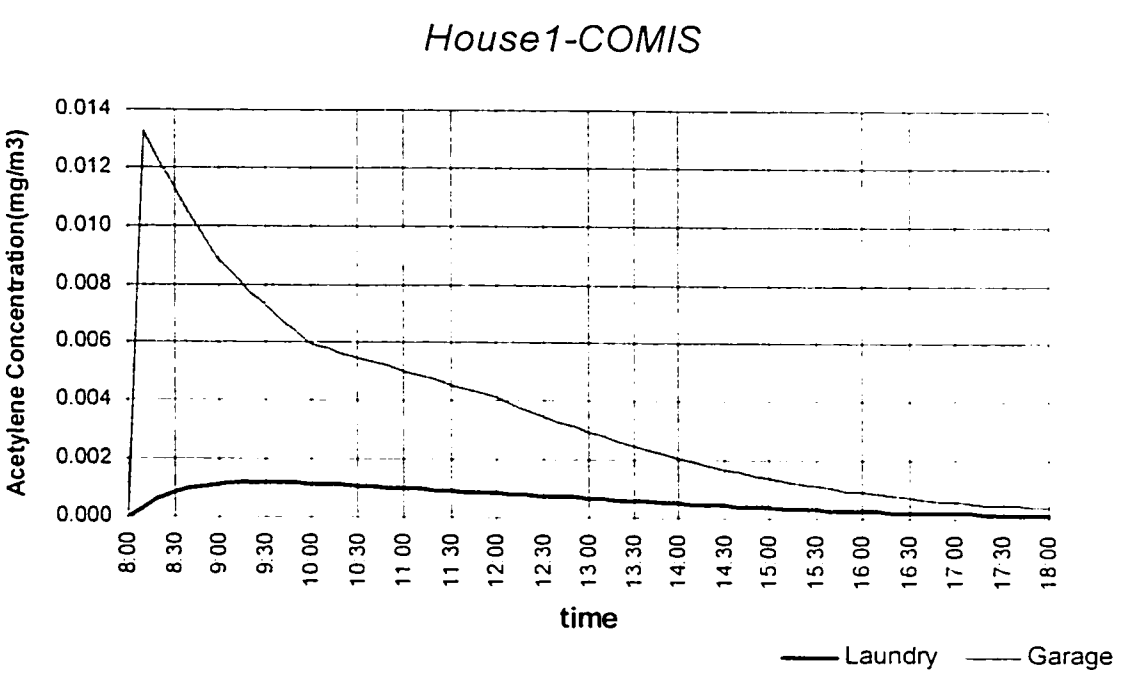

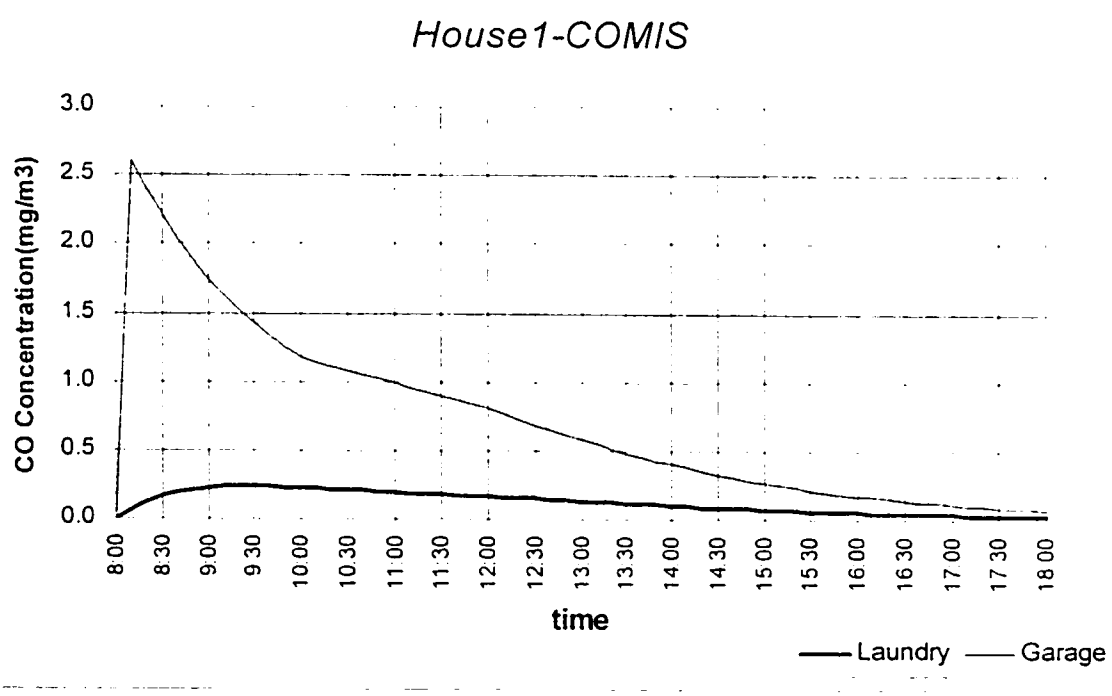

Figure 5.1 House-1 Concentration in Garage and Laundry Room Predicted by COMIS

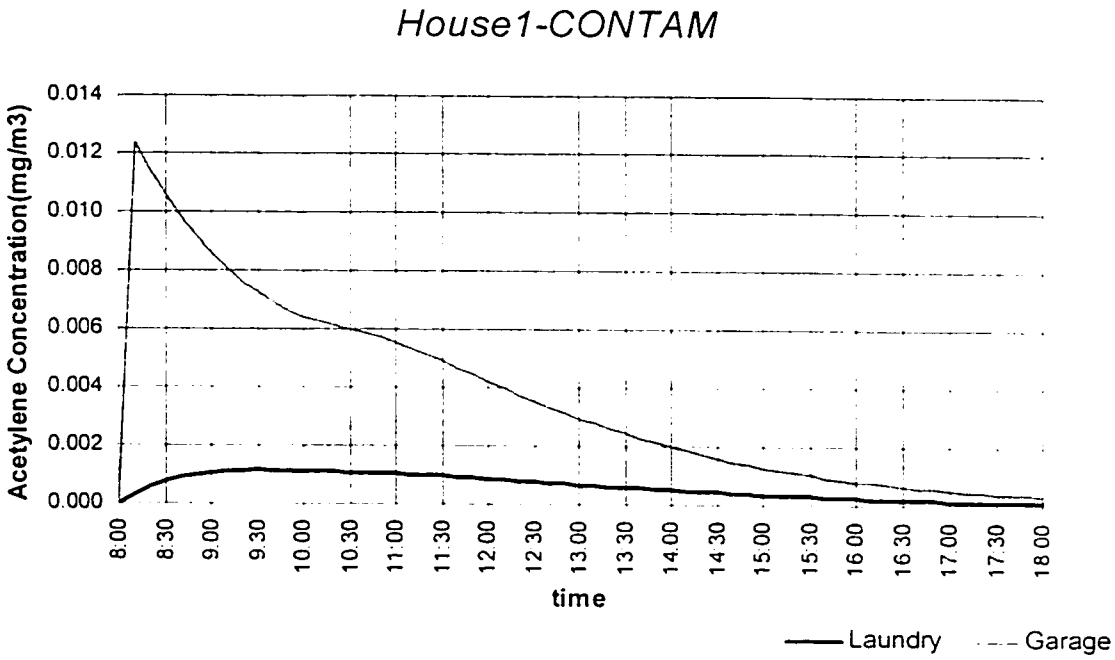

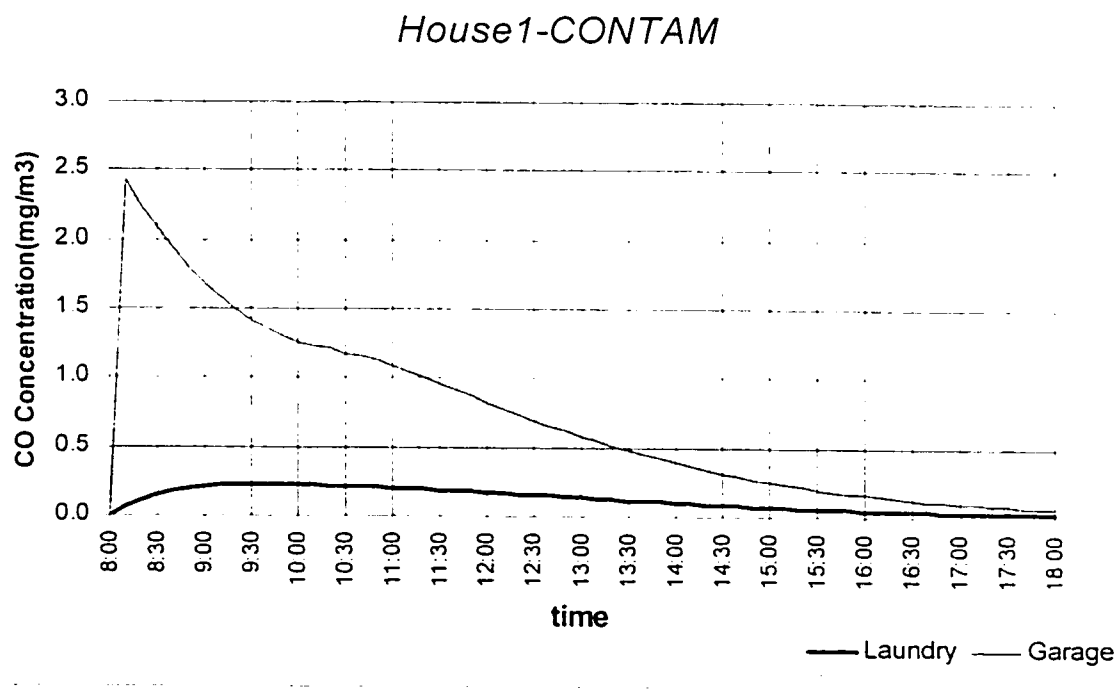

Figure 5.2 House-1 Concentration in Garage and Laundry Room Predicted by CONTAM

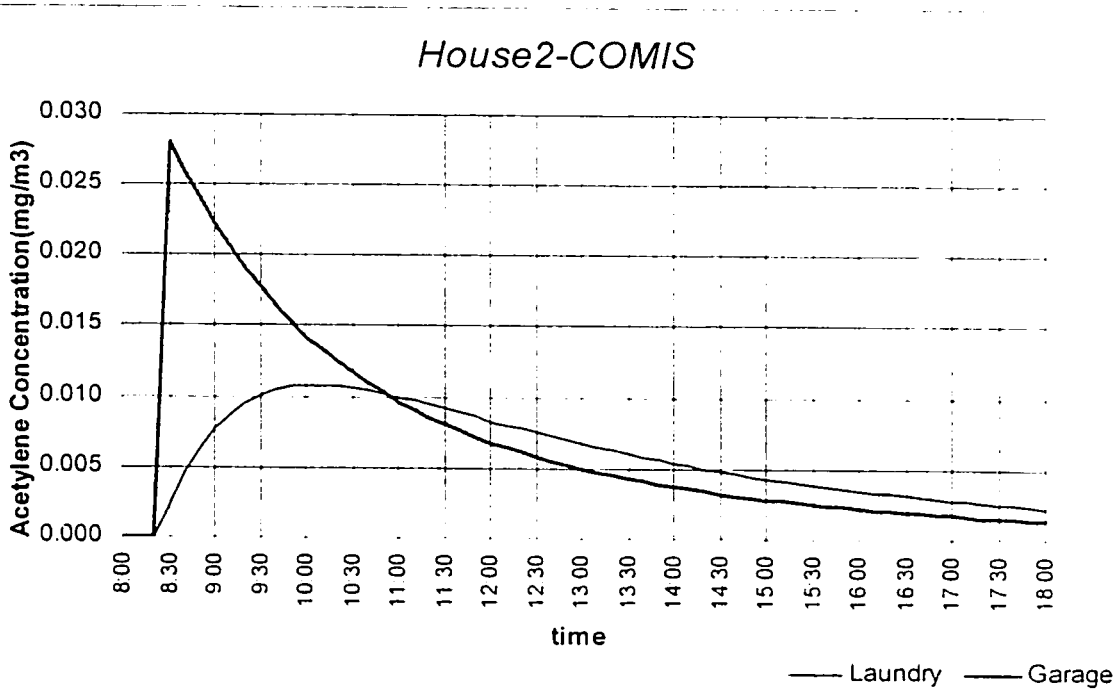

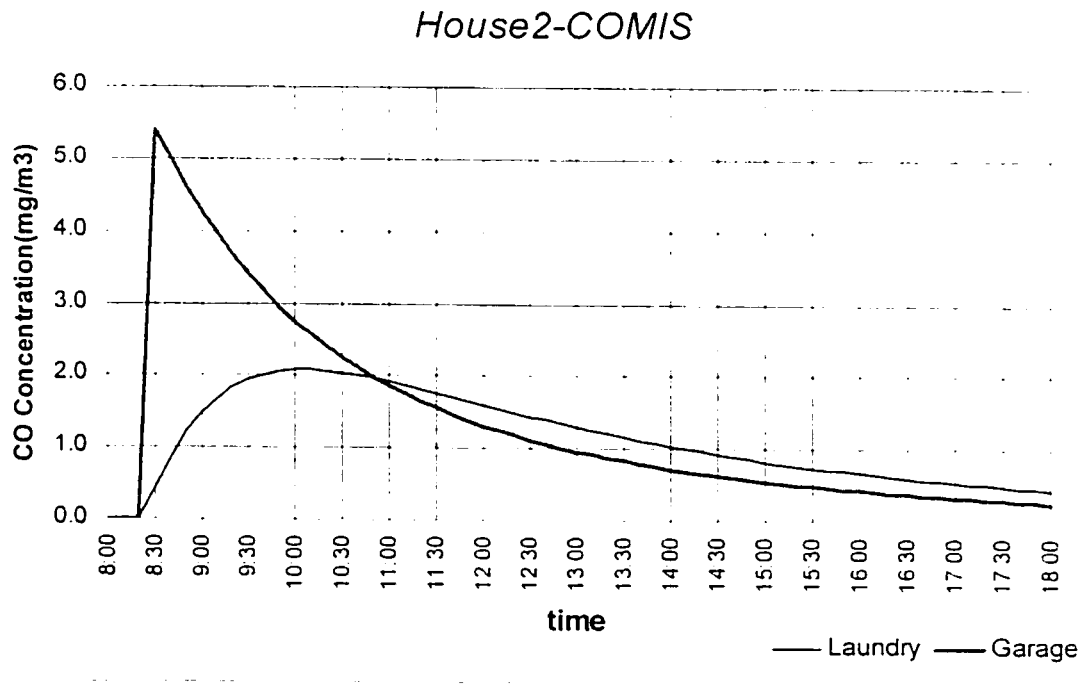

Figure 5.3 House-2 Concentration in Garage and Laundry Room Predicted by COMIS

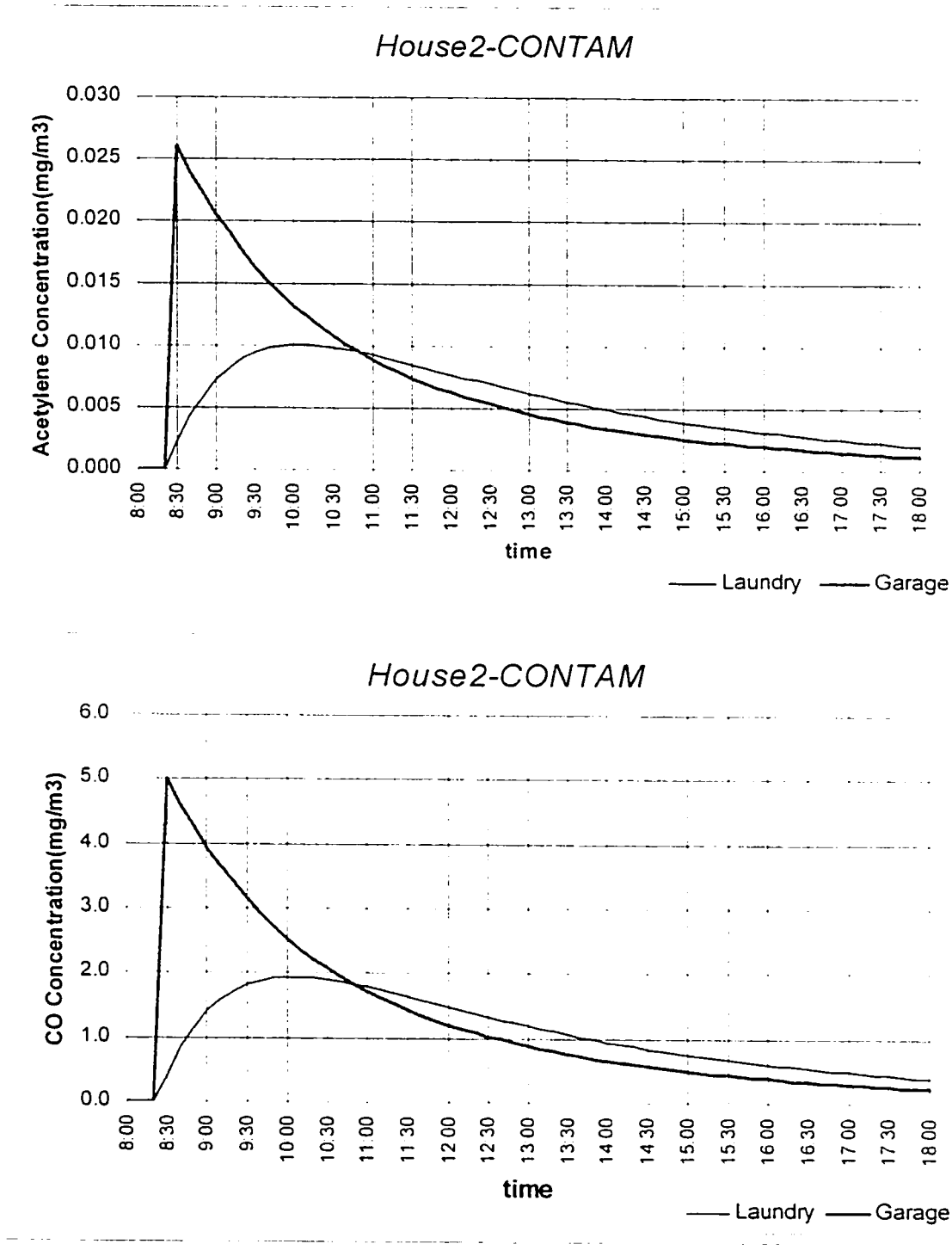

Figure 5.4 House-2 Concentration in Garage and Laundry Room Predicted by CONTAM

5.4 Air Contaminant Concentration Predicted by Two-zone Approach

In the case of the multi-zone approach, the building is modelled considering each room in the building as a single control volume and the stairway shaft as an additional control volume. In this section, two-zone simulationis used where each house is modelled as being comprised of two zones namely the garage and the house. The additional assumption here is that the air flows freely between all the rooms and the air contaminants are completely mixed instantaneously.

Good agreement between the prediction of the two-zone and the multi-zone approach for the pressure drop between the house and garage is expected, since the interior doors, in multi-zone case, modelled in Chapter4 as large openings, and the simulation results verified that the pressure difference between zones is very small.

Two-zone approach simulations are based on the configuration of the buildings in multi-zone simulations, just to remove the interior walls in the houses. The results of pressure drop between the garage and the house are the same as the predictions in chapter4. Therefore, the impact of the two-zone approach on the contaminant concentration predictions can be evaluated. Figure 5.5 to Figure 5.8 show the carbon monoxide and acetylene concentrations in the garages and houses predicted by COMIS and CONTAM.

From comparing Figure 5.1 and Figure 5.5 (COMIS results), it can be seen that for the garage, CO and acetylene concentration levels and variations predicted by the two-zone

approach is the same as that by the multi-zone approach. But, the concentrations in the house predicted by the two-zone approach are much lower than by the multi-zone approach and the time of peak values in the house (two-zone approach) is about one and half hour later than in the laundry room (multi-zone approach). The reason is that in the two-zone approach, the contaminant concentration level in the house is calculated based on the total volume of the house, and not based on the volume of the laundry room, which is used by the multi-zone approach.

The same results can be found from the comparison of Figure 5.2 and Figure 5.6 (CONTAM results), and from the comparison of Figure 5.3 and Figure 5.7, Figure 5.4 and Figure 5.8 (house-2).

From these comparisons of simulation predictions, it can be concluded that the impact of considering the buildings as two-zone (garage and house) or multi-zone on the indoor air contaminant concentration predictions is very big and there are good agreements between COMIS and CONTAM predictions.

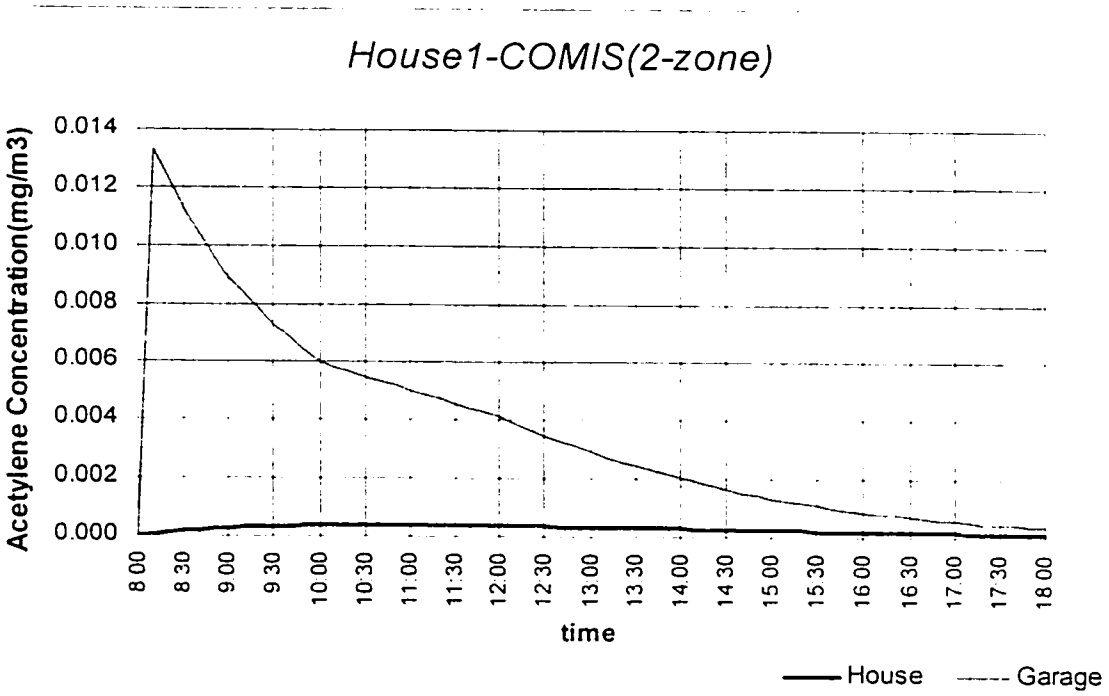

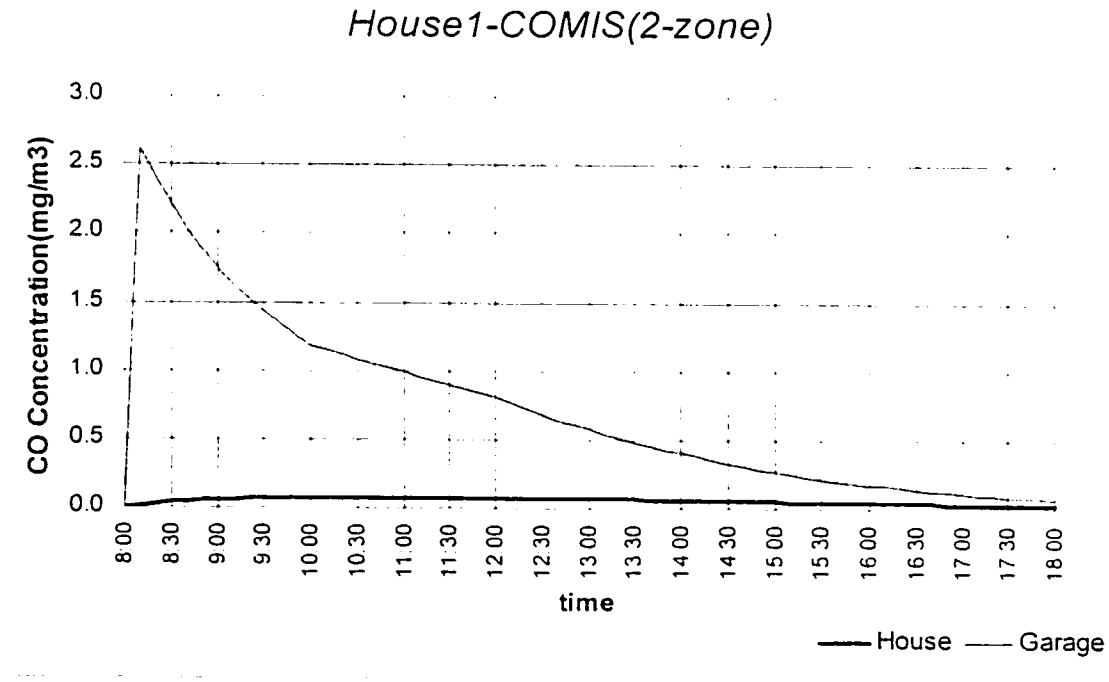

Figure 5.5 House-1 Concentration in Garage and House Predicted by COMIS (two-zone approach)

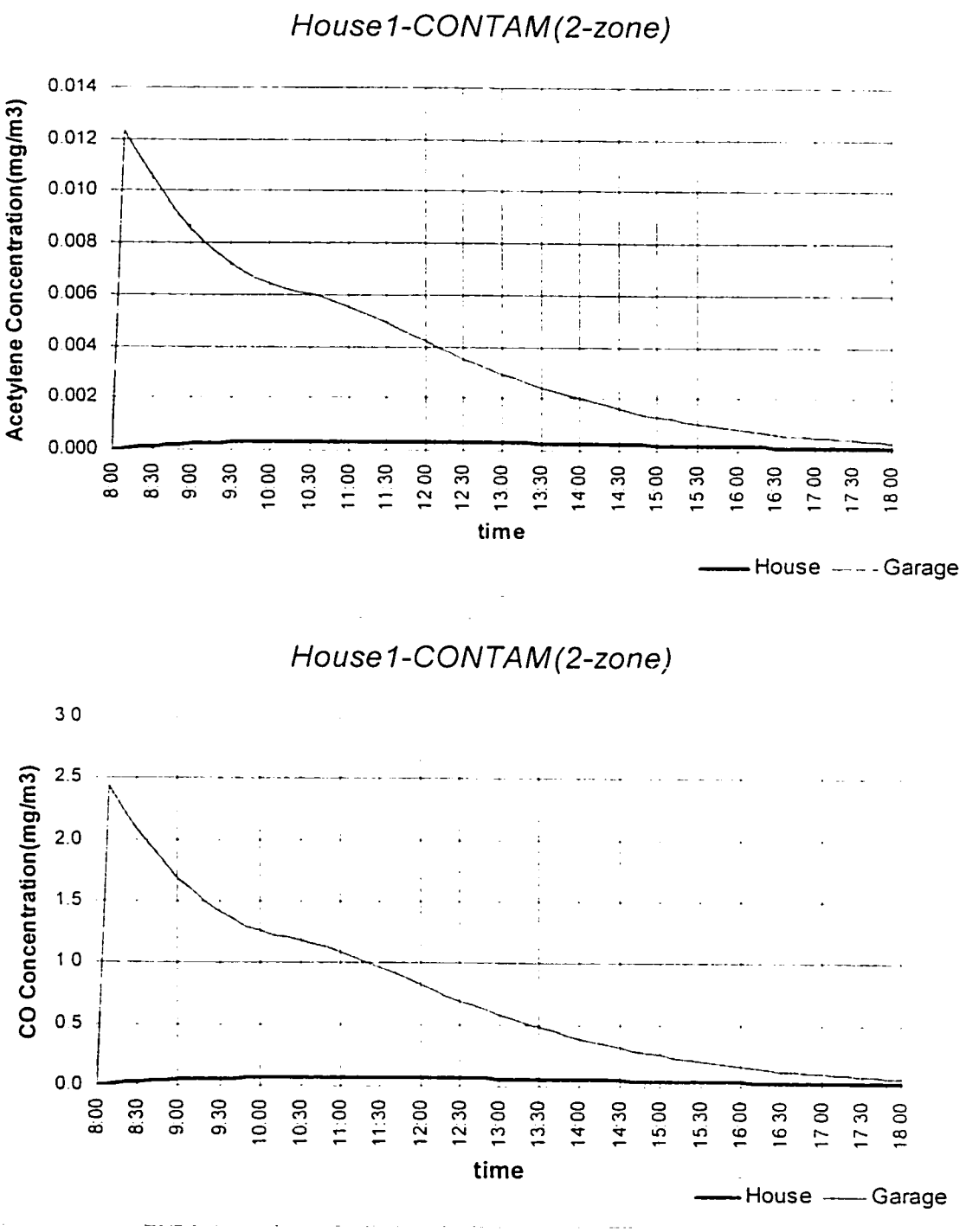

Figure 5.6 House-1 Concentration in Garage and House Predicted by CONTAM (two-zone approach)

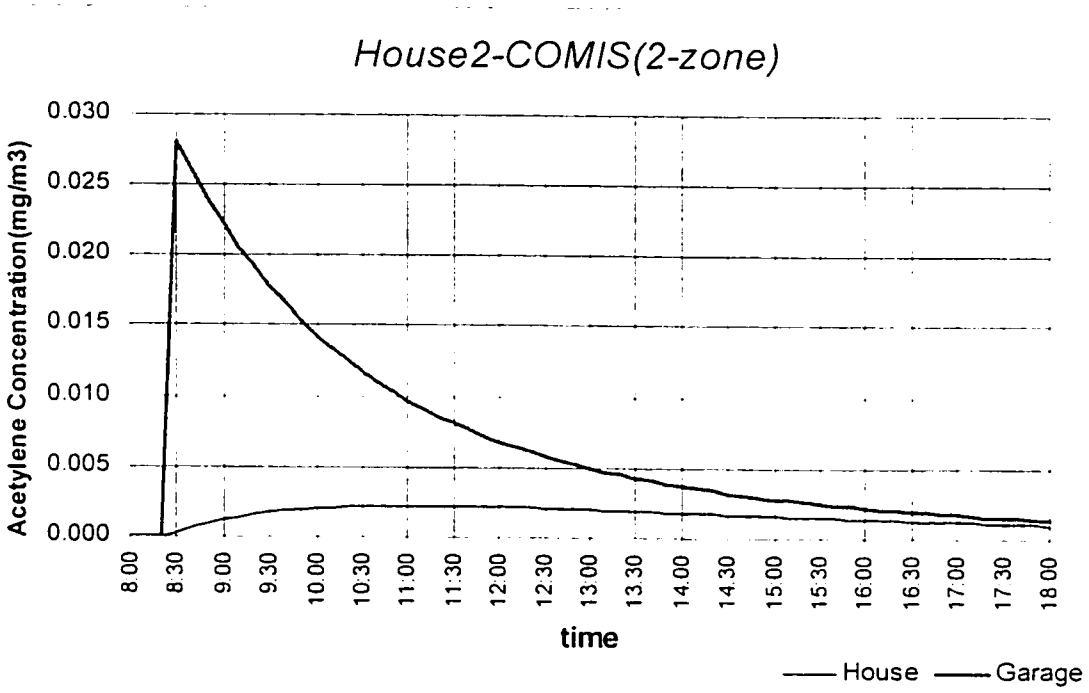

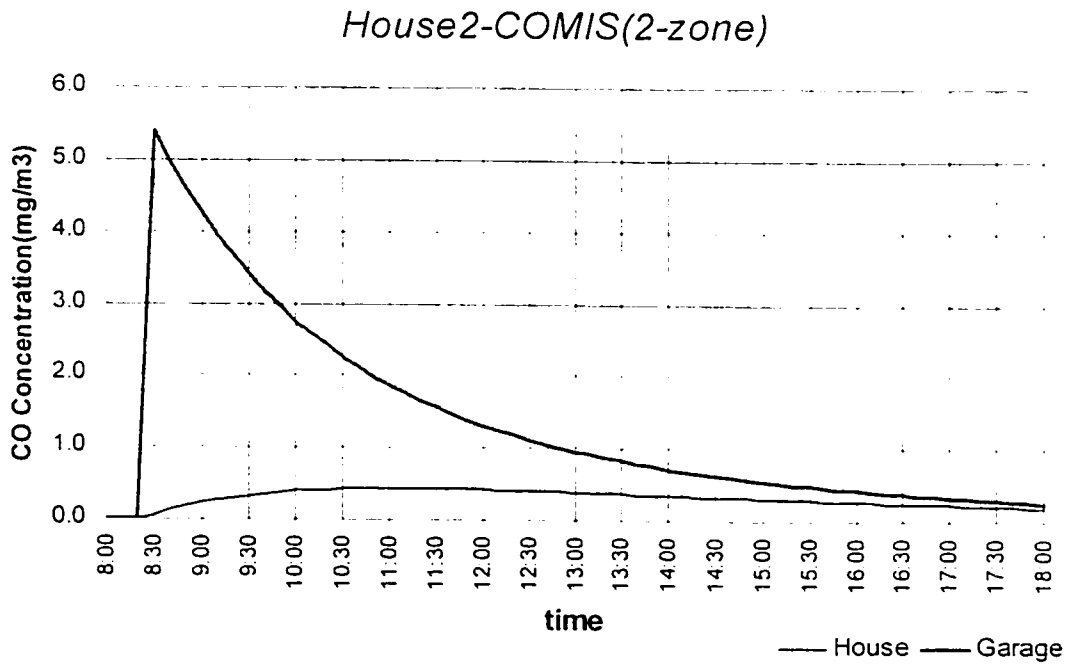

Figure 5.7 House-2 Concentration in Garage and House Predicted by COMIS (two-zone approach)

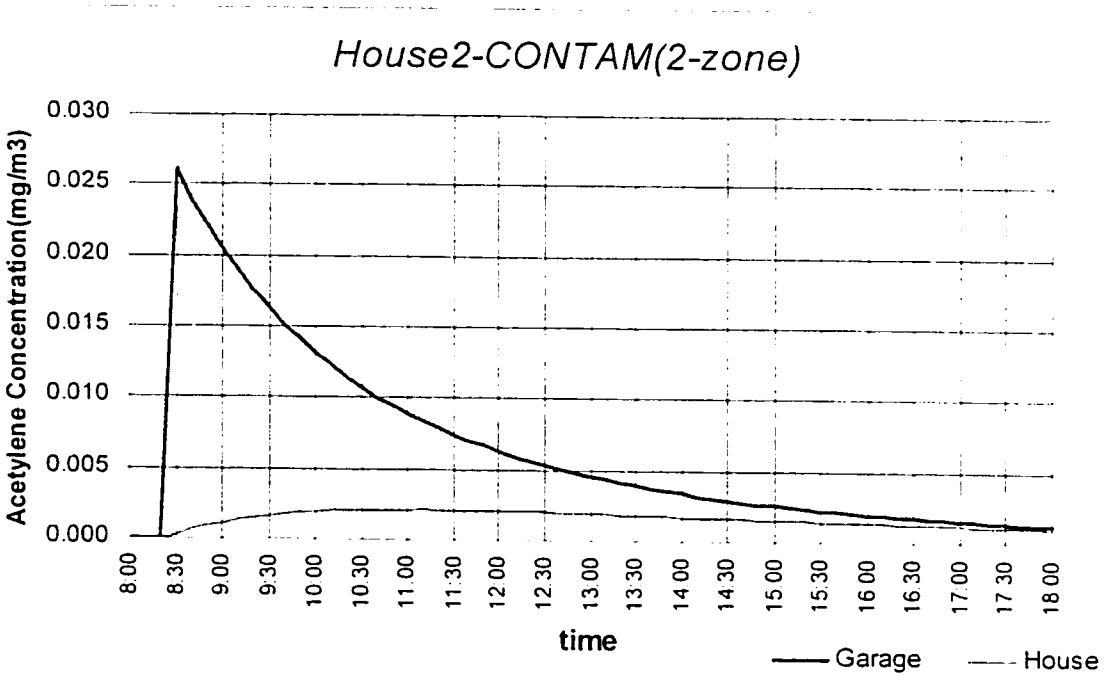

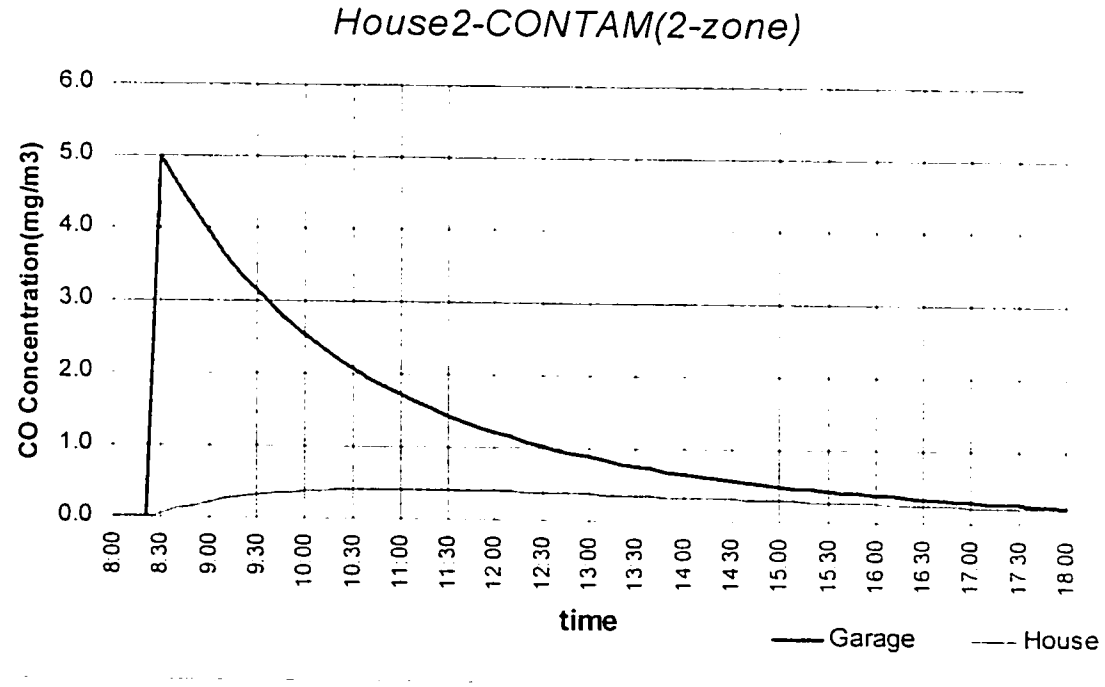

Figure 5.8 House-2 Concentration in Garage and House Predicted by CONTAM (two-zone approach)

CHAPTER 6

Conclusions and Future Works

6.1 Conclusions

In general, similar principles are used in the three multi-zone airflow models, COMIS, CONTAM and ESP-r, to describe various airflow/pressure relationships including the definitions for driving forces (wind pressure, thermal buoyancy and the mechanical ventilation systems) and airflow elements, and similar algorithms are used to solve the non-linear equations. Furthermore, two of the models, COMIS and CONTAM, are capable of computing the contaminant concentrations in building, but ESP-r does not have this kind of module to calculate the contaminant transport.

In this validation study, the three models' predictions were compared with two sets of experimental data, one was collected from a controlled environment test under both summer and winter conditions, and the other one was from field measurements of two single-family houses.

The results of the first validation show that there are significant differences between predicted and measured airflow rates from one zone to another, and even for the total airflow rates in each zone. This is acceptable because they agree with the experimental evaluation of COMIS presented in the final report of COMIS evaluation (Furbringer et al,

1996). However, there is good agreement between the predictions made by COMIS, CONTAM and ESP-r.

In the second validation, a method was developed first to distribute the global air leakage characteristics of the whole house with the garage through cracks and gaps on exterior walls and roof. From the comparisons it can be seen that there are good agreement between the predictions and experiments, as well as between the three models. Therefore, it can be concluded that the methodology for air leakage distribution is correct, and the performances of COMIS, CONTAM and ESP-r for predicting airflow rates in singl-family house are similar.

Then another study was carried out by using COMIS and CONTAM to predict contaminant concentration in the house and garage caused by morning vehicle coldstart exhaust. The predictions indicate that the contaminants infiltrate the house from the garage and the peak concentration in the laundry room adjacent to the garage is much less than in the garage and there is some time delay between the two peak values. The concentration predictions from COMIS and CONTAM are very close, but the difference caused by individual airflow and contaminant simulation time steps should be given attention.

From the concentration comparison between the two houses, it is predicted that the air-tightness of garage/house interface wall has a big impact on the indoor air contaminant dispersion in the houses.

In the case of two-zone simulation approach, each house is modeled as being comprised of two zones namely the garage and the house. The concentration in the house predicted by two-zone approach is much lower than in the laundry room predicted by multi-zone approach because modeling the house and garage as two-zone compartments did not provide information about the spatial contaminant concentration.

6.2 Contributions

The main contribution of this thesis is the development of a procedure for distributing the air leakage characteristics using the global building fan pressurization test data.

The other contribution is the validation of three airflow models with the experimental data collected in a controlled environment test in laboratory and the field measurements of two single-family houses.

6.3 Future Works

It is hopped that ESP-r will be integrated with a pollutant transport module to predict indoor air contaminant concentration, and further field experiments will be done to provide more complete test data (e.g. airflow rate, contaminant concentration, on-site

wind pressure profile, leakage data, indoor temperature and fan flow rate, etc.) in order to validate the models further.

The works have been carried out so far concentrated on validation of airflow models with measurement data from single or multi-story residential buildings. Future works must be concentrated on validation of airflow models with measurement data from mechanically ventilated office buildings.

REFERENCES

Allard, F. (1992) "Air Flow Through Large Openings", Energy and Buildings, Vol. 18, pp. 133-145.

Allard, F. (1998) "Natural Ventilation in Buildings—A Design Handbook", James & James Ltd, London, UK.

Amara, F. (1993) "Contribution a la Caracterisation aeraulique des Batiments. Etude de Transferts aerauliques dans les Locaux multizone", Ph.D thesis at INSA, Lyon, France.

ASHRAE (1997). Handbook, Fundamental. American Society of Heating, Refrigerating, and Air-Conditioning Engineers, Inc. Atlanta, USA.

Axley, J. (1988) "Progress Toward A General Analytical Method for predicting Indoor Air Pollution in Buildings – Indoor Air Quality Modelling Phase III Report", NBSIR 88-3814, National Institute of Standards and Technology.

Dols, W. Stuart (2001), "A Tool for Modeling Airflow & Contaminant Transport", ASHRAE Journal, Vol.43, No.3, pp.35-42

Dols, W.S., G.N. Walton, et al. (2000) "CONTAMW 1.0 User Manual", NISTIR 6476. National Institute of Standards and Technology.

ESRU (Energy Systems Research Unit, University of Strathclyde), (1997) "ESP-r User Guide Version 9 Series", University of Strathclyde, Glasgow, UK.

ESRU (Energy Systems Research Unit, University of Strathclyde), (1996) "Data Model Sumarry - ESP-r Version 9 Series", University of Strathclyde, Glasgow, UK.

Feustel, H.E. (1992) "Annex 23 'Multizone Airflow Modeling' An International Effort", International Symposium – Air Flow in Multizone Structures, Budapest, September 9, 1992. pp. 1-8. Technical University of Budapest.

Feustel, H.E. (1999) "COMIS – An International Multizone Airflow and Contaminant Transport Model", Energy and Buildings, Vol. 30 (1999), pp.3-18.

Feustel, H.E. and Dieres, J. (1992) "A Survey of Airflow Models for Multizone Structures", Energy and Buildings, Vol. 18 (1992), pp.79-100.

Feustel, H.E. and Kendon, V.M. (1985) "Infiltration Models for Multicellular Structures" Energy and Buildings, Vol. 8 (1985)

Feustel, H.E. and Raynor-Hoosen, A., (1990) "Fundamentals of the Multizone Air Flow Model – COMIS", International Energy Agency, AIVC Technical Note 29.

Feustel, H.E. and Smith B.V. (1997) "COMIS 3.0 – User's Guide", Lawrence Berkeley National Laboratory, US.

Furbringer, J.-M., Roulet, C.-A. and Borchiellini, R. (1996) "Annex 23: Multizone Air Flow Modelling—Final Report, Evaluation of COMIS", Swiss Federal Institute of Technology, Lausanne. LESO.PB, Institute of Building Technology. IEA, ECBCS (International Energy Agency, Energy Conservation in Buildings and Community Systems Programme)

Grosso, M., (1992) "Wind Pressure Distribution Around Buildings: A Parametrical Model", Energy and Buildings, Vol. 18, pp. 101-103.

Grot, R.A. (1991) "User Manual NBSAVIS CONTAM88", NISTIR 4585, National Institute of Standards and Technology.

Haghighat, F. (1989) "Air infiltration and indoor air quality models – a review", International Journal of Ambient Energy, Vol.10, pp. 115-122.

Haghighat, F. and Megri, A.C. (1999) "Predicting the Airflow, Distribution of Vehicle Exhaust and Vehicle Evaporation Emissions through Residential Buildings from

Attached Garage with the CONTAM Model", project report prepared for Air & Waste Section of Health Canada.

Haghighat, F. and Megri, A.C. (1996) "A comprehensive Validation of Two Airflow Models – COMIS and CONTAM", Indoor Air 1996; 6: 278-288

Hensen, J.L.M. (1991) "On the thermal interaction of building structure and heating and ventilating system", Doctoral dissertation Eindhoven University of Technology, (ISBN 90-386-0081-X)

Herrlin, M.K. (1992) "Air-Flow Studies in Multizone Buildings—Models and Application", Final Report for BFR Project #900461-8, Department of Building Services Engineering, Royal Institute of Technology, S-100 44 Stockholm, Sweden.

Hong, T., Chou, S.K., Bong, T.Y. (2000) "Building Simulation: an Overview of Developments and Information Sources", Building and Environment, Vol.35 (2000), pp.347-361.

Klote, J.H. (1981). "A Computer Program for Analysis of Smoke Control Systems", NBSIR 80-2157, National Bureau of Standards (U.S.).

Liddament, M. and Allen, C. (1983) "The Validation and Comparison of Mathematical Models of Air Infiltration", Technical Note AIC 11, Great Britain.

Orme, M. (1999) "Applicable Models for Air Infiltration and Ventilation Calculations", International Energy Agency, AIVC Technical Note 51.

Orme, M., Liddament, M. and Wilson, A. (1994) "An Analysis and Data Summary of the AIVC's Numerical Database", International Energy Agency, AIVC Technical Note 44.

Upham, D. Rebecca, Yuill, K. Grenville, and Bahnfleth, P. William (2001) "A Validation Study of Multizone Airflow and Contaminant Migration Simulation Programs as applied to Tall Buildings", ASHRAE Transactions 01(2)

Walton, G.N. (1997) "CONTAM96 User Manual", NISTIR 6056 National Institute of Standard and Technology.

Walton, G.N. (1994) "CONTAM93 User Manual", NISTIR 5385 National Institute of Standard and Technology.

Walton, G.N. (1989) "AIRNET – A Computer Program for Building Airflow Network Modelling", National Institute of Standards and Technology (NIST), USA.

Yoshino, H., Zhao, Y., Kobayashi, H. and Utsumi, Y. (1995) "Simulation and Measurement of Air Infiltration and Pollutant Transport Using a Passive Solar Test House", ASHRAE Transactions 95(2): pp.1091-1099

Zhao, Y., Yoshino, H. and Okuyama, H. (1998) "Evaluation of the COMIS Model by Comparing Simulation and Measurement of Airflow and Pollutant Concentration", Indoor Air 1998, 8: pp.123-130

APPENDICES

A 1. Air Tightness Test Information – Record of Field Data

A 1.1. House-1

A 1.1.1. House and Garage Description (illustrated in Figure A.1 and A.2)

◊ House Age – *29* or Year Built – *1968*, Number of Storeys – *1*

◊ Type of Construction – *Raised bungalow, split entrance*

◊ Primary Heating Fuel – *Electricity*, Supplementary Heating Fuel – *Wood*

◊ Compass orientation of garage to house – *W.-S.W.*

◊ Orientation of garage door – *N.-N.W.*

◊ Description of garage attachment to the house – *one full wall*

◊ Size of the Garage (how many cars the garage holds?) – *two*

◊ Size of the Garage Vehicle door – *double door*

◊ Survey of garage interior finishing – *all drywalled*

◊ Survey of garage exterior walls and ceiling – *uninsulated*

◊ Garage is not heated

◊ Chimney height above main floor ceiling – *2.25m*

◊ Fireplace flue is a rectangular clay tile – *8¼" x 13¼"*

◊ Fireplace opening – 1.0m wide by 0.5m high, the hearth is 0.23m above the floor.

◊ House volume – 419.1m^3, garage volume – 115.7m^2, common surface area – 17.8m^2

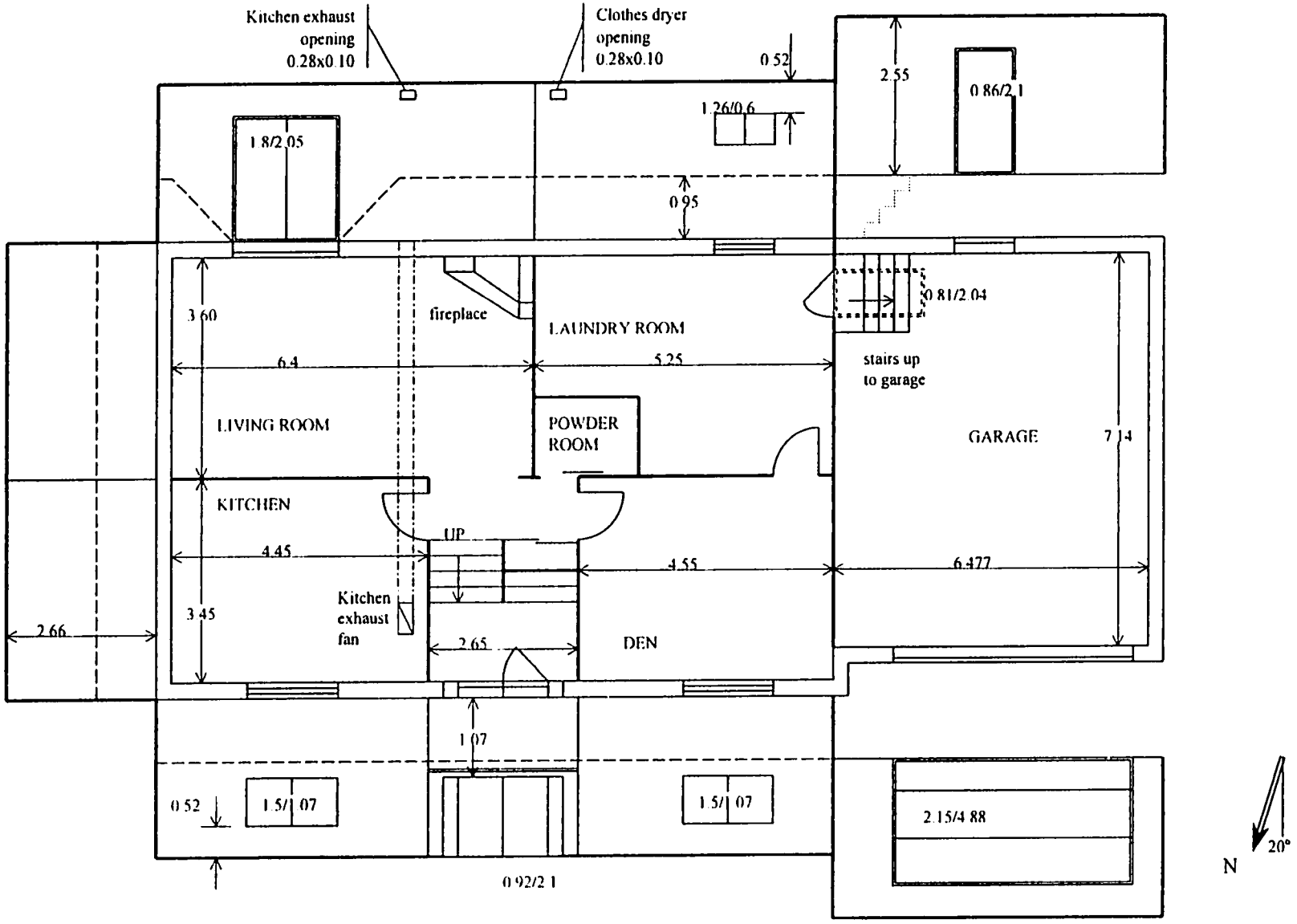

Figure A.1 Basement Plan of House-1

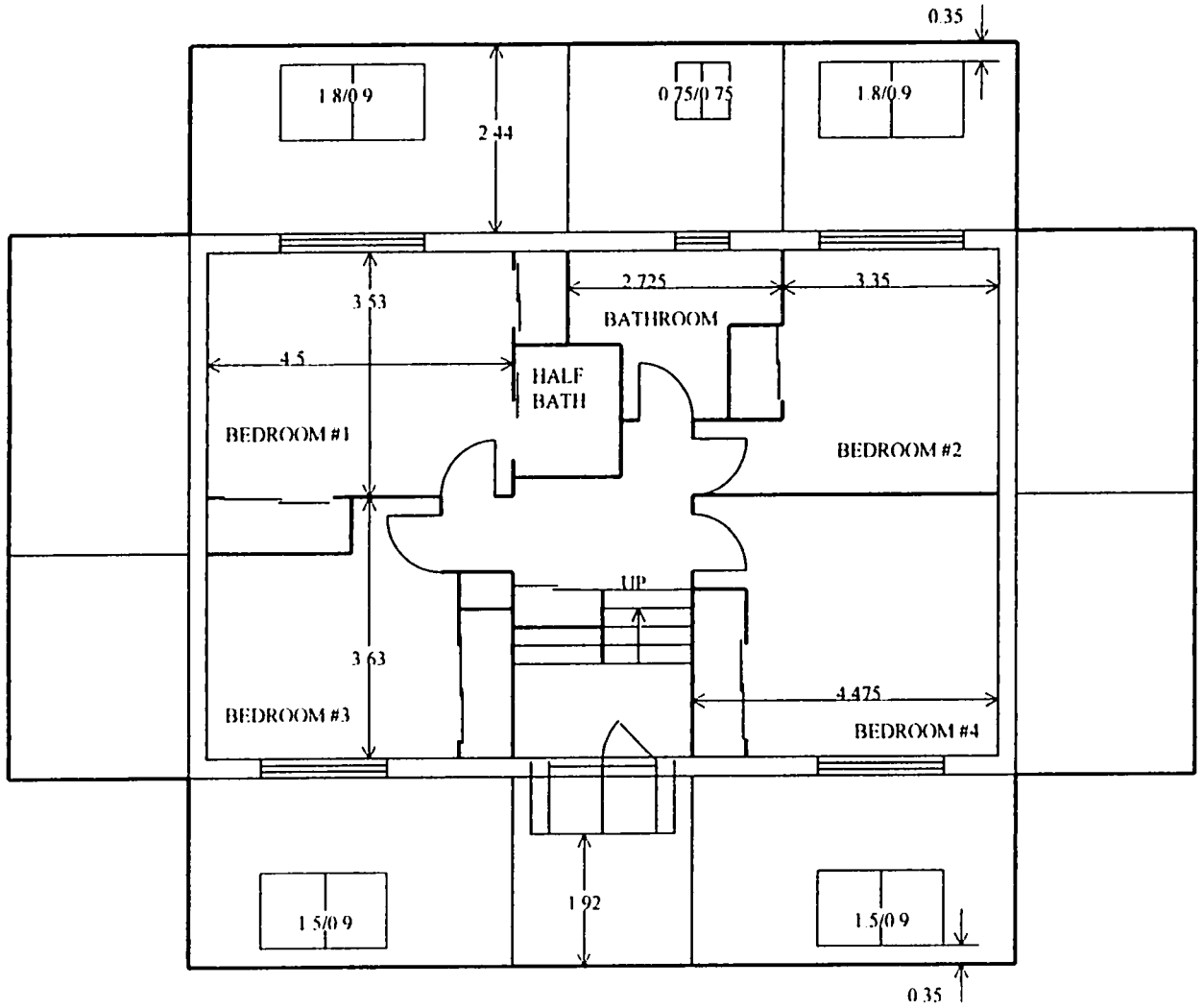

Figure A.2 Main Floor Plan of House-1

A 1.1.2. Observations

Record the visual observation of major air leakage paths from common surfaces of garage and the house during the garage pressurisation test.

◊ Leakage around the door from the garage to the basement (requires better weather stripping)

◊ Significant leakage from the header area along garage wall into the laundry room

◊ Electrical outlet on garage wall in main floor back bedroom

A 1.1.3. House air leakage paths

◊ Windows and doors (shrink wrap during the winter reduces air change by about ½ air change as tested in the past)

◊ Header area (main floor & split entrance landing)

◊ Disconnected bathroom exhaust fan (may leak into attic, and duct leading to exterior)

◊ Kitchen exhaust fan damper

◊ Clothes dryer damper

◊ Fireplace damper

A 1.1.4. Air tightness test results

	Test1 House Airtightness without Garage	**Test2** House Airtightnes with Garage/house $\Delta P=0$	**Test3** Garage Airtightness with Garage/house $\Delta P=0$
Air Change /Hr at 50 Pa	6.41	5.53	29.95
ELA at 10 Pa, cm^2	939	909	1,630
K, L/(s.Pa^n)	44.48	50.76	117.88
n	0.72	0.65	0.54
correlation coefficient	0.999	0.992	0.991

A 1.1.5. Weather Data

time-of-day (s)	ambient temperature (K)	barometric pressure (Pa)	wind speed (m/s)	wind direction (0=N, 90=E, 180=S, ...)
0	267.1	99690	2.5	45
3600	266.6	99420	3.06	45
7200	266.5	99200	3.61	45
10800	266.5	99080	3.06	45
14400	266.5	99070	3.06	45
18000	266.3	99110	2.5	45
21600	266.5	99150	3.61	45
25200	264.8	99330	4.72	45
28800	267.9	99400	4.72	45
32400	269.8	99500	5	67.5
36000	272.2	99590	4.72	67.5
39600	273.3	99610	4.17	67.5
43200	274.8	99640	3.06	67.5
46800	275	99680	3.61	67.5
50400	275.8	99830	3.61	67.5
54000	276	99970	3.06	90
57600	276.3	100090	4.17	67.5
61200	276.1	100300	3.06	67.5
64800	275.8	100520	1.94	90
68400	275.2	100660	1.94	90
72000	274.6	100740	3.61	67.5
75600	274.2	100860	3.61	45
79200	274.2	101020	4.72	67.5
82800	274.1	101130	4.17	67.5
86400	274.1	101220	4.17	67.5

A 1.2. House-2

A 1.2.1. House and Garage Description (illustrated in Figure A.3 and A.4)

◊ House Age – *19* or Year Built – *1978*, Number of Storeys – *1*

◊ Type of Construction – *Raised basement with garage in basement*

◊ Primary Heating Fuel – *Gas*, Supplementary Heating Fuel – *Wood*

◊ Compass orientation of garage to house – *W.-S.W.*

◊ Orientation of garage door – *S.-S.E.*

◊ Description of garage attachment to the house – *one full wall and full ceiling above*

◊ Size of the Garage (how many cars the garage holds?) – *one*

◊ Size of the Garage Vehicle door – *single door*

◊ Survey of garage interior finishing – *all finished*

◊ Survey of garage exterior walls and ceiling – *insulated*

◊ Garage is not heated

◊ Chimney height above main floor ceiling – *1.5m*

◊ Fireplace flue diameter – *8"*

◊ Fireplace opening is 0.71x0.71m^2, the hearth is 0.035m above the floor.

◊ Windows have letters on the different glazing units to indicate the type of window. The F is for fixed, C for casement.

◊ Furnace is a sealed combustion unit.

◊ House volume – 480.4m^3, garage volume – 69.4m^2, common surface area – 50.5m^2

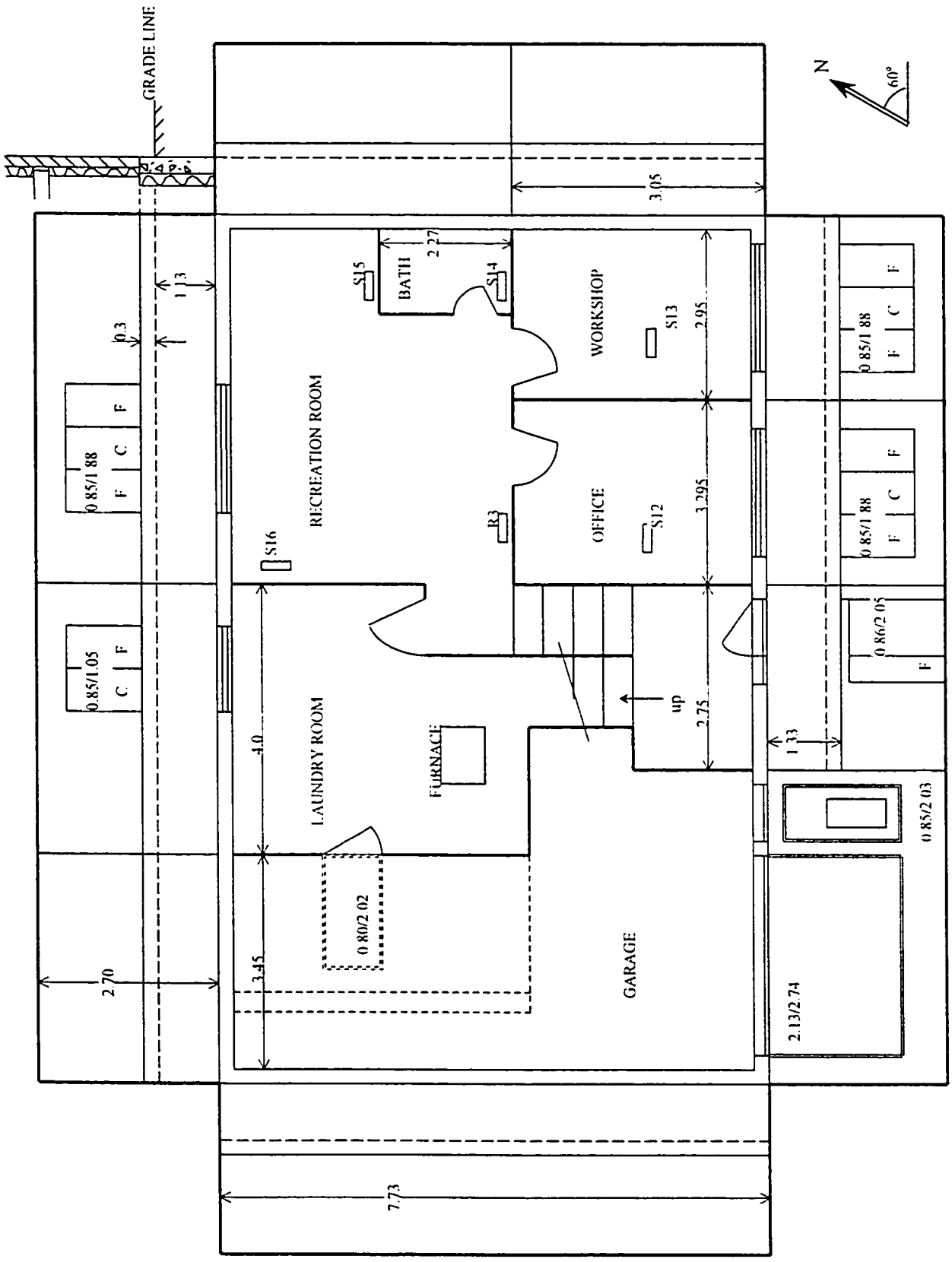

Figure A.3 Basement Plan of House-2

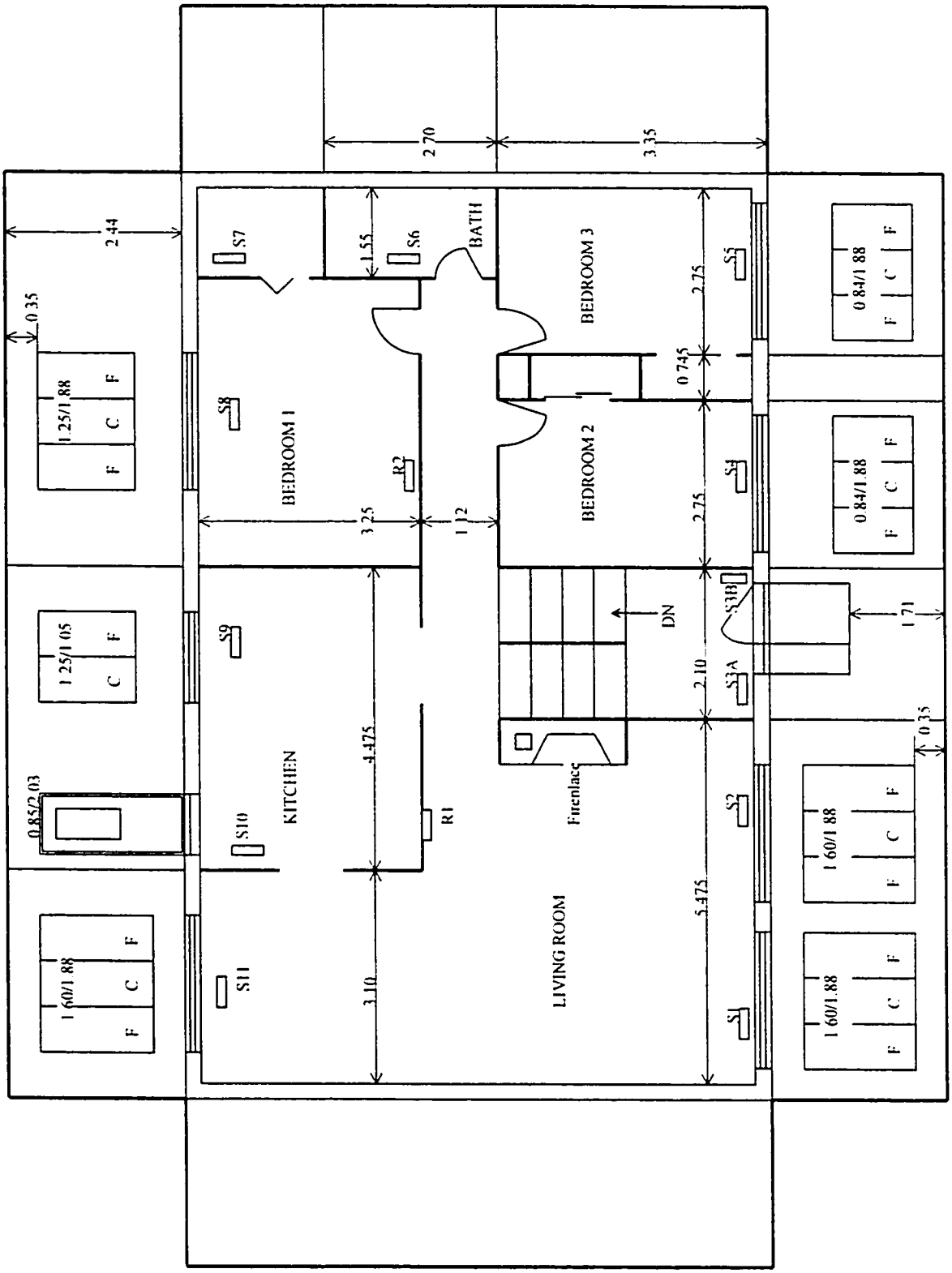

Figure A.4 Main Floor Plan of House-2

A 1.2.2. Observations

Record the visual observation of major air leakage paths from common surfaces of garage and the house during the garage pressurisation test.

◊ Main floor, dining room – heat register boot has slight leak

◊ Main floor, living room – heat register boot has slight leak (none at register closest to door)

◊ Basement, door to garage – weather-stripping and perimeter of door, joist space above wall between garage and basement (mostly to the front of the house past the centre steel beam), at steel beam

A 1.2.3. House air leakage paths

◊ Windows and doors

◊ Header area

◊ Electrical service entrance in the workshop

◊ Pocket door between kitchen and hallway (air leak into the attic)

◊ Attic hatch in bedroom 2 ceiling

A 1.2.4. Air tightness test results

	Test1 House Airtightness without Garage	**Test2** House Airtightnes with Garage/house $\Delta P=0$	**Test3** Garage Airtightness with Garage/house $\Delta P=0$
Air Change /Hr at 50 Pa	3.98	3.58	12.14
ELA at 10 Pa, cm^2	570	514	332
K, $L/(s.Pa^n)$	21.43	19.38	18.68
n	0.82	0.82	0.65
correlation coefficient	0.998	0.990	0.992

A 1.2.5. Measured airflow rates of the mechanical air distribution system

Ref #	Type	Flow Range L/s	Flow Rate L/s	Duct diam .(in)	Duct length (m)	Comments
S1	floor register	10-15	14	5"	3.43	(1)
S2	floor register	15-20	16	5"	3.43	(1)
S3A	floor register	25-30	29	5"	3.65	(2)
S3B	wall register	15-20	17	5"	3	(3)
S4	floor register			5"	3.43	(1) not accessible for measurement
S5	floor register	10-15	11	5"	3.43	(1) register louvers closed
S6	floor register	25-30	30	5"	0.8	(1)
S7	floor register	10-15	13	5"	3	(1) register louvers closed
S8	floor register	15-20	20	5"	3.3	(1)
S9	floor register			5"	2.8	(1) not accessible
S10	floor register	5-10	8	5"	2.6	(1)
S11	floor register	10-15	15	5"	3.3	(1)
S12	ceiling register	25-30	25	5"	2.2	(4)
S13	ceiling register	25-30	26	5"	2.2	(4)
S14	wall register	5-10	6	5"	2.7	(5)
S15	wall register	25-30	26	5"	3.4	(5)
S16	wall register	< 5	< 5	5"	5.3	(5)
R1	wall register			5"	2	Double register width
R2	wall register	30-35	34	5"	4.7	
R3	wall register	35	35	5"	4.8	

Comments: (1) at main floor height, 2.70m above basement floor.

(2) at 1.33m above basement floor

(3) at 2.33m above basement floor

(4) at 2.45m above basement floor

(5) at 0.13m above basement floor

Main supply and return trunks sizes are shown on the duct work diagram, Figure A.5.

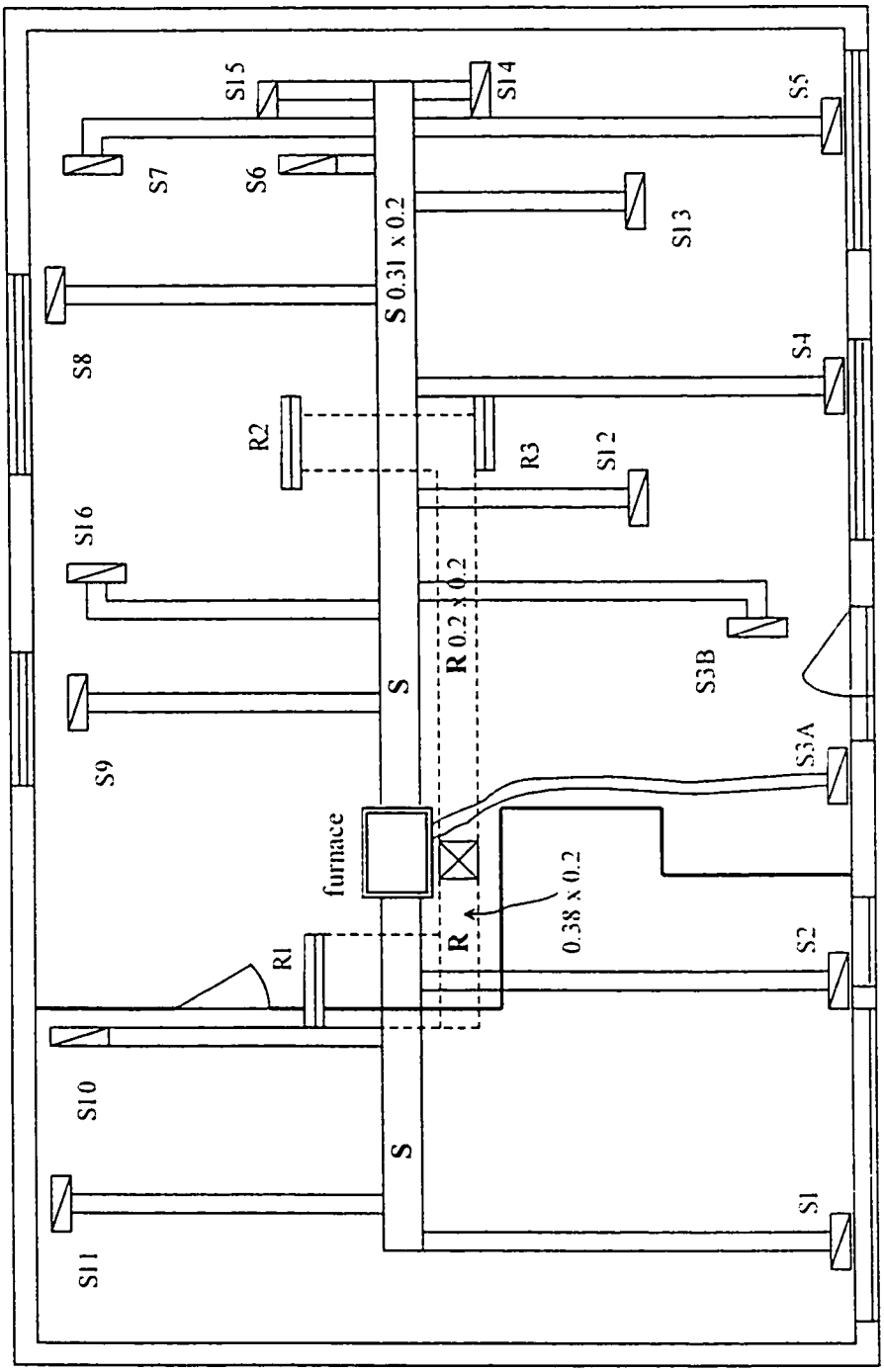

Figure A.5 Duct Work Diagram

A 1.2.6. Weather Data

time-of-day (s)	ambient temperature (K)	barometric pressure (Pa)	wind speed (m/s)	wind direction (0=N, 90=E, 180=S,...)
0	256	99690	1.11	180
3600	255.1	99420	1.67	180
7200	255.1	99200	1.94	180
10800	254.9	99080	1.94	180
14400	255	99070	1.94	180
18000	254.7	99110	0	0
21600	255.8	99150	0	0
25200	255.5	99330	1.67	90
28800	257	99400	1.11	67 5
32400	258.8	99500	1.11	67 5
36000	262.5	99590	0	0
39600	265.5	99610	0	0
43200	268.1	99640	1.67	90
46800	269.5	99680	2.5	90
50400	270.5	99830	2.5	180
54000	272.8	99970	4.72	202 5
57600	273	100090	5.28	202 5
61200	272.2	100300	7.22	202.5
64800	271.2	100520	5.56	202.5
68400	270.7	100660	4.72	202.5
72000	270.5	100740	4.72	202.5
75600	270.4	100860	3.06	180
79200	270.5	101020	3.06	135
82800	270.3	101130	3.61	135
86400	270.3	101220	3.61	135

A 2. Air Leakage Distribution Spreadsheet

A 2.1. Spreadsheet for House-1 Calculation

Zones	Orientation	Components	Dimensions (area or perimeter) (m^2 or m)	$C_{i,lit}$ (literature) ($dm^3.s^{-1}.m^{-1}.Pa^{-n}$)	$n_{i,lit}$ (literature)	$K_{i,lit}= C_{i,lit}$*Dimen ($dm^3.s^{-1}.Pa^{-n}$)	$Q_{i,lit}=K_{i,lit}$*(50Pa)$^{n}_{i,lit}$ ($dm^3.s^{-1}$)	K_i ($dm^3.s^{-1}.Pa^{-n}$)
BASEMENT								
DEN	NW	Wall	5.40	0.066	0 78	0.3564	7 5359	0 2923
	NW	Window	6.21	0.23	0.6	1.4283	14 9349	1.1714
	NW	Window/Wall	5 14	0 0025	0 6	0 01285	0 1344	0 0105
	NW	Wall/Ceiling	9.1	0 011	0 6	0 1001	1 0467	0.0821
						1 89765		
Laundry	SE	Wall	7.12	0 066	0 78	0 46992	9 9362	0 3854
	SE	Window	4.32	0 23	0 6	0 9936	10 3895	0 8149
	SE	Window/Wall	3.72	0 0025	0.6	0.0093	0 0972	0 0076
	SE	Wall/Ceiling	10.05	0.011	0.6	0 11055	1 1560	0 0907
	SE	Clothes Dryer (penetration)	0.76	0 8	0 6	0 608	6 3575	0 4987
		Clothes Dryer (damper)	0.0076	780	0 5	5.928	41.9173	4.8619
						8 11937		
Living Room	SE	Wall	6.10	0.066	0.78	0 4026	8 5128	0.3302
	SE	Door	9.75	0.15	0 6	1.4625	15 2925	1.1995
	SE	Door/Wall	7 70	0 0025	0 6	0.01925	0 2013	0 0158
	SE	Wall/Ceiling	12.80	0 011	0 6	0 1408	1 4723	0 1155
	SE	Kit_Exh (penetration)	0.76	0 8	0.6	0 608	6 3575	0 4987
	NE	Wall	5.55	0.066	0 78	0 3663	7 7452	0 3004
	NE	Wall/Ceiling	3.71	0 011	0 6	0 04081	0.4267	0 0335
		Fireplace (Damper)	0.066	410	0.5	27 06	191 3431	22 1934
						30 10026		
Kitchen	NW	Wall	5.3	0.066	0.78	0.3498	7 3963	0 2869
	NW	Window	6.21	0.15	0.6	0.9315	9 7401	0 7640
	NW	Window/Wall	5.14	0.0025	0.6	0.01285	0.1344	0 0105
	NW	Wall/Ceiling	9	0.011	0.6	0.099	1 0352	0 0812
	NE	Wall	5.32	0.066	0.78	0.35112	7.4242	0 2880
	NE	Wall/Ceiling	3.45	0.011	0.6	0 03795	0.3968	0 0311
		Kit_Exh (damper)	0.0076	780	0.5	5 928	41 9173	4.8619
						7 71022		
Corridor	NW	Wall	0.52	0.066	0 78	0 03432	0 7257	0.0281
	NW	Door	4.9	0.27	0 6	1 323	13 8338	1 0851
	NW	Door/Wall	5.4	0 0025	0 6	0 0135	0 1412	0 0111
	NW	Wall/Floor	2 64	0 015	0 6	0 0396	0 4141	0 0325
						1 41042		
MAINFLOOR								
Bedroom #4	NW	Wall	9.57	0 066	0.78	0.63162	13 3553	0 5180
	NW	Window	5.7	0.15	0.6	0 855	8.9402	0 7012
	NW	Window/Wall	4.8	0.0025	0.6	0.012	0 1255	0.0098
	NW	Wall/Ceiling	4.48	0 011	0.6	0.04928	0 5153	0 0404
	NW	Wall/Floor	4.48	0.011	0.6	0.04928	0 5153	0.0404
	SW	Wall	4.43	0.066	0.78	0.29238	6 1822	0.2398
	SW	Wall/Ceiling	3.63	0.011	0 6	0.03993	0.4175	0.0327

	SW	Wall/Floor	3.63	0.011	0.6	0.03993	0.4175	0.0327
						1 96942		
Bedroom #2	SE	Wall	6.55	0.066	0 78	0.4323	9 1408	0.3546
	SE	Window	6.3	0.15	0.6	0.945	9 8813	0 7750
	SE	Window/Wall	5.4	0.0025	0.6	0 0135	0 1412	0 0111
	SE	Wall/Ceiling	3.35	0.011	0.6	0.03685	0 3853	0.0302
	SE	Wall/Floor	3.35	0.011	0.6	0.03685	0 3853	0.0302
	SW	Wall	4.43	0.066	0.78	0.29238	6.1822	0.2398
	SW	Wall/Ceiling	3.53	0.011	0.6	0.03883	0 4060	0.0318
	SW	Wall/Floor	3.53	0.011	0.6	0.03883	0 4060	0 0318
						1 83454		
Bathroom	SE	Wall	6.09	0.066	0.78	0.40194	8 4988	0 3297
	SE	Window	3.75	0.15	0.6	0.5625	5.8817	0 4613
	SE	Window/Wall	3	0.0025	0.6	0 0075	0 0784	0 0062
	SE	Wall/Ceiling	2.73	0 011	0 6	0 03003	0 3140	0.0246
	SE	Wall/Floor	2.73	0.011	0 6	0.03003	0 3140	0 0246
	SE	Exh(penetration)	0.0076	780	0 5	5 928	41 9173	4 8619
						6 96		
Bedroom #1	SE	Wall	11 21	0 066	0.78	0 73986	15 6439	0 6068
	SE	Window	6.3	0.15	0.6	0.945	9 8813	0 7750
	SE	Window/Wall	5 4	0.0025	0.6	0 0135	0 1412	0 0111
	SE	Wall/Ceiling	5.2	0.011	0 6	0 0572	0 5981	0 0469
	SE	Wall/Floor	5.2	0.011	0.6	0 0572	0 5981	0 0469
	NE	Wall	10.38	0.066	0 78	0 68508	14 4856	0 5619
	NE	Wall/Ceiling	4.25	0.011	0.6	0.04675	0 4888	0 0383
	NE	Wall/Floor	4.25	0.011	0 6	0 04675	0 4888	0 0383
						2 59134		
Bedroom #3	NW	Wall	9.63	0 066	0.78	0 63558	13 4390	0 5213
	NW	Window	5.7	0.15	0 6	0 855	8 9402	0 7012
	NW	Window/Wall	4 8	0.0025	0 6	0 012	0 1255	0 0098
	NW	Wall/Ceiling	4 5	0 011	0 6	0 0495	0 5176	0 0406
	NW	Wall/Floor	4.5	0.011	0.6	0 0495	0 5176	0 0406
	NE	Wall	7.08	0.066	0 78	0 46728	9 8804	0 3832
	NE	Wall/Ceiling	2.9	0 011	0 6	0 0319	0 3336	0 0262
	NE	Wall/Floor	2.9	0 011	0.6	0 0319	0 3336	0 0262
						2 13266		
Corridor	NW	Wall	5.15	0 066	0 78	0 3399	7 1870	0 2788
	NW	Door	3	0 27	0 6	0 81	8 4697	0 6643
	NW	Door/Wall	3 4	0.0025	0 6	0 0085	0 0889	0 0070
	NW	Wall/Ceiling	2 64	0 011	0 6	0 02904	0 3037	0 0238
						1 18744		
CEILING			83.2	0 11	0 75	9 152	172 0852	7 5061
						75 06532	786 9647	61 5653
GARAGE								
	SE	Wall	14 55	0.52	0.67	7 566	104 0342	7 2148
	SE	Door	5.92	0.27	0.6	1 5984	16.7135	1 5242
	SE	Door/Wall	5.92	0.0025	0 6	0.0148	0.1548	0 0141
	SE	Wall/Ceiling	6.48	0.023	0.6	0 14904	1 5584	0 1421
	SE	Wall/Floor	6.48	0.023	0 6	0 14904	1 5584	0 1421
	SW	Wall	18	0.52	0 67	9 36	128.7021	8 9255
	SW	Wall/Ceiling	7.14	0 023	0.6	0 16422	1 7171	0 1566
	SW	Wall/Floor	7 14	0 023	0.6	0.16422	1.7171	0 1566
	NW	Wall	6.02	0.52	0.67	3.1304	43.0437	2.9851
	NW	Door	10.49	5.7	0.6	59.793	625.2193	57 0173
	NW	Door/Wall	9.18	0.0025	0.6	0 02295	0.2400	0.0219
	NW	Wall/Ceiling	6.45	0.023	0.6	0.14835	1.5512	0.1415
		Ceiling	46.4	0.11	0.75	5.104	95.9706	4.8671
				2762.8495		87 36442	1022.1805	83.3088

A 2.2. Spreadsheet for House-2 Calculation

Zones	Orientation	Components	Dimensions (area or perimeter) (m^2 or m)	$C_{i,lit}$ (literature) ($dm^3.s^{-1}.m^{-1}.Pa^{-n}$)	$n_{i,lit}$ (literature)	$K_{i,lit} = C_{i,lit} * Dimen$ ($dm^3.s^{-1}.Pa^{-n}$)	$Q_{i,lit} = K_{i,lit} * (50Pa)^{n}_{i,lit}$ ($dm^3.s^{-1}$)	K_j ($dm^3.s^{-1}.Pa^{-n}$)
BASEMENT								
Office	SE	Wall	2.92	0.066	0.78	0.19272	4.0750	0.1364
	SE	Window	2.96	0.13	0.6	0.3848	4.0236	0.2723
	SE	Window/Wall	5.46	0.0025	0.6	0.01365	0.1427	0.0097
	SE	Wall/Floor	3.3	0.011	0.6	0.0363	0.3796	0.0257
	SE	Wall/Ceiling	3.3	0.011	0.6	0.0363	0.3796	0.0257
						0.66377		
Workshop	SE	Wall	2.44	0.066	0.78	0.16104	3.4051	0.1140
	SE	Window	2.96	0.13	0.6	0.3848	4.0236	0.2723
	SE	Window/Wall	5.46	0.0025	0.6	0.01365	0.1427	0.0097
	SE	Wall/Ceiling	2.95	0.011	0.6	0.03245	0.3393	0.0230
	SE	Wall/Floor	2.95	0.011	0.6	0.03245	0.3393	0.0230
	NE	Wall/Ceiling	3.05	0.011	0.6	0.03355	0.3508	0.0237
	NE	Wall/Floor	3.05	0.011	0.6	0.03355	0.3508	0.0237
	NE	Wall	4.18	0.066	0.78	0.27588	5.8333	0.1952
	NE	Electrical Panel	1	0.21	0.5	0.21	1.4849	0.1486
						1.17737		
Half Bath	NE	Wall	3.11	0.066	0.78	0.20526	4.3401	0.1452
	NE	Wall/Ceiling	2.27	0.011	0.6	0.02497	0.2611	0.0177
						0.23023		
Recreation Room	NE	Wall	3.29	0.066	0.78	0.21714	4.5913	0.1537
	NE	Wall/Ceiling	2.4	0.011	0.6	0.0264	0.2760	0.0187
	NE	Wall/Floor	2.4	0.011	0.6	0.0264	0.2760	0.0187
	NW	Wall	6.96	0.066	0.78	0.45936	9.7129	0.3251
	NW	Window	2.96	0.13	0.6	0.3848	4.0236	0.2723
	NW	Window/Wall	5.46	0.0025	0.6	0.01365	0.1427	0.0097
	NW	Wall/Ceiling	6.25	0.011	0.6	0.06875	0.7189	0.0487
	NW	Wall/Floor	6.25	0.011	0.6	0.06875	0.7189	0.0487
						1.26525		
Laundry	NW	Wall	4.72	0.066	0.78	0.31152	6.5869	0.2204
	NW	Window	2.75	0.13	0.6	0.3575	3.7382	0.2530
	NW	Window/Wall	3.8	0.0025	0.6	0.0095	0.0993	0.0067
	NW	Wall/Floor	4.1	0.011	0.6	0.0451	0.4716	0.0319
	NW	Wall/Ceiling	4.1	0.011	0.6	0.0451	0.4716	0.0319
						0.76872		
Corridor	SE	Wall	5.82	0.066	0.78	0.38412	8.1220	0.2718
	SE	Door	5.82	0.27	0.6	1.5714	16.4312	1.1120
	SE	Door/Wall	7.1	0.0025	0.6	0.01775	0.1856	0.0126
	SE	Wall/Floor	2.75	0.011	0.6	0.03025	0.3163	0.0214
	SE	Wall/Ceiling	2.1	0.011	0.6	0.0231	0.2415	0.0163
						2.02662		
MAINFLOOR								
Bedroom #2	SE	Wall	5.16	0.066	0.78	0.34056	7.2010	0.2410
	SE	Window	2.94	0.13	0.6	0.3822	3.9964	0.2705
	SE	Window/Wall	5.44	0.0025	0.6	0.0136	0.1422	0.0096
	SE	Wall/Ceiling	2.75	0.011	0.6	0.03025	0.3163	0.0214
	SE	Wall/Floor	2.75	0.011	0.6	0.03025	0.3163	0.0214

		Attic Hatch	2.8	0.68	0.6	1.904	19.9090	1.3473
						2.70086		
Bedroom #3	SE	Wall	6.96	0.066	0.78	0.45936	9.7129	0.3251
	SE	Window	2.94	0.13	0.6	0.3822	3.9964	0.2705
	SE	Window/Wall	5.44	0.0025	0.6	0.0136	0.1422	0.0096
	SE	Wall/Ceiling	3.5	0.011	0.6	0.0385	0.4026	0.0272
	SE	Wall/Floor	3.5	0.011	0.6	0.0385	0.4026	0.0272
	NE	Wall	8.21	0.066	0.78	0.54186	11.4573	0.3834
	NE	Wall/Ceiling	3.35	0.011	0.6	0.03685	0.3853	0.0261
	NE	Wall/Floor	3.35	0.011	0.6	0.03685	0.3853	0.0261
						1.54772		
Bathroom	NE	Wall	6.62	0.066	0.78	0.43692	9.2384	0.3092
	NE	Wall/Ceiling	2.7	0.011	0.6	0.0297	0.3106	0.0210
	NE	Wall/Floor	2.7	0.011	0.6	0.0297	0.3106	0.0210
	Roof	F1	0.006	830	0.5	4.98	35.2139	3.5240
	Roof	F1(pene)	1	0.44	0.6	0.44	4.6008	0.3114
						5.91632		
Walk-in Closet	NE	Wall	4.09	0.066	0.78	0.26994	5.7077	0.1910
	NE	Wall/Ceiling	1.67	0.011	0.6	0.01837	0.1921	0.0130
	NE	Wall/Floor	1.67	0.011	0.6	0.01837	0.1921	0.0130
	NW	Wall	3.8	0.066	0.78	0.2508	5.3030	0.1775
	NW	Wall/Ceiling	1.55	0.011	0.6	0.01705	0.1783	0.0121
	NW	Wall/Floor	1.55	0.011	0.6	0.01705	0.1783	0.0121
						0.59158		
Bedroom Master	NW	Wall	9.12	0.066	0.78	0.60192	12.7273	0.4259
	NW	Window	3.76	0.13	0.6	0.4888	5.1111	0.3459
	NW	Window/Wall	6.26	0.0025	0.6	0.01565	0.1636	0.0111
	NW	Wall/Ceiling	4.7	0.011	0.6	0.0517	0.5406	0.0366
	NW	Wall/Floor	4.7	0.011	0.6	0.0517	0.5406	0.0366
						1.20977		
Kitchen	NW	Wall	7.87	0.066	0.78	0.51942	10.9829	0.3676
	NW	Window	3.55	0.13	0.6	0.4615	4.8256	0.3266
	NW	Window/Wall	4.6	0.0025	0.6	0.0115	0.1202	0.0081
	NW	Door	5.88	0.27	0.6	1.5876	16.6006	1.1234
	NW	Door/Wall	5.88	0.0025	0.6	0.0147	0.1537	0.0104
	NW	Wall/Ceiling	4.475	0.011	0.6	0.049225	0.5147	0.0348
	NW	Wall/Floor	4.475	0.011	0.6	0.049225	0.5147	0.0348
	Roof	F2	0.006	830	0.5	4.98	35.2139	3.5240
	Roof	F2(pene)	1	0.44	0.6	0.44	4.6008	0.3114
						8.11317		
Living Room	NW	Wall	4.59	0.066	0.78	0.30294	6.4055	0.2144
	NW	Window	4.46	0.13	0.6	0.5798	6.0626	0.4103
	NW	Window/Wall	6.96	0.0025	0.6	0.0174	0.1819	0.0123
	NW	Wall/Ceiling	3.1	0.011	0.6	0.0341	0.3566	0.0241
	NW	Wall/Floor	3.1	0.011	0.6	0.0341	0.3566	0.0241
	SE	Wall	7.4	0.066	0.78	0.4884	10.3270	0.3456
	SE	Window	8.92	0.13	0.6	1.1596	12.1252	0.8206
	SE	Window/Wall	13.92	0.0025	0.6	0.0348	0.3639	0.0246
	SE	Wall/Ceiling	5.475	0.011	0.6	0.060225	0.6297	0.0426
	SE	Wall/Floor	5.475	0.011	0.6	0.060225	0.6297	0.0426
	SW	Wall	18.94	0.066	0.78	1.25004	26.4314	0.8846
	SW	Wall/Ceiling	7.73	0.011	0.6	0.08503	0.8891	0.0602
	SW	Wall/Floor	7.73	0.011	0.6	0.08503	0.8891	0.0602
	Roof	Fireplace(damper)	0.0314	410	0.5	12.874	91.0329	9.1101
						17.06569		
CEILING			106.7	0.11	0.75	11.737	220.6910	8.3055
						55.01407	677.1706	38.9300

GARAGE	SE	Wall	5.41	0.066	0 78	0.35706	7 5498	0 1866
	SE	Door	5.76	0.27	0 6	1 5552	16.2618	0 8127
	SE	Door/Wall	5.76	0.0025	0.6	0.0144	0.1506	0.0075
	SE	Door(roller)	5.84	5.7	0.6	33.288	348.0725	17.3953
	SE	Door/Wall	9.74	0.0025	0.6	0.02435	0.2546	0 0127
	SE	Wall/Ceiling	4.8	0.011	0.6	0.0528	0.5521	0.0276
	SE	Wall/Floor	2.06	0.011	0.6	0.02266	0.2369	0.0118
	SW	Wall	10.59	0.066	0.78	0.69894	14.7787	0.3652
	SW	Wall/Ceiling	7.73	0.011	0.6	0.08503	0.8891	0 0444
	SW	Wall/Floor	7.73	0.011	0.6	0.08503	0 8891	0.0444
	NW	Wall	4.73	0.066	0.78	0 31218	6 6009	0.1631
	NW	Wall/Ceiling	3.45	0.011	0.6	0.03795	0.3968	0 0198
	NW	Wall/Floor	3.45	0.011	0.6	0.03795	0.3968	0.0198
		Ceiling	27.8	0.11	0 75	3.058	57 4996	1.5980
				2081 76		39 62955	454.5294	20 7093

A 3. Schematic Layouts of Simulation

These layouts are exported from CONTAM Sketchpad for House-1 and House-2 airflow simulations.

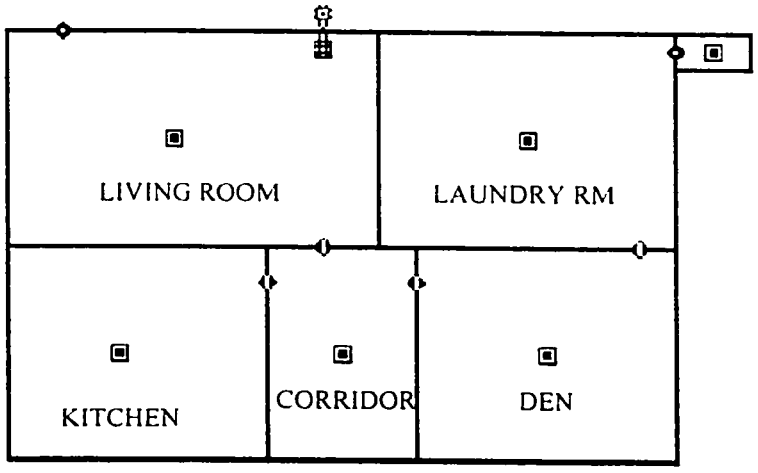

Figure A.6 Level-1 of the Basement in House-1

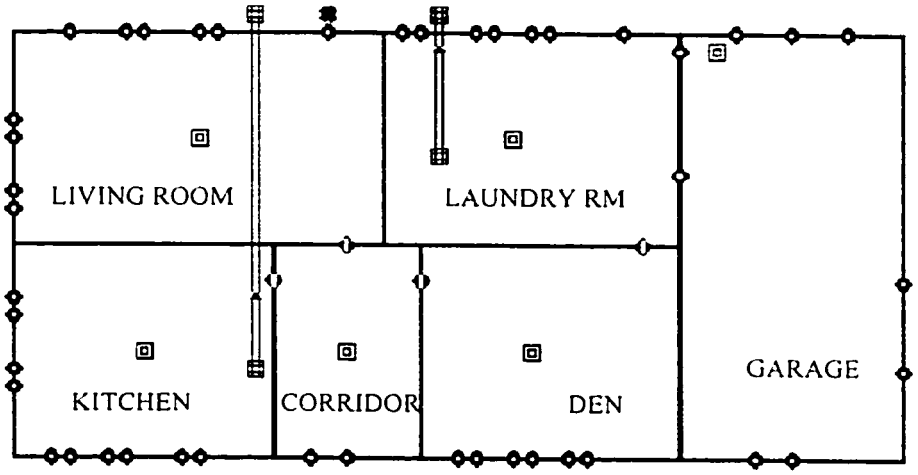

Figure A.7 Level-2 of the Basement in House-1

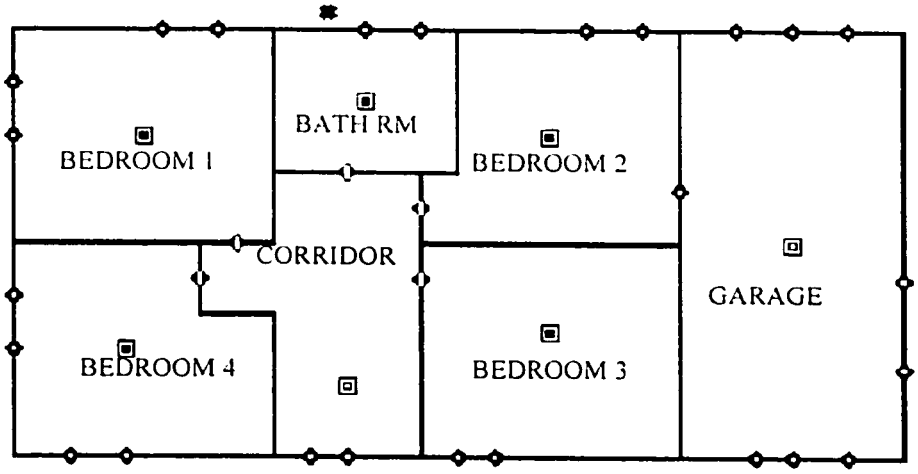

Figure A.8 Level-1 of the Main Floor in House-1

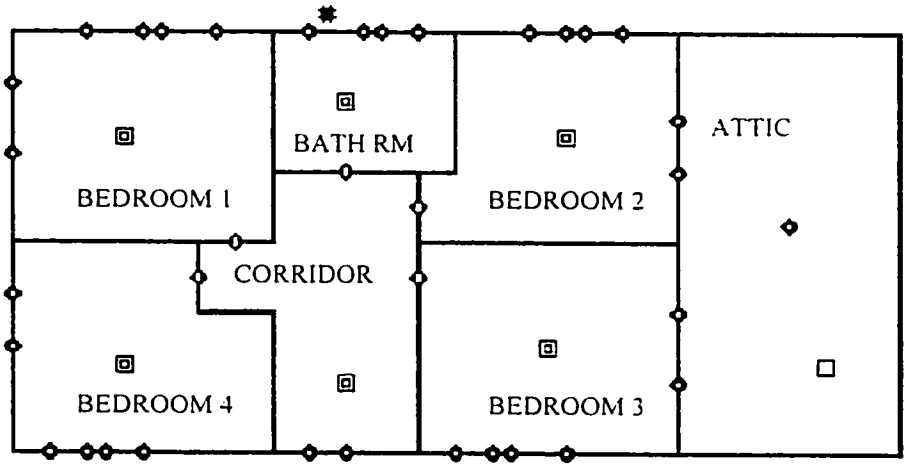

Figure A.9 Level-2 of the Main Floor in House-1

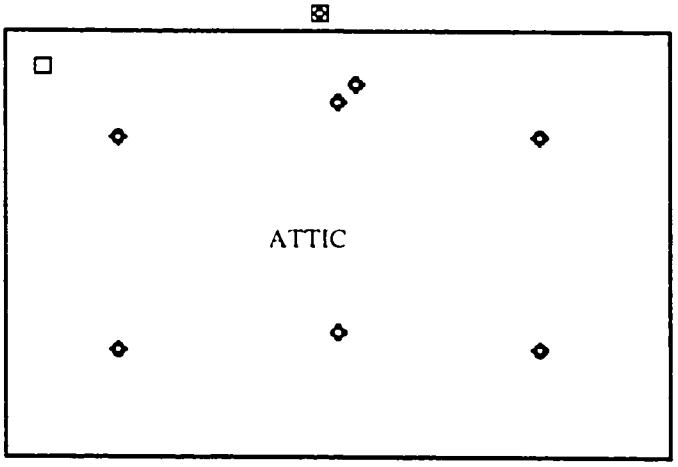

Figure A.10 Attic of House-1

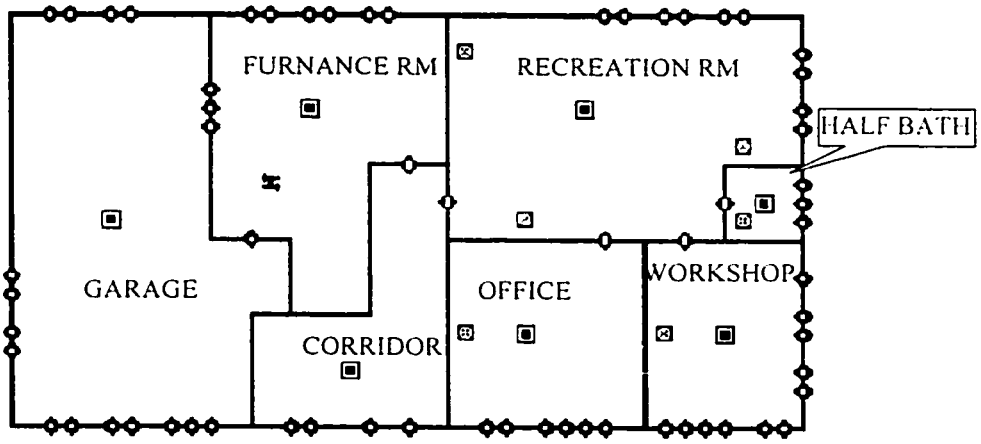

Figure A.11 Basement of House-2

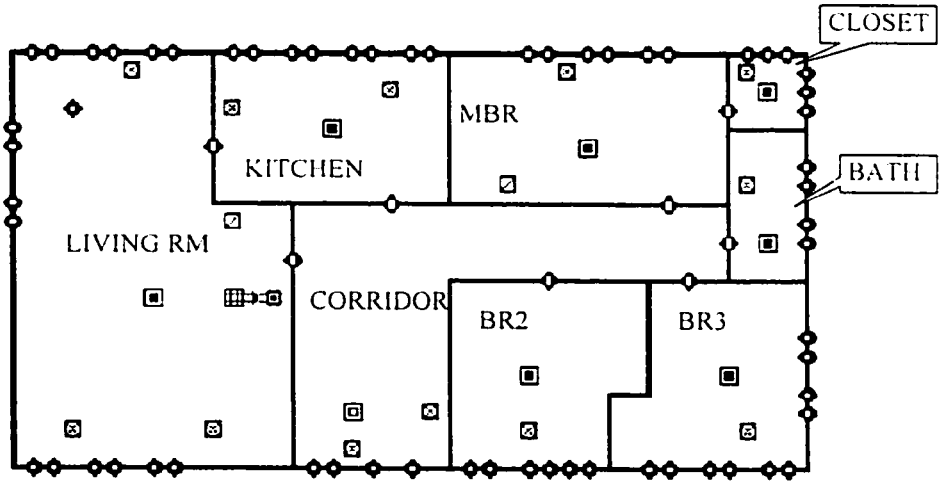

Figure A.12 Main Floor of House-2

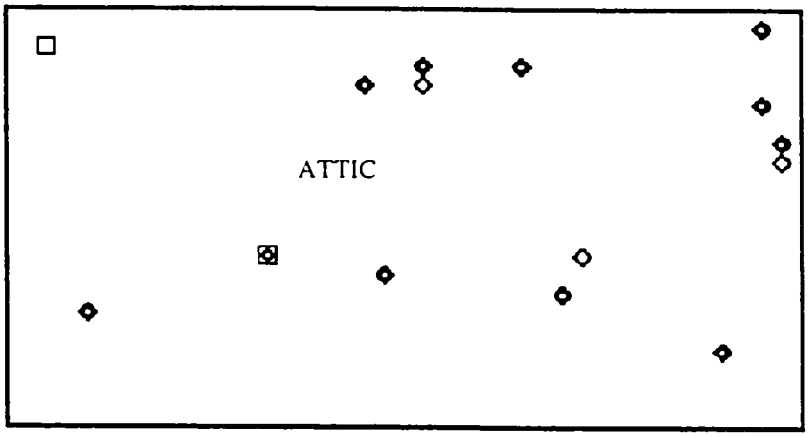

Figure A.13 Attic of House-2